$K^+\Lambda$ PHOTOPRODUCTION AT 1200 MeV

IN THE FORWARD HEMISPHERE

Thesis by

Charles W. Peck

In Partial Fulfillment of the Requirements

For the Degree of

Doctor of Philosophy

California Institute of Technology

Pasadena, California

1964

ACKNOWLEDGMENTS

This experiment was supervised by Professor Robert L. Walker. His interest, suggestions, criticisms and encouragement are deeply appreciated.

The assistance of Dr. D. Aitken in both mounting the experiment and much of the routine data accumulation is gratefully acknowledged.

Professor Robert F. Bacher was director of the laboratory during the performance of this experiment, and his presence was felt in many ways.

Mr. S. Ecklund actively assisted in taking part of the data. Furthermore, he and Mr. E. Adelberger performed many of the fringing field measurements on the magnet spectrometer. Mr. F. Wolverton spent many hours making detailed measurements on the optics of the focusing Cherenkov counter.

The principal electronic instruments used in this experiment were to a large extent conceived, designed, and tested by Mr. J. H. Marshall, III. The time and talent he lavished on them were clearly reflected in their remarkable reliability. In this experiment, almost no time was lost due to the malfunction of the experimental electronics.

The author is especially indebted to Dr. J. H. Mullins for his ready willingness to repair the synchrotron when it was broken and to improve it when it was operating. Without his ingenious solutions to the many difficult technical problems created by the transition from Phase II to Phase III operation of the machine, the high beam intensities, of crucial importance for this experiment, could hardly have been achieved so quickly. It would have been impossible to accumulate the large amount

of synchrotron operating time without the work of Mr. Edward Taylor, the synchrotron crew under the supervision of Mr. Larry Loucks, and the synchrotron operators under the supervision of Mr. Al Neubieser.

The financial support of the U. S. Atomic Energy Commission, the National Science Foundation, and the General Electric Foundation is gratefully acknowledged.

ABSTRACT

Measurements of the angular distribution of the cross section for the photoproduction of the $K^+ \Lambda$ system from hydrogen have been made in the center of mass angular interval from 15° to 85° at a lab photon energy of 1200 MeV. The reaction was identified by detecting K^+ mesons with a magnet spectrometer and a velocity selection system consisting of two Cherenkov counters. The angular distribution is very similar to those at lower energies in that it is peaked forward and is easily fit with a quadratic in $\cos \theta_{c.m.}$. Special emphasis was placed on the forward direction in an attempt to find evidence for the one-K-exchange pole. A Taylor-Moravcsik analysis of the data is presented, but the results are inconclusive. The total cross section for the reaction at this energy has been obtained by integrating the best fit to the measurements in the forward direction over the entire sphere. When this is compared with the total photoproduction cross sections at lower energies (also obtained by the integration of incomplete angular distributions), there appears to be no enhancement in the vicinity of 1700 MeV total center of mass energy, contrary to the case in the associated production by pions.

TABLE OF CONTENTS

APPENDICES

LIST OF TABLES

LIST OF FIGURES

To Margie

I. INTRODUCTION

The significant improvement achieved within the last couple of years in the intensity of electron synchrotrons has made possible the investigation of associated photoproduction at a level of precision comparable to the measurements on pion cross sections of five years ago. The current limitation on detailed quantitative knowledge of these reactions is the relatively primitive state of present detection schemes. For, whereas in pion photoproduction, a wide range of kinematical variables can be conveniently accommodated in a single experiment, this is not yet the case in K meson photoproduction. Of the many photon induced reactions leading to strange particle final states, surely the simplest experimentally is

$$\gamma + p \rightarrow K^+ + \Lambda$$

since its measurement represents but a straightforward extension of well established techniques developed for the study of the corresponding pion reaction. Not surprisingly, then, this is the best known strange particle photoproduction[1-4] and it will most likely retain that distinction in the foreseeable future. This thesis describes an experimental investigation of this process.

Theoretically, the two similar two body reactions

$$\gamma + p \rightarrow K^+ + \Lambda$$

and $$\gamma + p \rightarrow K^+ + \Sigma^0$$

leading to a charged K meson have a special significance in that they are potential sources of corroboratory evidence on the K and Σ parities (the Λ

parity being taken to be that of the nucleon) as well as the coupling constants $g^2_{NK\Lambda}/4\pi$ and $g^2_{NK\Sigma}/4\pi$. The method is much discussed in the literature[5-7] and hinges upon the simple pole in the reaction amplitude occurring at the unphysical value of the squared invariant momentum transfer, m^2_K. This contribution to the reaction amplitude is variously referred to as the retardation term, as the photoelectric term, as the one-K-exchange (OKE) pole. The latter name is descriptive of the Feynman diagram from which the term is normally calculated. Quite aside from its theoretical origins, there is quite strong experimental evidence that the amplitude for the reaction

$$\gamma + p \rightarrow \pi^+ + n$$

does indeed contain such a pole[7-8] with the expected extrapolated value. Thus, there is a well founded conviction that proper exploitation of this pole could yield information of considerable physical interest.

The experiment described in this thesis was deliberately designed to provide cross section measurements as near the forward direction as feasible in the hope that we could thereby demonstrate the necessity of including the OKE pole to describe the results, as in the pion case. Clearly, this would give one confidence in conclusions based upon the pole term. Unfortunately, at the highest energy which the synchrotron could reliably provide at the time the experiment was performed (end point energy = 1.28 BeV for a photon energy of 1.20 BeV), this hope remains unsatisfied; at this energy, a simple quadratic in cos θ fits the data quite nicely. Nevertheless, a Moravcsik extrapolation is included in the data analysis, although its physical significance seems doubtful.

In the case of pion photoproduction near threshold, it is well known that the phase of the production amplitude in a given channel of angular momentum and parity is simply the pion-nucleon scattering phase shift in that channel. However, for K photoproduction, even near threshold, there exists no such simple quantitative rule because of the large number of strong reactions coupled together at the high center of mass energies involved. Nevertheless, there is surely an intimate relation between the associated production by pions and the corresponding photoproduction, and any physical effect shown to be of importance in the reaction

$$\pi + N \rightarrow K + \Lambda$$

can be reasonably incorporated into a phenomenological analysis of

$$\gamma + N \rightarrow K + \Lambda \quad .$$

In fact, with sufficiently explicit models, some parameters are common between the theories of the two reactions. Several such models have been invented by various authors and they will be discussed.

This thesis consists of two parts: (a) the text proper which describes the most important features of the experiment itself and the principal results, and, (b) several appendices which give the technical details of method and data reduction of less general interest.

II. EXPERIMENTAL METHOD

The basic technique of measuring two-body photoproduction cross sections as used in this experiment is well known and has been described many times. It consists of illuminating a hydrogen target with a

bremsstrahlung beam and determining both the reaction and its kinematics by detecting one of the reaction products and measuring its production angle and energy. In this experiment, the K^+ meson was detected by using a magnet spectrometer to select reaction products with production angle and momentum defined to $\pm 0.7^{\circ}$ and $\pm 3.5\%$ respectively. Two Cherenkov counters selected K^+ mesons out of the momentum analysed beam. Since the Λ is the lowest mass system which can be photoproduced from hydrogen with a K^+ meson, we ensured the desired reaction by maintaining the maximum photon energy in the bremsstrahlung below that required for the production of the $K^+ \Sigma^{\circ}$ system. The general layout of the experimental area is illustrated in figure 1, and the spectrometer with its complement of scintillation and Cherenkov counters is shown schematically in figure 2. The solid angle was defined by A1 and the momentum aperture by S2. The Fan counters were arranged to detect particles scattered into the apparatus by the magnet pole pieces and the other scintillators were used to reduce accidental coincidences.

Since the precautions necessary to ensure proper momentum analysis with a magnet spectrometer are well known from pion photoproduction work, the principal experimental problem was the accurate separation of the K^+ mesons from the large flux of pions and protons. The most obvious K^+ meson signatures are its characteristic decay and its velocity. In order to avoid the large nuclear absorption correction inherent in stopping the mesons, we did not use the former possibility but relied entirely upon velocity dependent effects, particularly Cherenkov radiation.

The instrument which made this experiment possible was a focusing Cherenkov counter designed by Professor Robert L. Walker. Its location in the apparatus and its general configuration are shown in figure 2, and

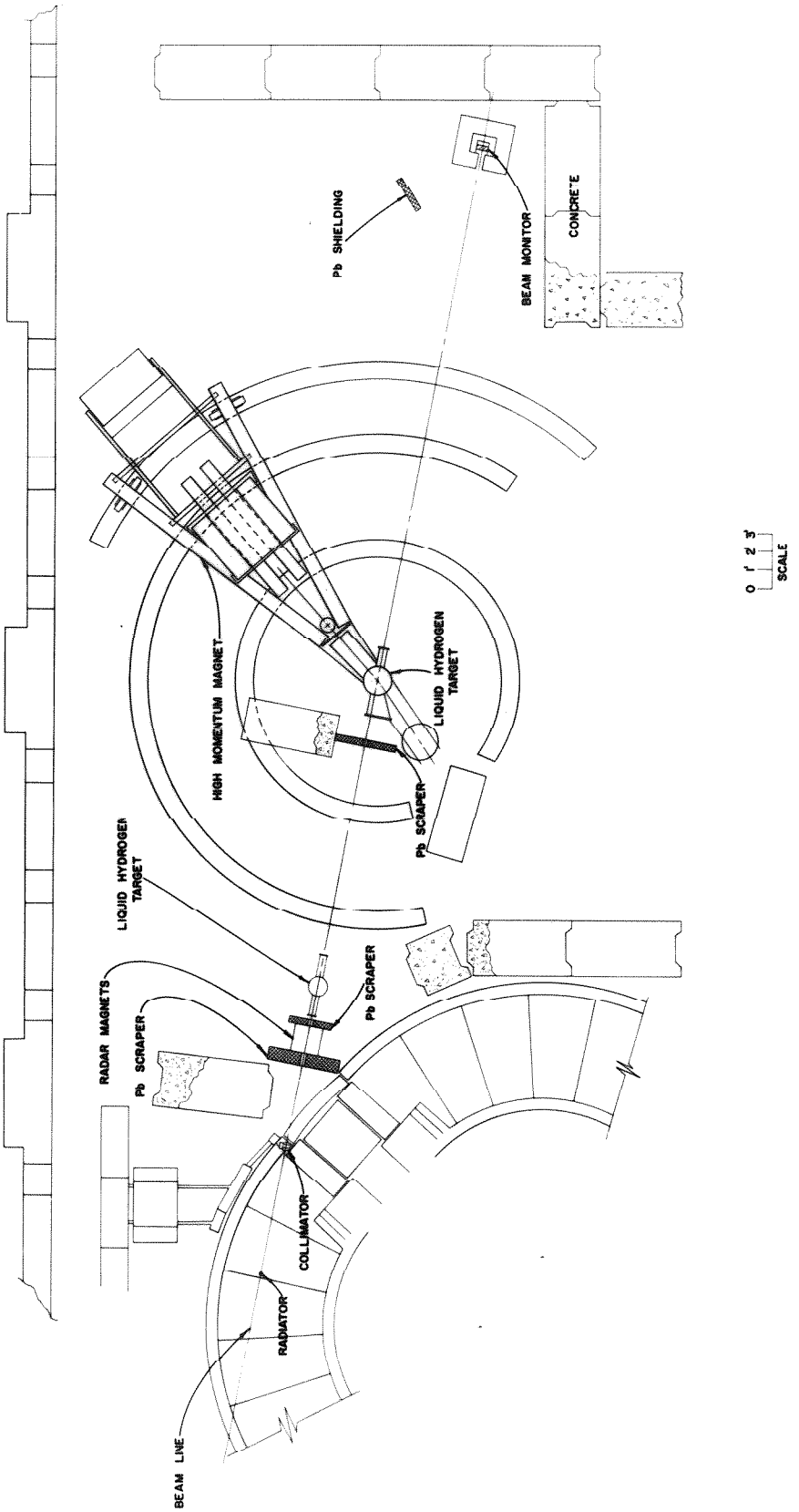

FIGURE 1

THE EXPERIMENTAL AREA

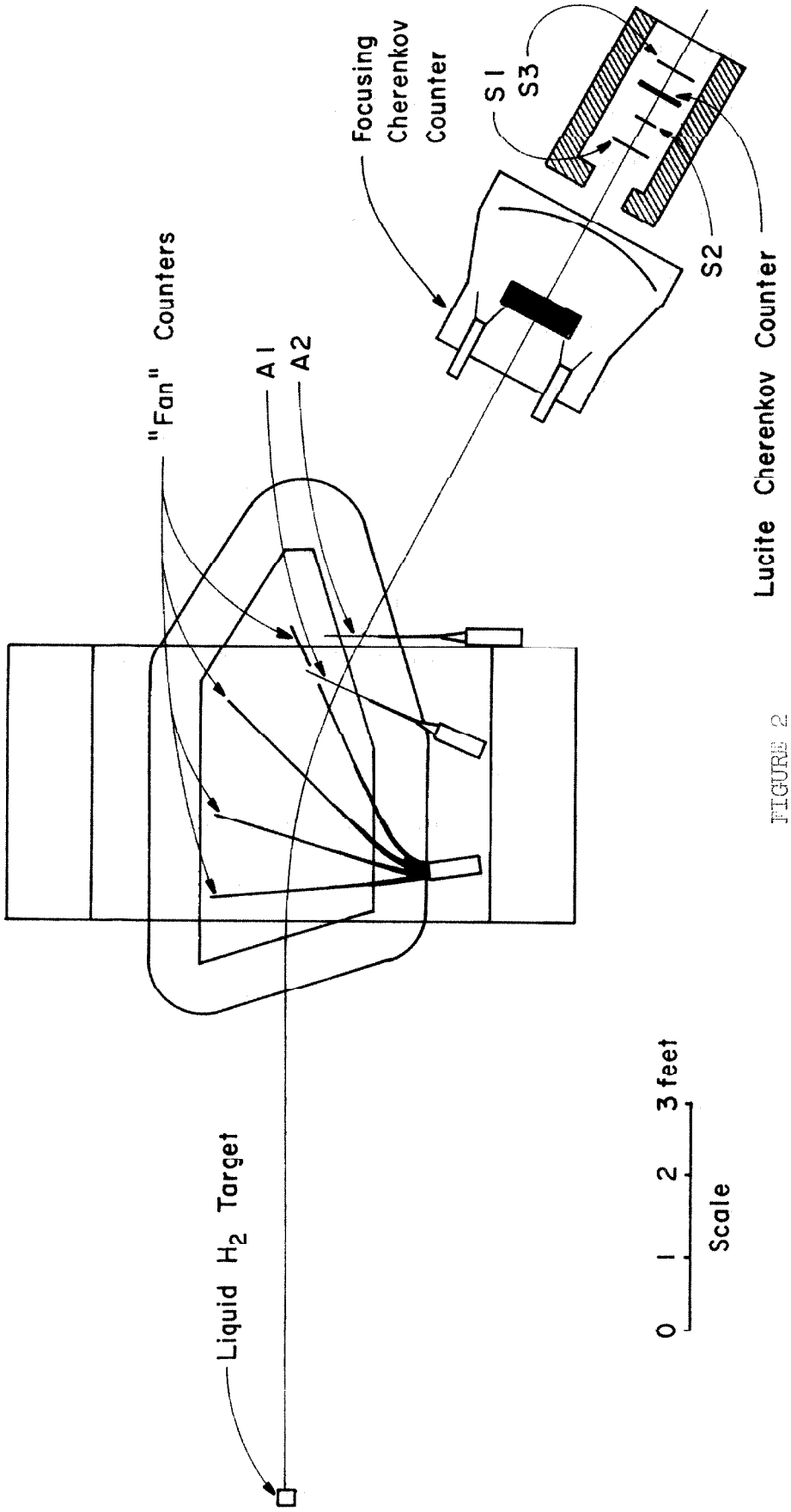

FIGURE 2

A SECTION THROUGH THE MEDIAM PLANE OF THE SPECTROMETER

figure 3 shows it in more detail. The cone of Cherenkov light generated in the 4 in. thick radiator is focused into a circular ring in the focal plane of a large spherical mirror. In this plane is an annular aperture viewed by phototubes. To a good approximation, the radius of the image depends only upon the particle's velocity and its center is determined by the particle's direction. Therefore, for the roughly collimated beam provided by the spectrometer, the phototubes respond only when the particle's velocity lies within a certain range. A typical velocity sensitivity curve for this instrument is shown in figure 4. With a fixed geometry, the velocity to which the counter is tuned depends only upon the refractive index of the radiator; mixtures of water and glycerine were used to adjust the index to that required by the K meson velocity at each of the several momenta used.

The resolution of a counter of this type is determined by a number of factors, but, for this experiment, the principal limitation was the divergence of the particle beam. Its sensitivity to protons was always small enough to present no serious problem (10^{-4} was an experimental upper limit), but alone it was insufficient to adequately separate highly relativistic particles from K mesons. For instance, at 812 MeV/c, the highest used in this experiment, its detection efficiency for fast particles was 0.4%. A second Cherenkov counter of threshold type was used to detect about 95% of the highly relativistic particles and so eliminate them by electronic anticoincidence. This counter (LC) was simply a Lucite slab viewed by phototubes normal to the average particle direction. The Cherenkov light from particles with $\beta > 0.9$ is efficiently piped to the phototubes by total internal reflection while for lower velocities the light escapes. Together, these two Cherenkov counters adequately eliminated the

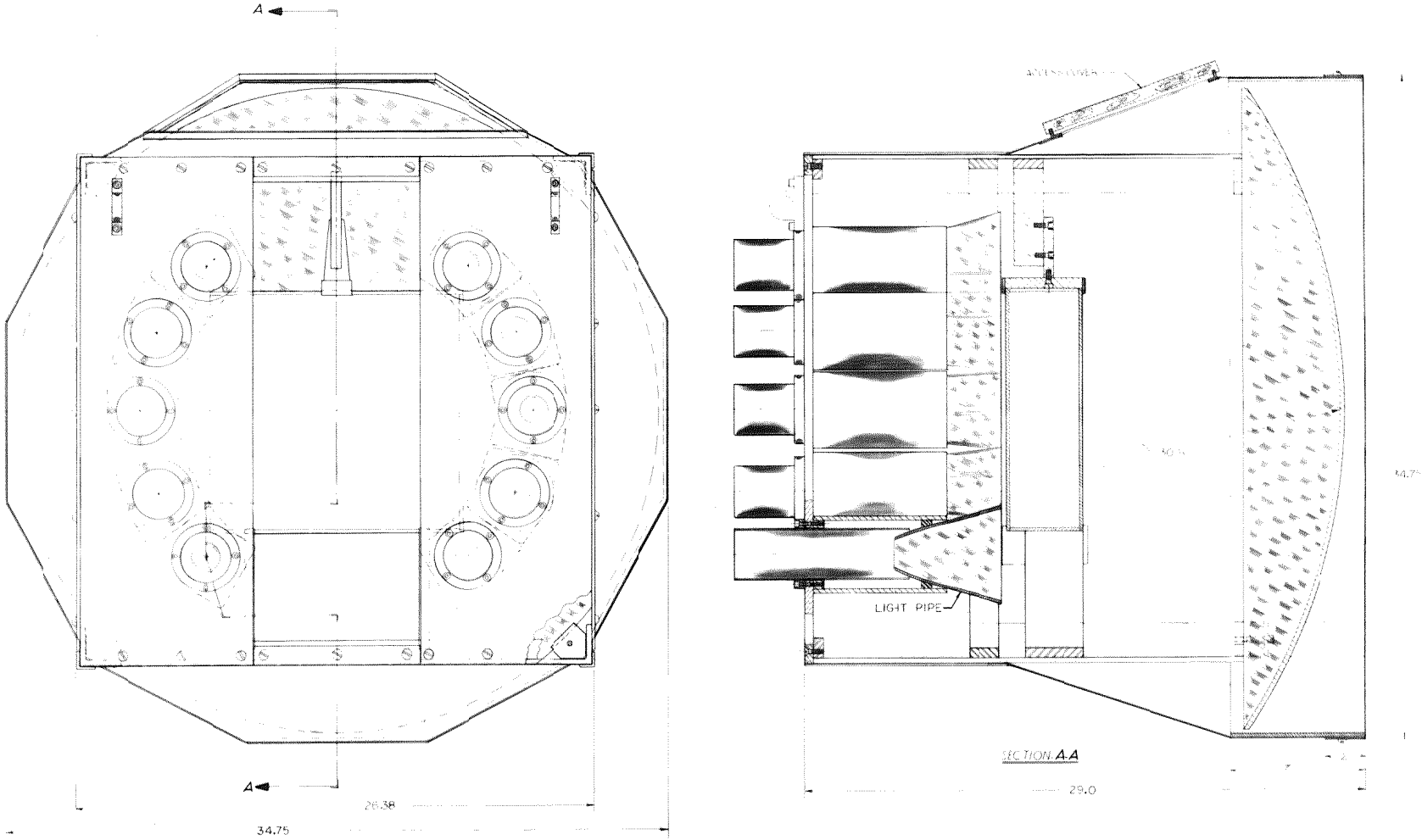

FIGURE 3

THE FOCUSING CHERENKOV COUNTER

FIGURE 4

A TYPICAL VELOCITY WINDOW DEFINED BY

THE FOCUSING COUNTER

These data were taken by using a proton beam, momentum analysed by the magnet with a resolution of 2.5% and the 12" scintillator at A1. The curve falls less steeply on the high momentum side because the amount of Cherenkov light is increasing and the cone angle is opening less rapidly.

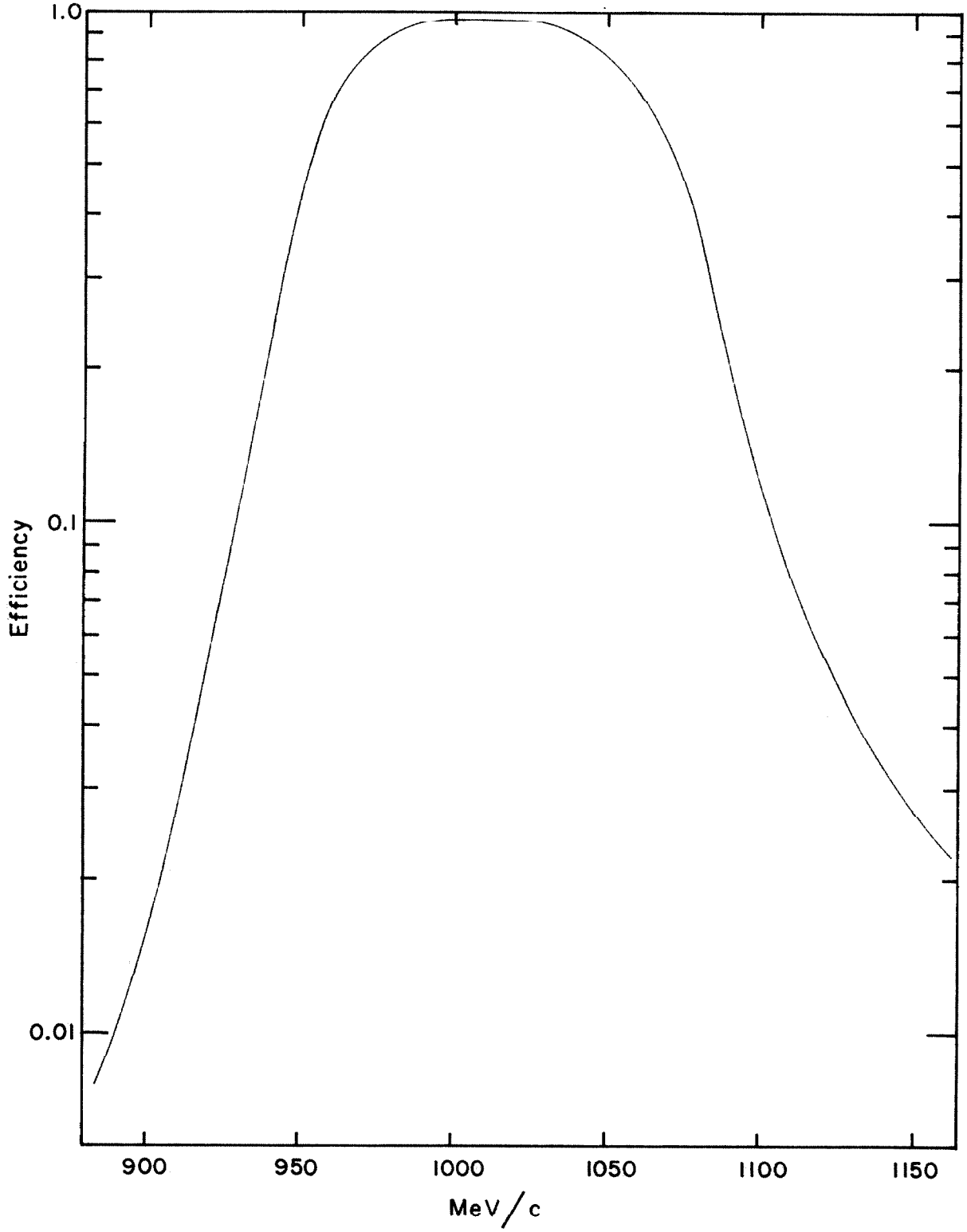
1.0
0.1
0.01
Efficiency
900
950
1000
1050
1100
1150
MeV/c

fast particle flux. Under the worst kinematical condition, an experimental upper limit to the detection efficiency for fast particles was 4×10^{-4}.

In brief, K^+ mesons were detected by a combination of momentum and velocity selection, and the reaction $\gamma + p \rightarrow K^+ + \Lambda$ was defined by setting the maximum photon energy in the bremsstrahlung just below that required to produce K^+ mesons (with the kinematical parameters required by the spectrometer) from the reaction $\gamma + p \rightarrow K^+ + \Sigma^0$.

III. EXPERIMENTAL PROCEDURE

Standard electronic logic requiring coincident pulses of adequate amplitude in each of the five scintillators A1, A2, S1, S2 and S3 was used to define the momentum analysed beam. Furthermore, signals from a set of counters (Fans) lying on the pole pieces of the magnet were included in anticoincidence to eliminate scattered particles. The counter S2 was divided into 3 parts to give finer momentum resolution when desired. Since the signals from the two Cherenkov counters were of special significance, their treatment was more elaborate. In particular, whenever the above requirements were satisfied, the signal from the focusing counter was measured in a pulse height analyser. Two spectra were accumulated, one when the Lucite counter was fired and one when it was not. This allowed us to monitor both the pion detection efficiency of the focusing counter and, roughly, the K detection efficiency of the Lucite counter.

In figure 5(A), a typical pulse height distribution observed in the focusing counter is presented. The huge rise in the distribution at small pulse heights when the Lucite counter was not used was due to pions. However, when LC was included in anticoincidence, this peak was greatly

FIGURE 5

TYPICAL PULSE HEIGHT SPECTRA OBSERVED

IN THE FOCUSING COUNTER

These data were accumulated during the runs on the 30° c.m., 1200 MeV point. Figure (A) shows the distribution taken with an end point energy of 1280 MeV and, for figure (B), it was 1130 MeV. In both cases, the dotted histogram was obtained when the signal from the Lucite Cherenkov counter was not used in the analyser triggering logic. For the solid histograms, this signal was included in anti-coincidence. The shaded histograms show the residues remaining after subtraction of a spectrum obtained with a Carbon target as discussed in the text. The exposure for figure (A) was 0.77×10^{14} eq. quanta and that for (B) was 0.35×10^{14} eq. quanta.

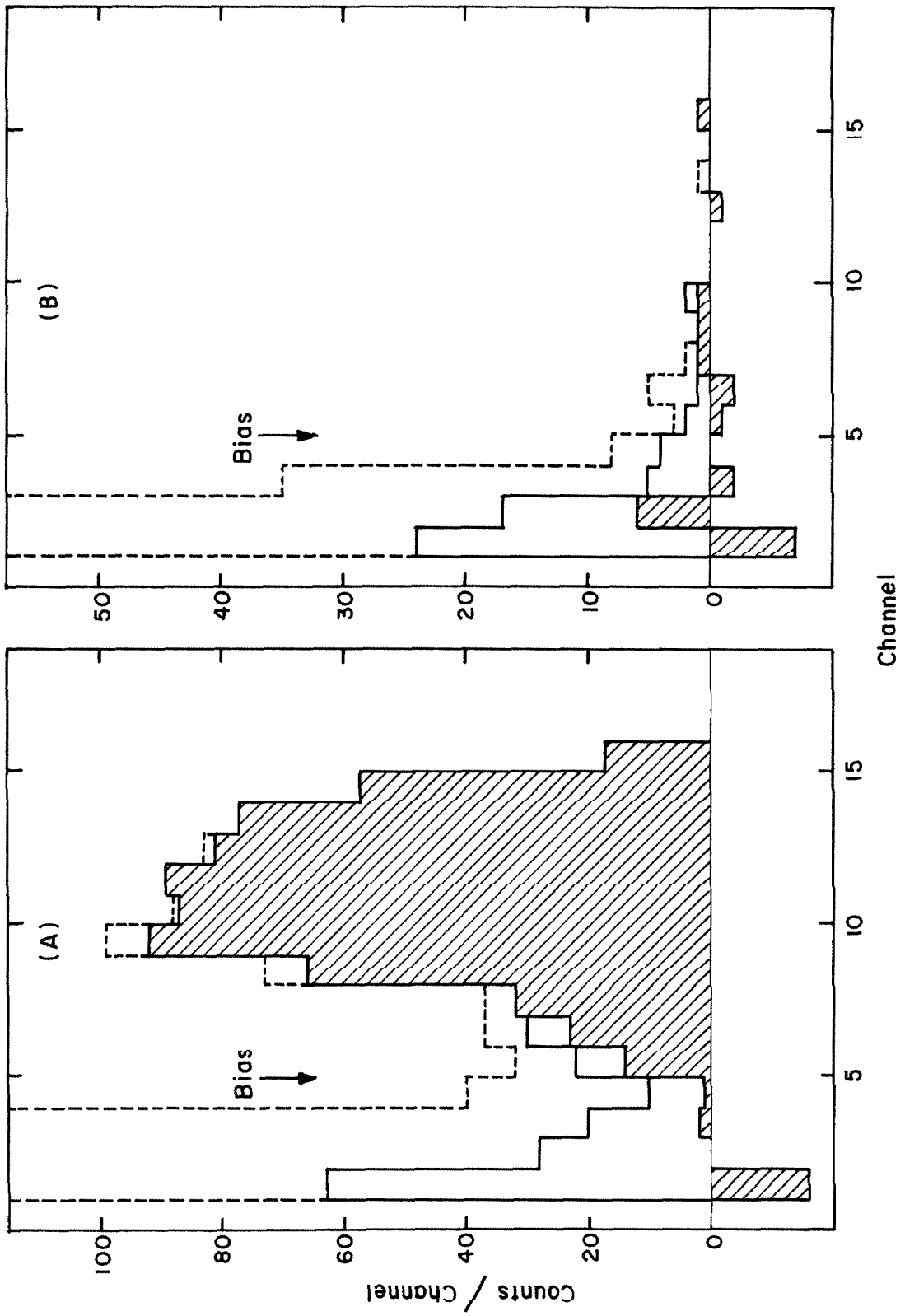
(A)
(B)
Bias
Bias
Counts / Channel
Channel
0
20
40
60
80
100
0
10
20
30
40
50
5
10
15

reduced, but there still remained a contamination of small pulses spilling into the K region. Similarly, when the maximum photon energy was set below that required for the $K^+\Lambda$ reaction, a distribution of small pulse heights appeared, as is shown in figure 5(B). A detailed investigation of this contamination was made in the hope of finding its origin and either eliminating it or, at worst, discovering how to correct for it. In the most unfavorable kinematical regions, about 30% of these particles appeared to be properly momentum-analysed pions and protons. We found that the remainder had velocities roughly equal to that for which the focusing counter was set by observing the pulse height distributions they made in the scintillators as well as by measuring their flight times. Thus, the fault was in inadequate energy selection by the spectrometer. Attempts to determine the mass of the offending particles by range measurements were inconclusive. The shielding of various parts of the apparatus with scintillators revealed no scattering source. Doubling the amount of matter at the positions of the aperture counters, A1 and A2, as well as at the focusing counter radiator, did not change the contamination, thus ruling out nuclear interactions of pions, protons, or neutrons as the origin of the difficulty. Calculations of low energy pions decaying in the magnetic field show that muons from this source cannot cause the trouble. In short, we were unable to attribute the contamination to any single source or simple combination of them. However, each test was made with but limited statistics so that each possibility may contribute something.

The simplest procedure of correcting for this contamination, in view of our ignorance of its origin, would be subtracting below threshold yields from those obtained above threshold. However, such a procedure is dangerous since it is known[11] that some types of contamination in K meson

photoproduction experiments show a dependence upon E_o. We found a purely empirical rule which appeared to effect the correction to a good approximation. With all logic and spectrometer settings the same as for a normal K run, the distribution in the focusing counter was observed with the hydrogen target replaced by Carbon and the maximum photon energy set well below that required to produce K mesons. For the 1200 MeV data, the Carbon distributions were taken with E_o = 1000 MeV. When compared to the spectrum obtained from below threshold hydrogen runs, both spectra being normalized to the same total flux of particles through the spectrometer (the rate PAR as defined in Appendix III was used), the agreement in both size and shape was within the statistical accuracy of the numbers. Similarly, when the spectrum from Carbon, normalized as above, was subtracted from the above threshold hydrogen data the tail of small signals was essentially eliminated. In figure 5, the shaded histograms show typical residues after such a subtraction. Except for further small corrections to be discussed shortly, the full target yield was taken as the number of counts above a suitable bias on the focusing counter signal, chosen as a compromise between a small "Carbon subtraction" and a high efficiency. This subtraction was largest at the most forward and most backward points, being 7% and 9% respectively, while for the middle angles it was typically 3%.

Below threshold rates were measured for six of the fourteen points. Table I compares these with the corresponding above threshold yields. Also, for the 35° c.m. point, the yield as a function of E_o was measured. Because of synchrotron energy limitations at the time this experiment was performed, we were unable to extend measurements to energies above that required for $K^+ \Sigma^o$ production and display the plateau between

TABLE I

PROOF OF K MESON IDENTIFICATION

Comparison of counting rates, C, at two different synchrotron end-point energies, E_o, one above the photon energy required for the reaction $\gamma + p \rightarrow K^+ + \Lambda$ and the other below it. The rates are normalized to 10^{13} eq. quanta.

k (MeV)	$\theta_{c.m.}$	E_o (MeV)	C
1200	15°	1280	90.1 ± 4.3
		1130	3.3 ± 3.4
1200	35°	1280	85.5 ± 3.0
		1130	$- 0.2 \pm .08$
1200	55°	1280	56.9 ± 2.8
		1130	0.5 ± 0.8
1200	70°	1280	30.6 ± 1.7
		1130	$- 0.5 \pm 0.4$
1200	85°	1280	18.8 ± 1.9
		1130	0.0 ± 1.0
1054	48°	1130	36.6 ± 2.7
		1000	$- 0.2 \pm 1.0$

these two sources of K^+ mesons in the full momentum aperture counting rate. However, even with the end point energy limitation, the resolution of a single one of the three momentum channels was sufficient to show the leveling off of its counting rate due to $K^+\Lambda$ production as the end point was raised. In figure 6, the equivalent yield in the central channel as a function of E_o is presented along with the expected curve. The measured points actually fall on three adjacent, similar curves, of course, one for each momentum channel, but these have been corrected for the different sensitivities of the three counters and suitably shifted along the horizontal axis to give a composite.

At small angles, the counting rate in each of the aperture counters, A1 and A2, was large, reaching a maximum of 3×10^5 counts/sec for the 15° c.m. point. The rate in the Fans was almost an order of magnitude larger. Corrections were calculated to account for dead time in the coincidence circuits, and the accidental anticoincidence rate of the Fans was continuously measured using reduced logic requirements. In the worst case, these corrections amounted to 1% and 5% respectively.

During exploratory work prior to the principal running of this experiment, the empty target yields at two wide angle points were measured. These were found to be about 7% of the full target yields, consistent with the known target construction and measured K^+ rates from Mylar. Except for the three smallest angles where the effective background target is not so well known, the empty target backgrounds were expected to be easily calculable from observed Mylar yields, and their direct measurement was left to the end of the experiment. Just after emptying the hydrogen, however, we found the target to be suddenly opaque whereas it had been transparent throughout the experiment. Closer investigation revealed a

FIGURE 6

THE DEPENDENCE OF THE K MESON

COUNTING RATE ON E_o

The fifteen data points were actually taken at only five end point energies, but the multiplexing of the momentum aperture allows the resolution shown. The shape of the smooth curve is that expected from the resolution of the spectrometer and the bremsstrahlung energy spectrum. The resolution function for S2 BC as shown in figure 14 and Boyden's[8] bremsstrahlung spectrum function were used. The amplitude and horizontal position of the calculated curve were adjusted to fit the data. The a priori curve based upon the energy calibrations of the synchrotron and the spectrometer was 15 MeV (1.3%) higher than that shown.

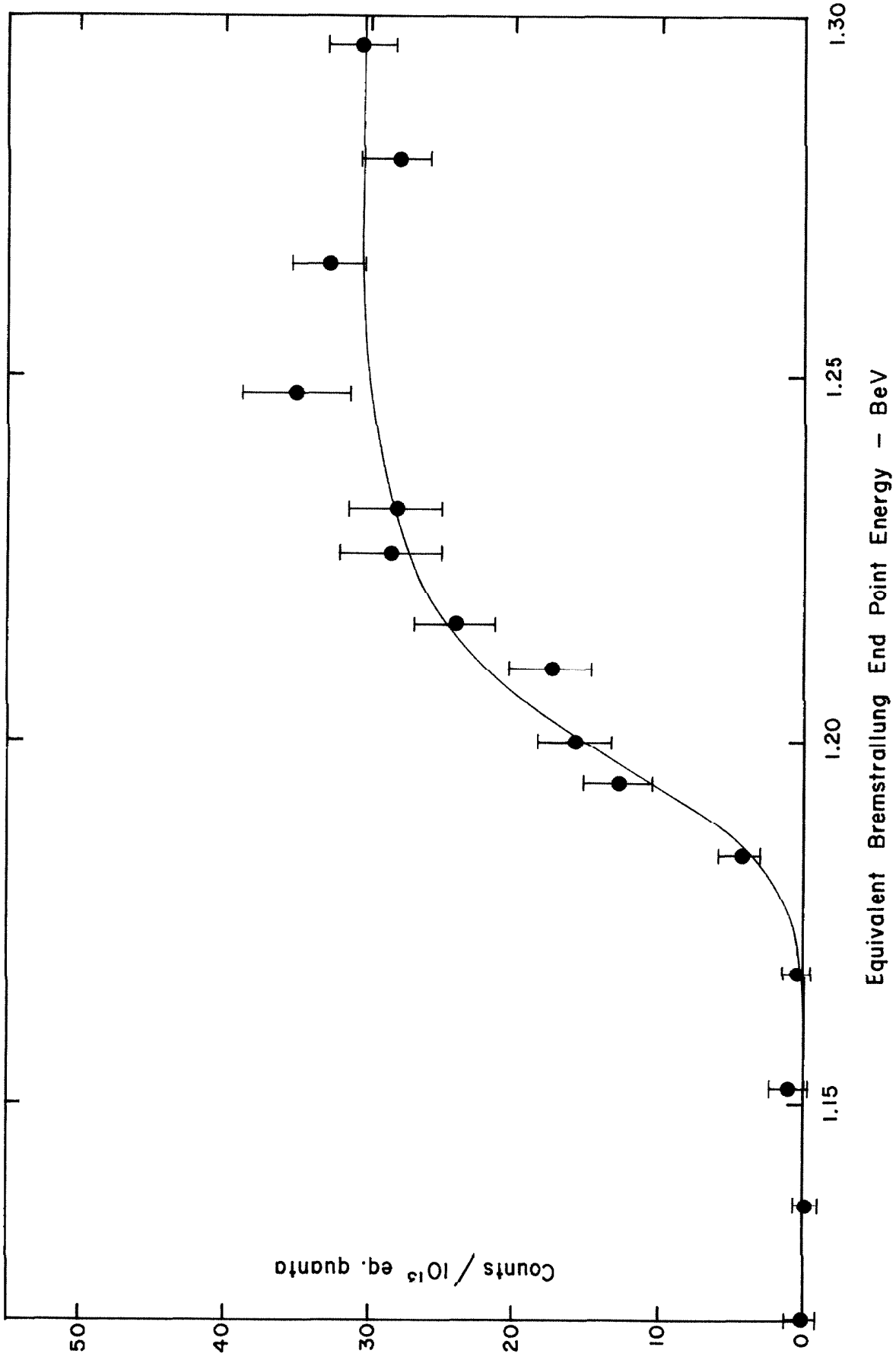
Counts / 10^{13} eq. quanta
0
10
20
30
40
50
1.15
1.20
1.25
1.30
Equivalent Bremstrallung End Point Energy - BeV

thin layer of matter condensed on the heat shields as well as on the outside of the Mylar cup. Since this contaminant seemed to have appeared during emptying, the target was disassembled and cleaned before proceeding. A full target check was immediately made and various monitoring rates were significantly smaller than before the incident. We were forced to conclude that the target had been contaminated to some extent during all but the earliest part of the experiment. However, the internal consistency of full target K rates taken at various times during the experiment as well as a proton rate measured frequently to $\pm$ 3% statistical accuracy leads us to believe that the target contamination was stable. Since reaccumulation of the data was not feasible, full target yields at four representative points, 15°, 30°, and 49° c.m. at 1200 MeV and the point at 1080 MeV, were remeasured. The assumption that the target contamination contributed a constant fraction of the full target yields was consistent with these data and the correction factor was determined to be .933 $\pm$ .035. Two points, that at 85° c.m., 1200 MeV, and the wider angle one at 1054 MeV, were completed during the exploratory work so that their backgrounds were known directly. The statistical uncertainty of $\pm$ .035 in this correction factor has not been included in the relative errors on the angular distribution but rather is combined with the systematic uncertainties.

Standard backgrounds were measured from the uncontaminated empty target using the same procedure as for the full target runs. At the smallest angle, it was 17% of the full target rate while, for the angles greater than 35° c.m., it was about 7%. For four of the points, the background was calculated from K^{+} rates observed with a 1" thick Mylar target.

IV. RESULTS

For the conditions of this experiment, the relation connecting the hydrogen yield, Y, to the differential cross section, $\frac{d\sigma}{d\Omega}$, is one of simple proportionality,

$$Y = \Gamma \frac{d\sigma}{d\Omega}$$

where Γ is a well known product of kinematical factors, target and spectrometer constants, detection efficiencies, the exposure, and a photon energy spectrum factor. As indicated above, the yields from hydrogen were obtained by correcting the full target counting rates for inadequate K meson identification, accidental anticoincidences and electronic dead time, target contamination, and empty target backgrounds. The detailed discussion of the factors entering into Γ is reserved for Appendix VI.

The principal results of this experiment are the fourteen cross sections given in Table II. The uncertainties listed in this table are statistical only; the overall systematic uncertainty is $\pm$ 6%. The three measurements at lower energies (1054 and 1080 MeV) were taken to connect this work with that from Cornell. The comparison is shown in figures 7(A) and 7(B). The angular distribution at 1200 MeV is displayed in figure 7(C). In these three figures, the dotted curves are calculated from the phenomenological model of Beauchamp and Holladay[20] (see Discussion below). The solid curves are simple quadratics in cos θ which best fit the data. In addition to the eleven cross sections at 1200 MeV measured in this experiment, a cross section of $1.34 \pm 0.41 \times 10^{-31}$ cm^2 at an angle of 127° was included to constrain the behavior of the fit in the backward direction. This value is the weighted average of three measurements of M. Daybell[43]

TABLE II

THE CROSS SECTIONS

k (MeV)	$\theta_{c.m.}$	$\frac{d\sigma}{d\Omega}$ $(10^{-31} cm^2)$
1200	15°	$3.79 \pm .27$
	25°	$3.34 \pm .15$
	30°	$3.41 \pm .19$
	35°	$3.00 \pm .14$
	42°	$2.84 \pm .15$
	49°	$2.82 \pm .16$
	55°	$2.76 \pm .16$
	63°	$2.41 \pm .16$
	70°	$2.02 \pm .14$
	78°	$1.94 \pm .17$
	85°	$1.54 \pm .18$
1080	46.5°	$2.79 \pm .18$
1054	31°	$2.84 \pm .22$
	48°	$2.33 \pm .19$

FIGURE 7

COMPARISON OF THIS EXPERIMENT WITH

PREVIOUS WORK

The solid curves drawn through the points are quadratic least squares fits. The dotted curves are calculated from the theory of Kuo[19] and Beauchamp and Holladay[20] with the parameters of the latter.

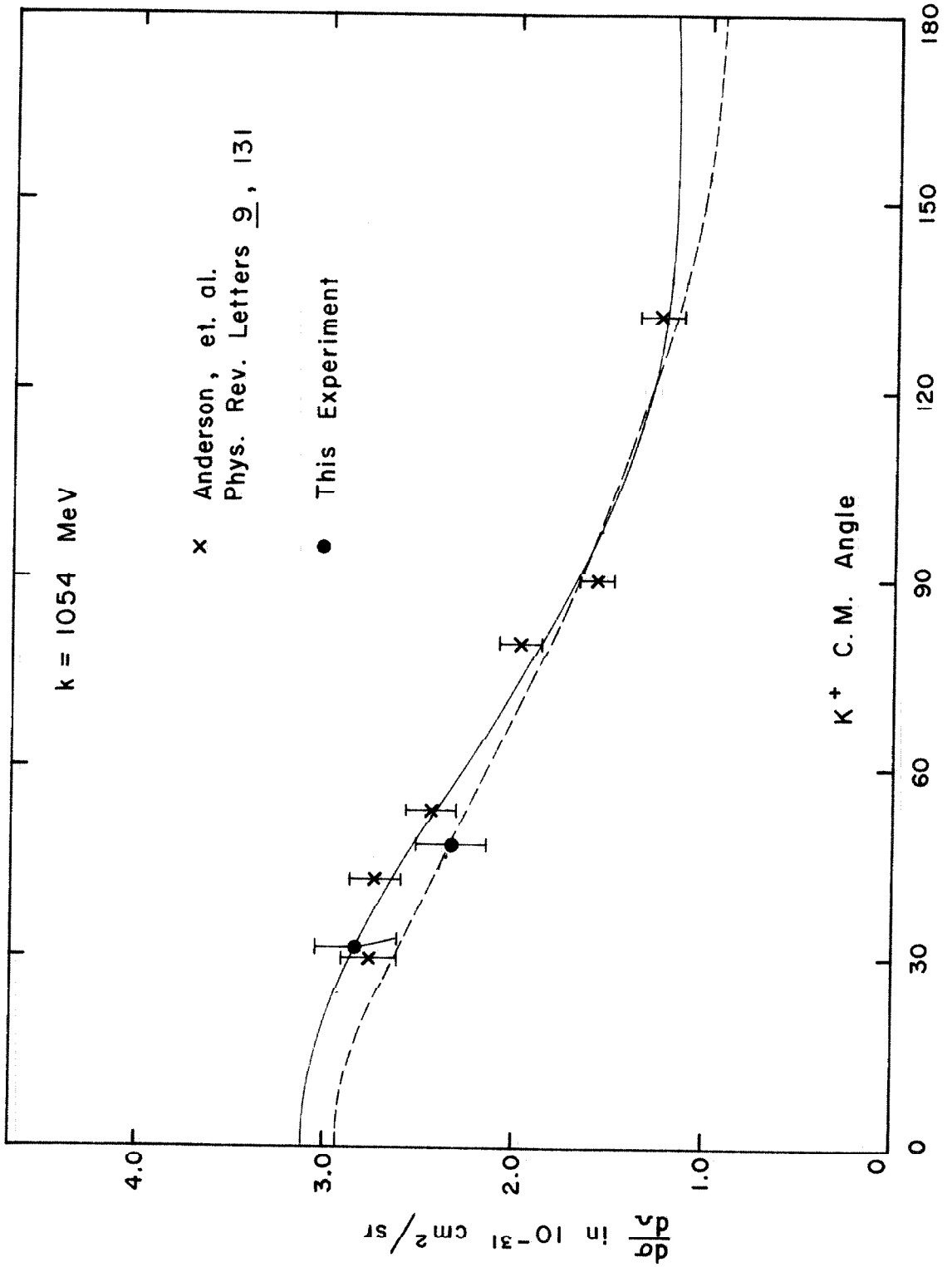
k = 1054 MeV
× Anderson, et. al.
Phys. Rev. Letters 9, 131
● This Experiment
K+ C.M. Angle
dσ/dΩ in 10−31 cm2/sr
0
30
60
90
120
150
180
1.0
2.0
3.0
4.0

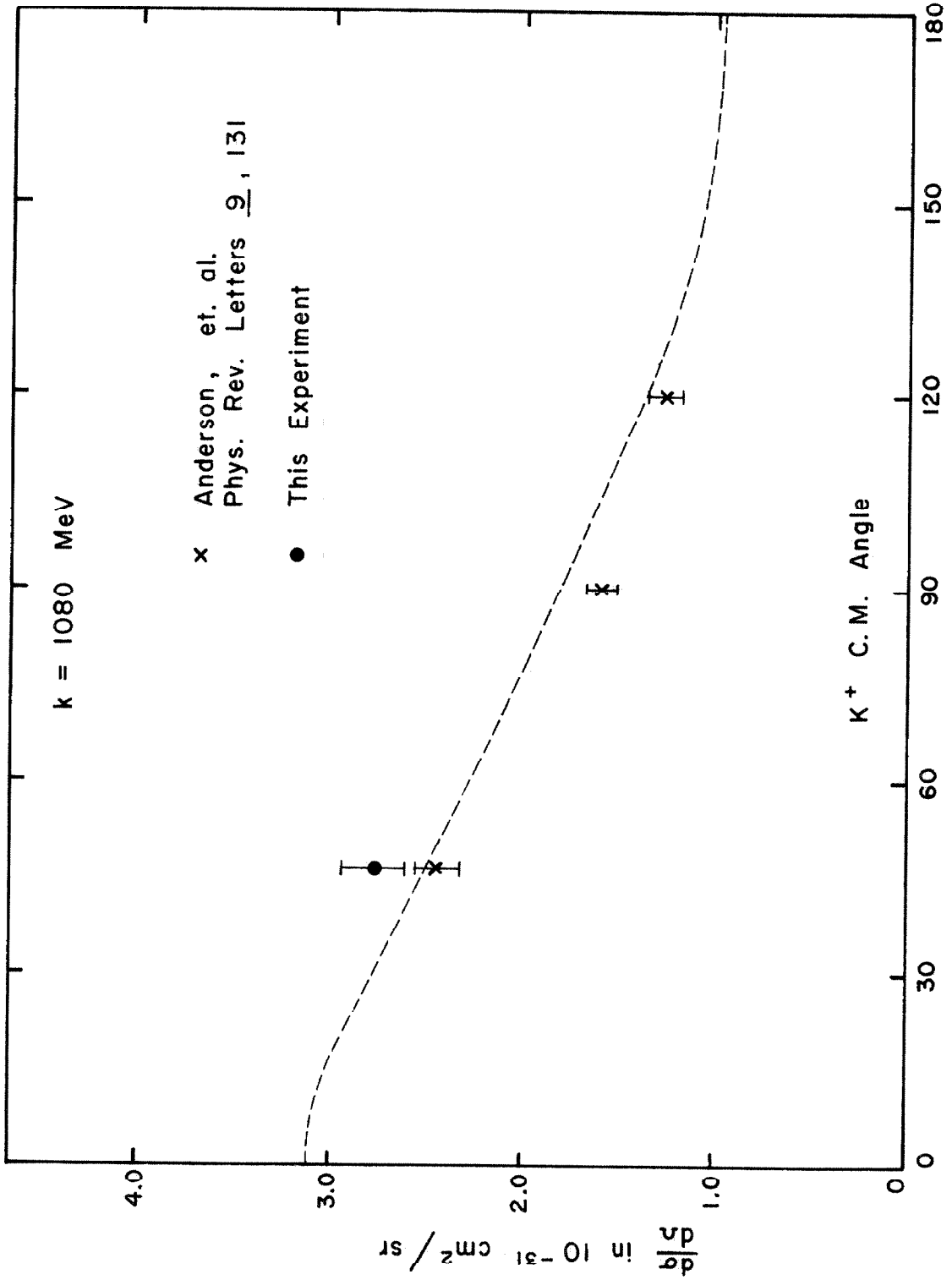
k = 1080 MeV
× Anderson, et. al. Phys. Rev. Letters 9, 131
● This Experiment
K+ C. M. Angle
dσ/dΩ in 10⁻³¹ cm²/sr
0
30
60
90
120
150
180
1.0
2.0
3.0
4.0

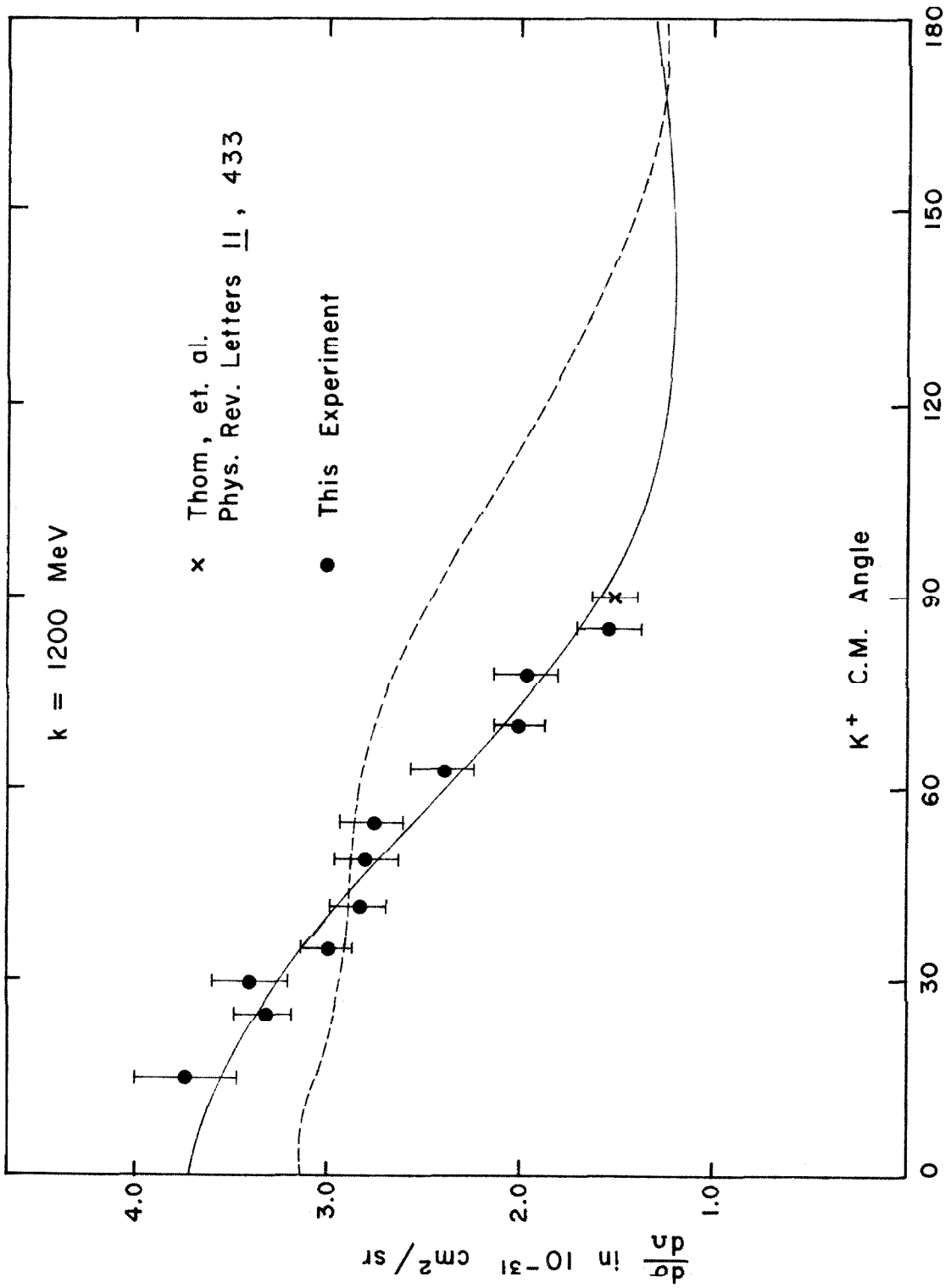
k = 1200 MeV
x Thom, et. al.
Phys. Rev. Letters 11, 433
● This Experiment
K+ C.M. Angle
dσ/dΩ in 10-31 cm2/sr
4.0
3.0
2.0
1.0
0
30
60
90
120
150
180

at lab photon energies of 1100, 1200 and 1300 MeV and c.m. angles of 120°, 127° and 134° respectively. The 1200 MeV distribution is actually fit fairly well by the simple linear function $a_o + a_1 \cos\theta$ (χ^2 probability of 18%); in the backward direction, however, this fit yields negative cross sections. A quadratic fit $a_o + a_1 \cos\theta + a_2 \cos^2\theta$ is considerably better (χ^2 probability of 83%). The coefficients for the quadratic form (in units of 10^{-31} cm^2) are

$$a_o = 1.60 \pm .11$$
$$a_1 = 1.18 \pm .33$$
$$a_2 = .87 \pm .34$$

Integration of this quadratic form gives a total cross section at 1200 MeV (total c.m. energy = 1770 MeV) of $2.0 \pm .15$ μb, the uncertainty being statistical only.

V. DISCUSSION

At the present time, there exists no established theory to describe the dynamics of the strange particles. However, the kinematics (i.e., conservation laws) and the kinematical parameters (charge, mass, spin, parity, isospin, hypercharge) of the particles involved in this experiment are all known with a high degree of certainty. These, then, form the basis upon which any dynamical theory must be built. The most fruitful idea for describing the dynamics of the strong interaction is that of Yukawa, in which, by analogy with electromagnetism, the force between two particles is mediated by a third. One is then led to the characteristic three particle interactions (πNN, $K\Lambda N$, $K^*\Lambda N$, $\pi\Lambda\Lambda$, πNN^{**}, etc.) into which electromagnetism

can be incorporated in a natural way (γNN, $\gamma\pi\pi$, γKK, etc.). All of the discussion will be based upon this general view of strong interaction dynamics.

With respect to the strange particles, perhaps the most important dynamical parameters to be determined are the K-nucleon-hyperon coupling constants. In particular, the SU(3) unitary symmetry predicts a relationship between the three coupling constants $g_{\pi NN}$, $g_{K\Lambda N}$ and $g_{K\Sigma N}$ so that knowledge of the two strange particle constants would be of interest. As always in this thesis, however, we shall be concerned only with the K^+ Λ system and the discussion will be restricted to the coupling constant $g_{K\Lambda N} = g_\Lambda$. In the literature, several approaches have been taken to determine this number, such as analyses[12] of the reaction $p + \bar{p} \rightarrow \Lambda + \bar{\Lambda}$ the binding energies of the hypernuclei[13], and the reaction $\pi^- + p \rightarrow K^o + \Lambda$ [14]. All of this work suggests that $g^2_{K\Lambda N}/4\pi$ is small (between 1 and 3) compared to the corresponding πNN coupling constant. The first indication of this smallness, however, came from the early photoproduction data[1]. Assuming a pseudoscalar K meson, Gell-Mann[15] applied the Kroll-Ruderman[16] approximation to the threshold photoproduction and obtained a coupling constant $g^2_\Lambda/4\pi$ of the order of unity. This approximation, however, is based upon a theorem for low energy photons producing particles with mass small compared to that of the nucleon. In fact, when a first order correction for the pion mass is made, the approximation yields the correct pion-nucleon coupling constant from the threshold pion photoproduction data[17]. However, it is expected that the relatively large mass of the K meson renders the theorem only suggestive rather than definitive in the strange particle case.

In the past several years, the method of extrapolating physical data to a pole in an unphysical kinematic region has been much discussed as a means of determining coupling constants. Here again, the analysis[7-9] of reactions involving pions has yielded the expected coupling constant but so far no one has been successful in extending the method to the strange particles. An attempt in this direction is described in section 1 below where the $K^+\Lambda$ angular distribution at 1200 MeV is extrapolated to the one-K-exchange pole. The extrapolation method of learning interesting physical constants from experimental data is especially attractive because of the simplicity of the dynamical assumptions involved. However, in practice, because of experimental uncertainties in data, the pole term must dominate the cross section before one can expect to obtain believable results and this does not seem to be the case in $K^+\Lambda$ photoproduction at the energies so far investigated.

Aside from the particular problem of determining $g_\Lambda^2/4\pi$ from the photoproduction data, there is a more general one of finding the physical processes which contribute to the reaction. One approach to this problem is to describe the data with a few parameters consistent with conservation of angular momentum and parity, in our case, the multipole amplitudes. Since various processes, and in particular final state resonant interactions, contribute in a characteristic way to these amplitudes, one could hope that a reasonable physical interpretation could result from such an analysis. On the other hand, full fledged models, parametrized by a few constants, can be postulated and the parameters tailored to force the model to fit existing data. In either case, however, intrinsic ambiguities and incomplete data make firm conclusions very difficult to justify. The angular distributions of cross sections for $K^+\Lambda$ photoproduction are not

yet sufficiently well known to allow meaningful multipole analyses. On the other hand, two essentially different phenomenological models have been proposed for this process. In section 2 below, these are discussed, but as just implied, the conclusions are only tentative at best.

1. Moravcsik Extrapolation

Moravcsik[5] has pointed out that the pole in the analytically continued $K^+\Lambda$ ($\pi^+ n$) photoproduction amplitude due to the exchange of a K^+ (π^+) meson (see figure 8, diagram 1) should be separable from all other processes contributing to the reaction. The reason is that this singularity is nearer the physical region than that due to any other known virtual process and, consequently, in a kinematical region covering both this pole and the physical region, one hopes that the contribution to the cross section from all other processes can be accurately approximated in a simple way. For the one-meson-exchange term, the amplitude is proportional to $1/(1 - \beta \cos\theta)$ where β is the meson velocity and θ, its angle in the center of mass system. This leads to the following form for the cross section:

$$\frac{d\sigma}{d\Omega} = \frac{g_\Lambda^2}{4\pi} \frac{e^2}{4\pi} R(W) \frac{1 - \cos^2\theta}{(1 - \beta \cos\theta)^2} + F(W,\theta)$$

where

$$R(W) = \frac{1}{8} \left(\frac{q}{k}\right)^3 \frac{(m_\Lambda - m_p)^2 - m_K}{\omega^2 W^2}$$

W - total energy

q = K meson momentum

ω = K meson energy

k = photon energy

FIGURE 8

THE VARIOUS FEYNMAN DIAGRAMS WHICH
MIGHT CONTRIBUTE TO $K^+\Lambda$ PHOTOPRODUCTION

In addition to the ten diagrams shown here, there can be those involving the exchange of excited hyperons ($Y^*(1405)$, for example) in the u-channel. These particles, however, are so massive that they are not expected to affect photoproduction at the energies considered in this thesis and so have not been included.

Electric Born Terms

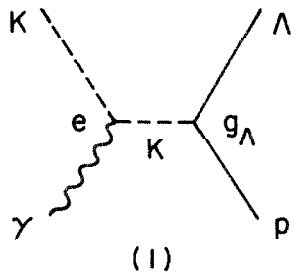

(1)

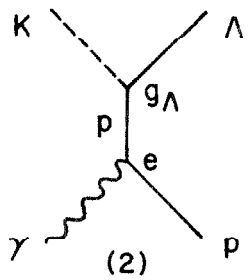

(2)

Magnetic Borns Terms

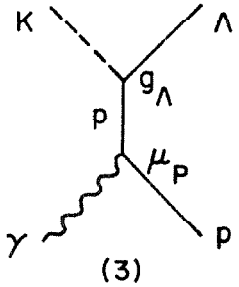

(3)

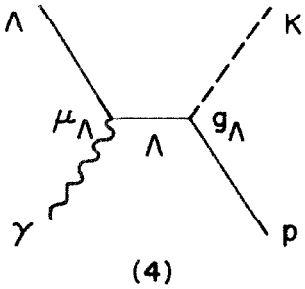

(4)

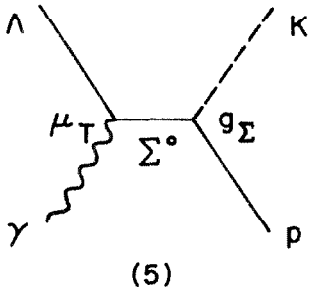

(5)

K* Exchange Terms

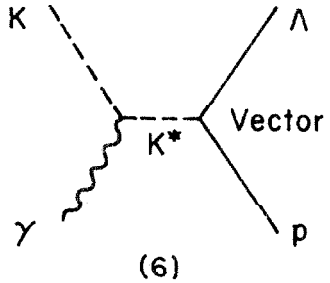

(6)

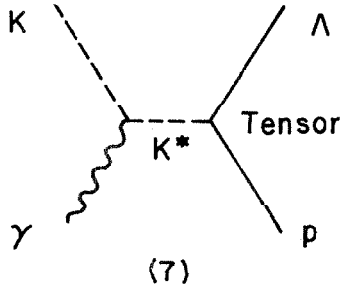

(7)

Resonance Terms

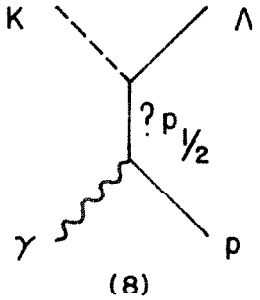

(8)

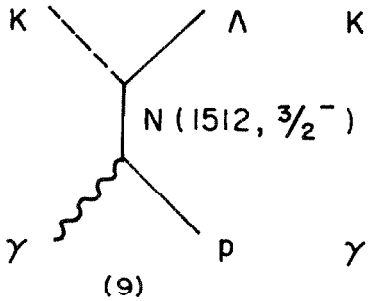

(9)

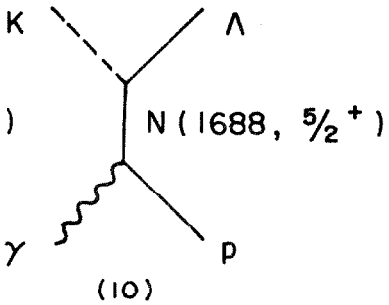

(10)

with all quantities being taken in the center of mass system. In general, all that is known about the function $F(W,\theta)$ is that it contains at most a first order pole at $\cos\theta = 1/\beta$. Consequently, we have*

$$\lim_{\cos\theta \to 1/\beta} (1 - \beta\cos\theta)^2 \frac{d\sigma}{d\Omega} = \frac{g_\Lambda^2}{4\pi} \frac{e^2}{4\pi} R(W) (1 - 1/\beta^2) \quad .$$

The crux of the practical utilization of this fact as suggested by Moravcsik lies in the assumption that $(1 - \beta\cos\theta)^2 F(W,\theta)$ at a fixed W can be accurately represented by a polynomial in $\cos\theta$ in a region covering the unphysical point $\cos\theta = 1/\beta$. In the case of pion photoproduction there is reason to believe that this is possible since there is no known meson with mass near that of the pion. For K^+ photoproduction, however, the exchange of the $K^*(888)$ (figure 8, diagrams 6 and 7) gives a pole in an amplitude contributing to $F(W,\theta)$ at

$$\cos\theta = 1/\beta^* = 1/\beta + (m_{K^*}^2 - m_K^2) / (2kq)$$

where k and q are defined above. At the present time, there is no reason to believe that K^* exchange is not important, so that, at high energies anyway, a simple polynomial expansion of $(1 - \beta\cos\theta)^2 \frac{d\sigma}{d\Omega}$ may not be adequate. However, at the energy of this experiment, the $K^*(888)$ pole occurs at $\cos\theta = 2.98$ while that of the K^+ itself is at 1.75. Since the relative strength of these two singularities is not known, it is impossible

---

* In keeping with the practice adopted by Moravcsik, this limit is sometimes referred to in this thesis as the residue at the pole. This usage is not to be confused with the standard mathematical definition of the residue at a first order pole.

to prove that the Moravcsik procedure is adequate at this energy, but the poles are sufficiently separated that a cubic fit in the function

$$\left(\frac{1 - \beta x}{1 - \beta^{*} x}\right)^{2}$$

in the region $1.0 < x < 0$ is quite good out to $x = 1.75$. Although at higher energies a more sophisticated approach will be necessary to disentangle the effects of these two singularities, the simple polynomial fit appears satisfactory at 1200 MeV.

In figure 9, the polynomial fits to $(1 - \beta \cos \theta)^2 \frac{d\sigma}{d\Omega}$ are shown, and the relevant parameters of the statistical analysis are given in Table III. The relation between extrapolated values and the coupling constant is shown in figure 10. It is clear that even the first order polynomial fits the data quite well, but if one insists on using higher orders, quartic seems to be preferred. This simply reflects the fact that a quadratic fits the angular distribution very well. Thus, contrary to the significant reduction in the order of the fitting polynomial when the pole is included in the analysis of the $\pi^{+}n$ photoproduction[8], the $K^{+}\Lambda$ data does not suggest any need for its inclusion. Furthermore, at $k_{lab} = 1200$ MeV, the total c.m. energy (1770 MeV) is not very far from that of the $F_{5/2}$ nucleon resonance (1688 MeV) so that one might expect F-waves to contribute to the angular distribution. This can be taken as evidence for the need of at least a sixth order extrapolating polynomial, for which the data are quite inadequate. Accordingly, we do not place much confidence in the resulting residue.

FIGURE 9

MORAVCSIK EXTRAPOLATIONS

The curves are polynomial fits to the values of $(1 - \beta \cos \theta)^2 \frac{d\sigma}{d\Omega}$, the order of the polynomial being shown on the curve.

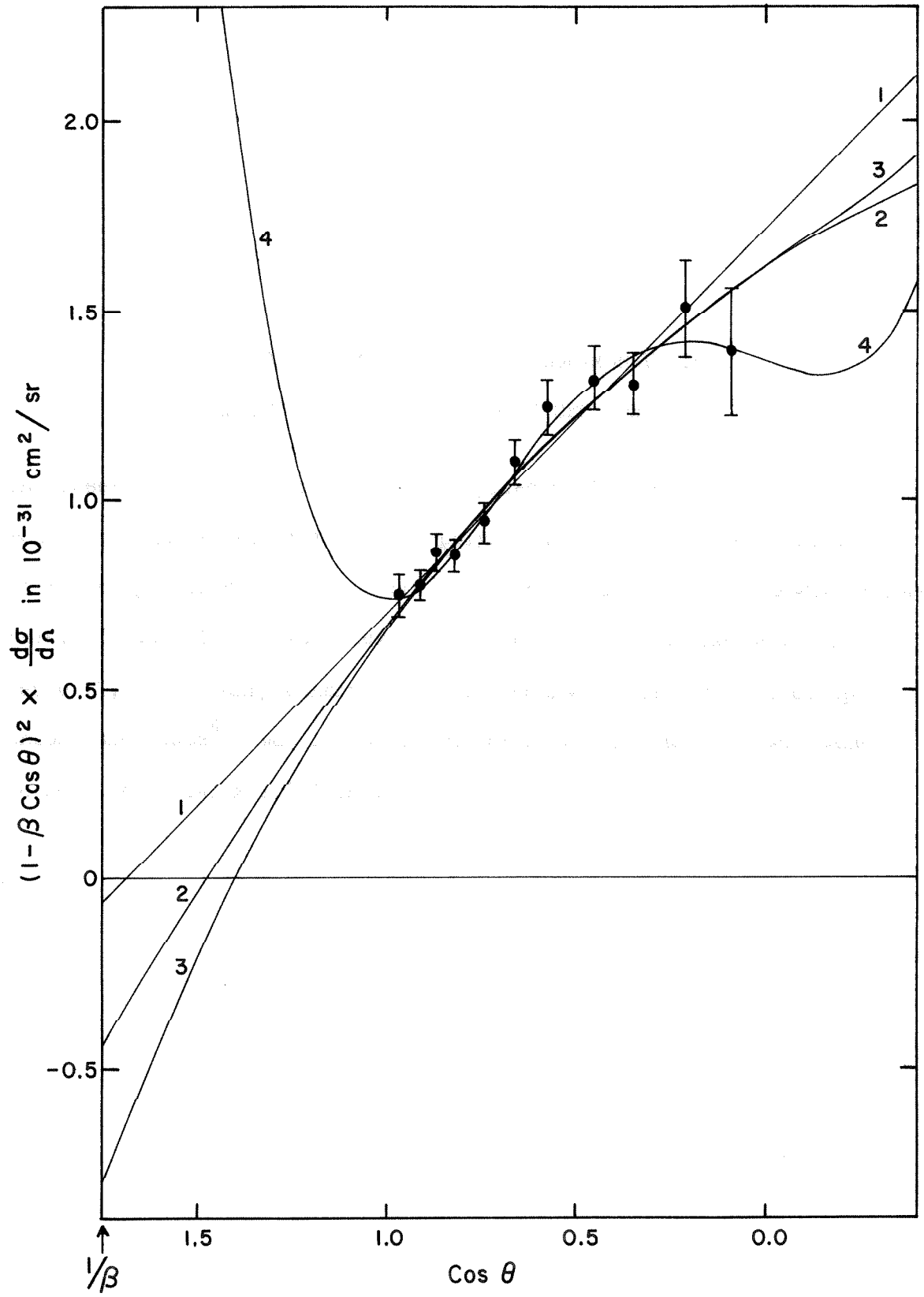
2.0
1.5
1.0
0.5
0
-0.5
1
2
3
4
$(1-\beta\,Cos\,\theta)^2 \times \frac{d\sigma}{d\Omega}$ in 10^{-31} cm^2/sr
1.5
1.0
0.5
0.0
$1/\beta$
Cos θ

TABLE III

STATISTICAL PARAMETERS FROM TAYLOR-MORAVCSIK

ANALYSIS OF 1200 MeV CROSS SECTIONS

The observed cross sections are multiplied by $(1 - \beta \cos \theta)^2$ and the resulting numbers are fitted with polynomials in $\cos \theta$. The evaluation of the polynomials at $\cos \theta = 1/\beta$ gives the residue at the one-K-exchange pole. In addition to the eleven cross sections at 1.2 BeV given in Table II, a "boundary condition" in the backward direction based upon unpublished data[43] was imposed. The cross section at 127° was taken to be $1.34 \pm 0.41 \times 10^{-31}$ cm^2.

Order of Polynomial	1	2	3	4	5
Degrees of Freedom	10	9	8	7	6
$\chi^2_{OBS.}$	8.24	7.17	7.05	3.73	3.60
Residue ($10^{-31} cm^2$)	- .07	- .46	- .81	7.31	15.4
Error on Residue	.09	.38	1.11	4.59	22.2
Prob. $\chi^2 \geq \chi^2_{OBS.}$	60%	62%	53%	81%	73%

FIGURE 10

THE EXTRAPOLATED VALUE AT THE OKE POLE

IN TERMS OF THE COUPLING CONSTANT

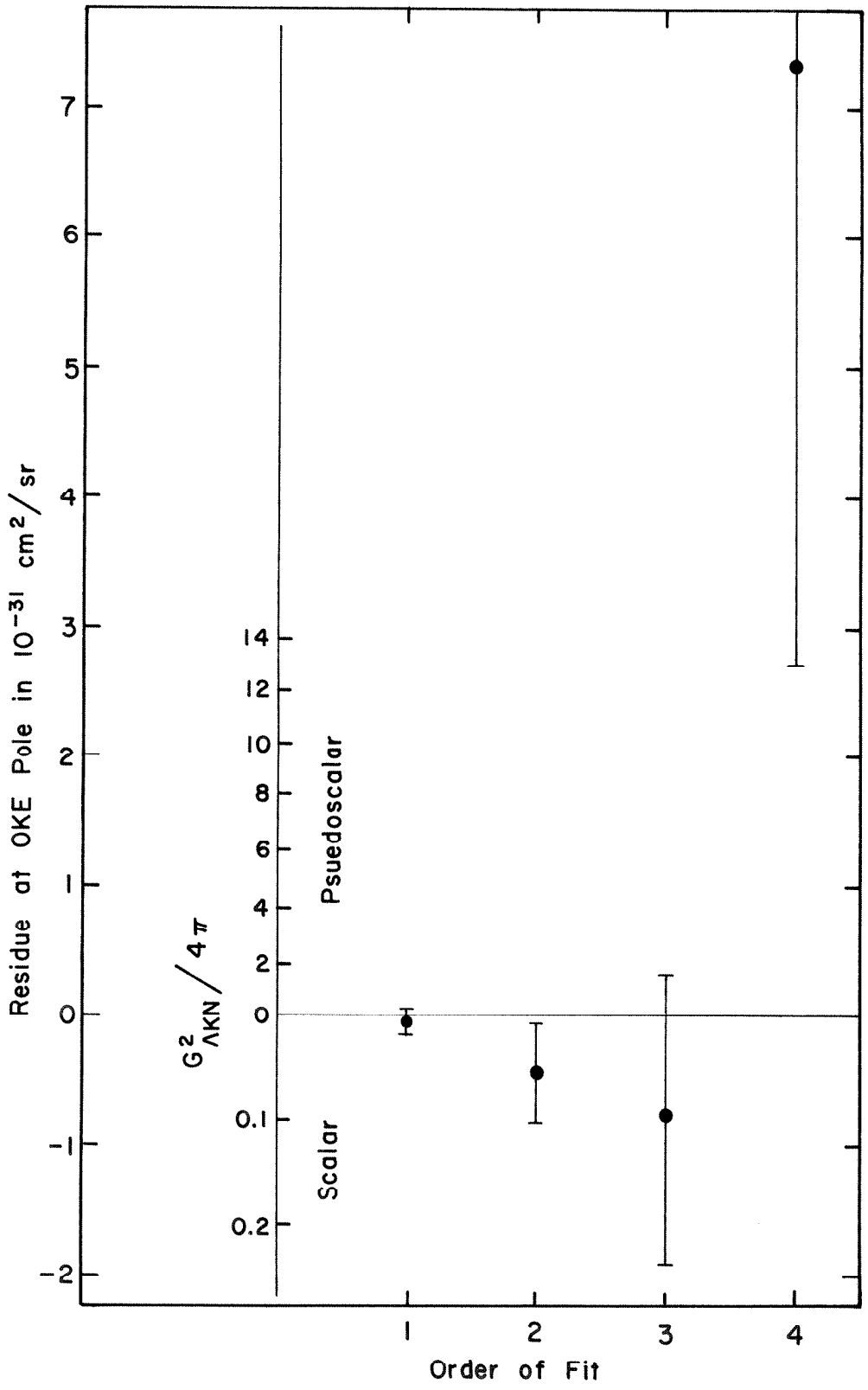
Residue at OKE Pole in 10^{-31} cm^2/sr
7
6
5
4
3
2
1
0
-1
-2
$G^2_{\Lambda KN}/4\pi$
14
12
10
8
6
4
2
0
0.1
0.2
Psuedoscalar
Scalar
1
2
3
4
Order of Fit

2. Resonance Models

The energy dependence of the total cross section for $K^+\Lambda$ photoproduction is shown in figure 11, and it is clear that there is no hint of any resonant structure. On the other hand, the bottom half of the figure shows the total cross sections for the reaction

$$\pi^- + p \rightarrow K^o + \Lambda$$

and it shows a big bump centered at about 1700 MeV. If this characteristic of the associated production by pions is due to a final state interaction, one can reasonably expect something to happen in photoproduction. However, since there are virtual processes contributing to the charged photoproduction which cannot occur in the above reaction, it is conceivable that the resonant features are masked in photoproduction. In any case, two phenomenological resonance models have been proposed to describe the reaction $\gamma + p \rightarrow K^+ + \Lambda$.

The first of these was motivated by an analysis by Kanazawa[18] of the pionic $K^o\Lambda$ production. He noted that the angular distributions of both the cross section and Λ polarizations in the vicinity of the bump are very simple. This suggests that, if a final state resonance causes the bump, it is in a low order angular momentum state and he concluded that either $S_{1/2}$ or $P_{1/2}$ was the most likely candidate. A similar analysis by Hoff[14] has recently been performed with the same conclusion. Kuo[19] and, independently, Deauchamp and Holladay[20] proposed a photoproduction model including the electric Born terms, the magnetic Born term for the proton, the two K^* terms, and a $P_{1/2}$ resonance (see figure 8, diagrams 1,2,3,6,7,8). The model was characterized by six constants, two of which (the position and width of the resonance) were fixed by the $\pi^-p \rightarrow K^o\Lambda$ reaction. The other four

FIGURE 11

COMPARISON OF ASSOCIATED PRODUCTION BY PIONS

WITH THE PHOTOPRODUCTION

The total cross sections for the photoproduction were obtained by integrating linear or quadratic fits in $\cos\theta$ to the data of Anderson, et al.[2], Sadoff, et al.[3], and this thesis. Since the angular distributions are not very complete, the error bars obtained from the statistical analysis may be optimistic. The data for the $\pi^- p \rightarrow K^o \Lambda$ reaction can be found in reference 14.

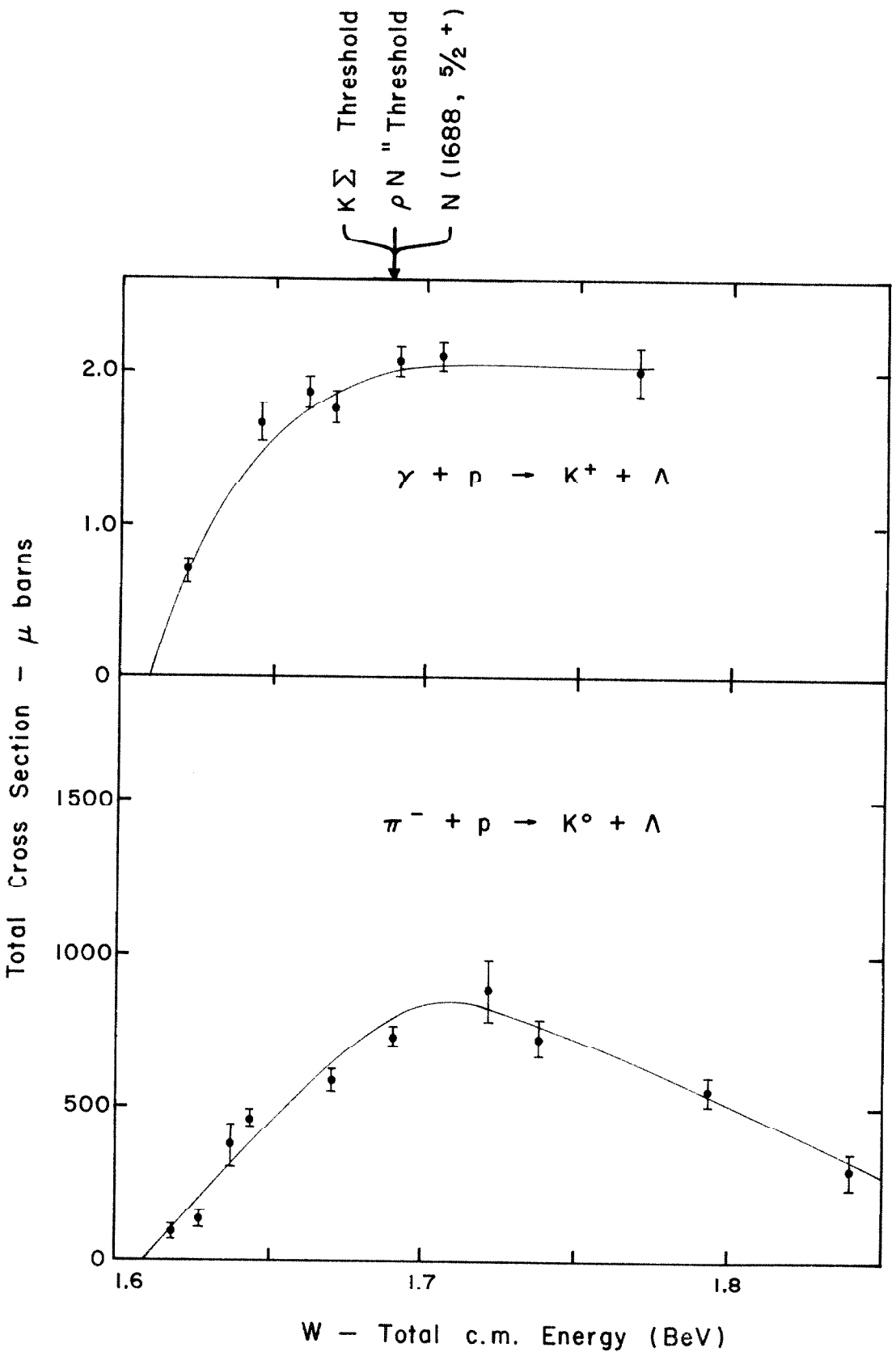
K Σ Threshold
ρ N " Threshold "
N (1688, 5/2 +)
2.0
1.0
0
γ + p → K+ + Λ
1500
π⁻ + p → K° + Λ
1000
500
0
1.6
1.7
1.8
Total Cross Section - μ barns
W — Total c.m. Energy (BeV)

parameters were adjusted to fit the Cornell data of Anderson, et.al.[2] Although the model fits the data used to adjust its parameters quite well, it yields the wrong sign for the Λ polarization[1], and it gives too flat an angular distribution at 1200 MeV. Figure 7(C) shows the comparison.

It has been noted by many people that the bump in the $\pi^- p \rightarrow K^o \Lambda$ total cross section occurs at the mass of the N(1688, $5/2^+$). The simplicity of the cross section angular distributions, however, makes one reluctant to draw the natural inference. Nevertheless, it has been shown by Rimpault[21] that the data allows a large resonant $F_{5/2}$ partial wave if the lower state amplitudes are appropriately adjusted. This fact adds weight to the likelihood that the photoproduction data contain F-waves. Two resonance models based upon all the diagrams in figure 8, with the exception of the $P_{1/2}$ resonance, have been proposed, one by Hatsukade and Schnitzer[22] and the other by Gourdin and Dufour[24]. Hatsukade and Schnitzer[23] have also used the data of Anderson, et.al., to determine their parameters but the author of this thesis has been unable to reproduce their calculated angular distributions using the published parameters. Discussions with the two theorists have not resolved the difficulty, but the discrepancy seems to be purely numerical rather than one of interpretation. Consequently, an independent attempt has been made to find sets of parameters which will make the model of Hatsukade and Schnitzer and/or that of Gourdin and Dufour fit the observations.

Before the discussion of the numerical work, the differences in these two similar resonance models should be indicated. Since the Feynman rules for evaluating the five Born diagrams are well established, the amplitudes arising from these virtual processes are the same in both theories. However, the mode of calculating the other diagrams is evidently

not so well established. Hatsukade and Schnitzer calculated the detailed contribution due to the two K^* diagrams and the two nucleon resonances by the Cini-Fubini approximation[25] of dispersion theory with all subtractions set equal to zero. For the two nucleon resonances, this results in resonant amplitudes in the appropriate angular momentum states ($D_{3/2}$ and $F_{5/2}$) as expected, but there are also contributions from these diagrams in all lower order states of both parities. The situation is analogous to the fact that diagram 2 of figure 8 gives rise to both $S_{1/2}$ and $P_{1/2}$ amplitudes. On the other hand, Gourdin and Dufour simple use a Breit-Wigner resonance formula for the appropriate angular momentum state to describe the effects of the N(1512) and N(1688). With appropriately adjusted subtractions in the Cini-Fubini approximation, of course, agreement can be achieved. It should perhaps be noted here that the Cini-Fubini approximation of the K^* terms (with all subtractions ignored) gives formulas different from those of Kuo. In particular, if one evaluates the kinematic function multiplying the resonant denominator in the K^* invariant amplitudes given by Kuo at the pole (i.e., find the residue at the pole), he obtains the Hatsukade-Schnitzer version. Once again, appropriate subtractions can resolve the discrepancy. At the present state of interpretation of experiments in high energy physics, however, such differences of detail between phenomenological models as outlined in this paragraph are surely not significant; even the gross features of the interpretation remain to be settled. In the numerical work, the K^* formulas of Hatsukade and Schnitzer have been used.

The selection of parameters to optimize the agreement of theory with observations has been made by the method of least squares. However, since the theoretical expressions for the observed cross sections are

quadratic in the parameters, the function to be minimized (χ^2) is quartic in them so that non-linear minimization methods must be employed. In all the numerical work, the "Variable Metric" method of W. C. Davidon[26] has been used. The cross sections given in this thesis and those of Anderson[2] and Sadoff[3] were the input data. Altogether, there are 44 data points ranging in lab photon energy from 954 MeV to 1200 MeV. Older data were not used because they are less precise (thereby increasing computation time with little increase in information) and because some of them are quite inconsistent with the new data. Since it was felt that any theory should predict something, no Λ polarization data were included in making the fits; giving the correct polarization was the burden of the theory only.

The method of carrying out the computation was as follows. The strengths of the resonances and all the magnetic Born terms were first fixed to be zero, and g_Λ and the two K^* couplings varied to obtain a fit. Under these conditions, a value of χ^2 about four times the number of degrees of freedom was obtained. Statistically, this would be considered very poor, but qualitatively the theoretical curves looked reasonably good. The three magnetic Born terms* were then "turned on"; the proton anomalous moment was fixed at 1.79 nucleon magnetons and the Λ moment, μ_Λ, and the

---

* The motivation for treating the magnetic Born terms on a different footing than the electric ones was the difficulty experienced by J.Kilner[9] when these terms were included in an analysis of $\pi^o p$ photoproduction. He found that it was extremely difficult to reconcile the large effect of the pole in the u-channel associated with the nucleon moment with the observed cross sections in the backward direction.

product $g_\Sigma \mu_T$ (diagrams 4 and 5, figure 8) were allowed to vary. In spite of the two added parameters, the resulting fit was actually slightly worse than obtained when the magnetic terms were ignored. Similarly, when the resonance terms were allowed to vary, the fit was not improved significantly nor was any appreciable polarization predicted. This result followed regardless of which version of the effect of the resonances was used, that of Hatsukade and Schnitzer or that of Gourdin and Dufour.

As rather strongly suggested by the total cross sections, there is no current evidence for any resonant behavior in $K^+\Lambda$ photoproduction. On the other hand, the Λ polarization remains unexplained. Since the polarization angular distributions are quite sensitive to resonances, further data of that type may make resonance models more attractive. Although it cannot be considered firm evidence that the exchange of the K^* meson has anything to do with photoproduction, it is noteworthy that whenever K^* terms (both couplings) were included in the analysis as outlined above and other similar ones (of too little intrinsic interest to describe in detail) the fits improved significantly.

VI. CONCLUSIONS

The data presented in this thesis have neither raised nor resolved any questions in elementary particle physics. It appears, however, that the somewhat mysterious enhancement in the total cross section for $\pi^- p \to K^o \Lambda$ near W = 1700 MeV does not happen in photoproduction. For whereas the pionic cross section decreases by about 30% between 1700 and 1770 MeV, the total cross section obtained from the angular distribution given in this thesis is the same, to within the statistics, as at the lower energies. To be sure, the angular distribution was not

measured in the backward direction in this experiment and the total cross section was calculated under the assumption that the best quadratic fit (in cos θ) to the forward hemisphere data gives reasonable behavior in the backward direction. Nevertheless, even if the cross section in the range from 120° to 180° be only half what the fit indicates (see figure 7(C)), the total cross section would be reduced by only 10% of the value obtained here. Furthermore, the detailed analysis of all the photoproduction data gives no hint of any resonance behavior.

The inconclusive Taylor-Moravcsik extrapolation was more disappointing than surprising. It was hoped that this analysis would give good evidence for the negative parity assignment of the K meson. However, if the coupling constant $g_{\Lambda}^{2}/4\pi$ really is of the order of unity, even a convincing determination of the sign of the extrapolated value will be difficult at this energy, as figure 9 indicates.

APPENDIX I

BREMSSTRAHLUNG, TARGET, AND SPECTROMETER

A. The Photon Beam

Bremsstrahlung resulting from monoenergetic electrons in the synchrotron falling upon a 0.2 radiation length thick tantalum target was passed through a lead collimator and three lead scraping walls before hitting the hydrogen target. Early in the experiment, it was learned that the counting rates of several monitored signals (Appendix III) were fairly strongly dependent upon the precision of the beam alignment. Consequently, an effort was made to keep the beam as "clean" as possible by centering it in both angle and position in the primary collimator and maintaining all scraping walls well within the shadow of the collimator. Furthermore, the radiator was moved closer to the center of the synchrotron aperture than its historical position since this greatly reduced the size of the penumbra at the top and bottom of the collimated beam. During this experiment its radius was 146.0". Finally, the position of the radiator was changed with the end-point energy to compensate for the slight changes in the shape of the equilibrium orbit with magnetic field in the synchrotron.

The nominal end-point energy was set and monitored with instruments provided in the synchrotron control system, the beam-energy meter. Since this meter is calibrated under the assumption of a circular equilibrium orbit at 145" while the radiator was at 146", its readings should in principle have been increased by 0.37%. This was not done, however, since not only is the circularity of the orbit open

to question, but also the experiment itself provided information on the end-point energy (see figure 6). In all references to the end-point energy, E_o, the direct reading of the beam energy meter is meant unless stated otherwise.

The canonical representation of the bremsstrahlung spectrum is

$$N(k)\,dk = \frac{W}{E_o}\,B(k,E_o)\,\frac{dk}{k}$$

with $$\int_o^{E_o} B(k,E_o)\,dk = E_o$$

where $N(k)\,dk$ = number of photons in energy interval dk at energy k,

$W = \int N(k)k\,dk$ = total energy in the beam,

E_o = energy of electron producing the radiation.

No independent measurement of the shape function $B(k,E_o)$ was made for this experiment, but rather the curve obtained by Boyden[8] was used to reduce the data. The basic instrument used to measure the total energy in the beam, W, was Wilson's quantameter. However, since the particular quantameter available was not large enough to contain the lateral size of the beam during normal data collection, other monitors were used and special measurements were made to calibrate these against the quantameter.

During the experiment, two such monitors were employed, one, an ion chamber with 1 in. copper walls* located in the beam catcher,

*This chamber was an old-style "Cornell air chamber".

and the other, a well-shielded two scintillator counter telescope* viewing the H_2 target at 90° to the bremsstrahlung beam. This latter was used for those measurements with the lab angle less than about 15° since the magnet yoke intercepted the beam under these conditions. It was calibrated against the ion chamber before and after each such small angle run with a statistical precision of about 0.2% and the exposure monitored by it reduced to the equivalent ion chamber reading. After the completion of this experiment, it was discovered** that the telescope's location with respect to the hydrogen target depended slightly upon the angle to which the spectrometer was set. The relationship between the telescope's counting rate and the spectrometer's angle was determined from data taken during this experiment. The largest correction resulting from this effect was 1.3% for the 15° c.m. point.

An intercomparison of the beam catcher ion chamber with the quantameter was made several times during the experiment. Table IV gives the results of these measurements and compares them with previous calibrations of the same chamber. The quantity (RS) is defined as

$$(RS) = \frac{\dfrac{\text{reference monitor}}{\text{ion chamber}}}{\dfrac{\text{reference monitor}}{\text{quantameter}}} \qquad \frac{(P/T)\ \text{ion chamber}}{(P/T)\ \text{quantameter}}$$

---

* The use of such a monitor was recommended by Professor Walker; it was built and adjusted by S. Ecklund.

** The author is indebted to Professor Walker for noticing this unsuspected peculiarity of the apparatus.

TABLE IV

CALIBRATION CONSTANTS OF THE ION CHAMBER

A beam intensity of 1.0 is taken as typical for this experiment, i.e., 3-4 x 10^{10} electrons per pulse in the synchrotron spilled out smoothly for about 80 msec. The air chamber reference monitor was placed immediately after the primary collimator; it could only be used with beam intensities on the order of 0.1 since it saturated rapidly with increasing intensity. The telescope refers to that viewing the H_2 target as discussed in the text. The data of 1961 was obtained from reference 27.

Date	11 Oct. 1961			26 May 1963		6 Aug. 1963		13 Aug. 1963	27 Sept. 1963
Beam Intensity	0.1			0.1		1.0		1.0	1.0
Reference Monitor	Air Ch.			Air Ch.		Tel.		Tel.	Tel.
E_o(MeV)	1000	1130	1280	1000	1130	1130	1280	1280	1280
RS	1.070	1.114	1.160	1.086	1.139	1.143	1.186	1.182	1.170

where P is gas pressure in the chamber measured in mm Hg and T is the absolute temperature of the gas. The calibration[27] of the ion chamber is then

$$U = 13.10 \times 10^{18} \frac{(RS)}{(P/T)_{\text{ion chamber}}} \quad \text{MeV/coul.}$$

One sees that the calibration constant of the chamber is about 1.7% higher than it was during Phase II operations of the synchrotron; the reason for this change is not known. The average value of the several new measurements was used in the data reduction.

The total energy in the beam, W, is simply UQ, where Q is the total charge deposited in the chamber. This was measured by a standard laboratory integrator, which generated an electrical signal, a Beam Integrator Pulse (BIP hereafter), after accumulating a charge M. The integrator was calibrated several times during the experiment and Table V gives the results. Since this measurement could be made with high accuracy, the 0.5% fluctuation in M was taken as real and included in the data reduction.

Finally, the ion chamber was open to the atmosphere so that its gas density fluctuated with the weather. During the first half of the experiment, records of pressure and temperature were not maintained; the data from the latter half, however, were properly corrected for the fluctuating atmosphere. The average gas density observed during the latter half of the experiment was used in reducing the earlier data and the r.m.s. fluctuation of the density (0.44%) was included in the uncertainty of these measurements.

TABLE V

CALIBRATION OF THE ION CURRENT INTEGRATOR

The calibration is for instrument No. 0249 on Scale 4.

Date (1963)	M (μCoul/BIP)
May 8	2.274
Jun 2	2.277
Jun 9	2.273
Jun 20	2.268
Aug 3	2.261
Aug 14	2.263

B. The Hydrogen Target

The liquid H_2 target used in this experiment has been described in detail in earlier theses[28] from the Synchrotron Laboratory. Since no changes were made in it, reference to earlier work will suffice. In spite of the long succession of successful experiments performed with it, the H_2 target proved to be the Achilles' heel of this one. The uncertainty in the empty target background resulting from condensation of matter on the target structure has been mentioned in the text and is discussed more fully in Appendix IV.

C. Scintillation Counter Sizes, Locations, and Uses

Similarly, the spectrometer used in this experiment was essentially the same as described several times in the past[8,9,28]. However, its complement of scintillation counters was different. Due to the increased photon beam intensity relative to that attainable in the past, the solid angle subtended by the detector was defined by a scintillator, A1, placed near the exit of the magnetic field in contrast to the earlier practice of using a front scintillator to define the extent of the solid angle in one direction (vertical) and the rear Fan counters (see below) to limit it in the other direction. The main reason for using this configuration was the excellent shielding afforded by the magnetic field and the iron yoke. This counter was constructed in such a way that the scintillator proper was easily removable so that different sizes could be used.

In addition to A1, a second "aperture" counter, A2, located immediately after A1, was always used. In preliminary running, it was found that, with the scintillation plastic removed from A1, the system still had a very small response to minimum ionizing particles. It was inferred that these triggered A1 by Cherenkov light in its Lucite light pipe. Although this would be a negligible effect for all but the most precise pion experiments, it was feared that these objects could be mistaken for K mesons and so contribute to the contamination. Consequently, a counter fully covering A1's scintillator but not its light pipe was required in the detection logic. The effectiveness of A2 in reducing contamination was clearly demonstrated in a few runs in which it was not used. Since one pays for the help this counter provides in added complexity, increased multiple scattering and nuclear absorption, as well as an increased likelihood for making errors, a preferable solution would have been the replacement of the A1 Lucite light pipe with air.

On the pole pieces of the magnet, eight long thin scintillators were mounted and their signals used in anticoincidence. These counters, referred to as the "Fans", were designed to detect and so eliminate particles which can scatter from the pole pieces. They were originally used by Brody[29] and have been described by him.

In the vicinity of the focus of the magnet spectrometer, a three-scintillator telescope was used, S1, S2, and S3. The momentum aperture proper was geometrically established by S2 which was located at the conjugate point of the hydrogen target. The scintillator S1 was

used to provide a signal to drive one side of all fast coincidence circuits while S3 was required to ensure the passage of particles through the Lucite Cherenkov counter (see Appendix II) as well as to reduce the rate of accidental counts in the telescope. In order to provide improved momentum resolution, the momentum aperture S2 was broken into four pieces as shown in figure 12. This splitting of the momentum aperture proved especially useful in providing instrumental checks.

In Table VI constructional details of scintillation counters are tabulated, while figure 2 in the main text indicates their locations in the spectrometer.

D. Spectrometer Momentum Calibration and Acceptance

The magnetic field vs. central momentum relation for the spectrometer was originally obtained by Donoho[30] with the stretched wire method, later remeasured by Dixon[31] with the same method, and compared with the synchrotron end-point calibration several times.[8,9,28] Since there are deviations of several percent in the various results, a third method* was employed prior to performing the experiment reported in this thesis; it consisted of a "brute force" measurement of the fringing field. The procedure used in the measurements and the method of analysis

*The technique was recommended by Professor Walker, the measurements made by S. Ecklund, E. Adelberger, and the author, and their analysis performed by the author.

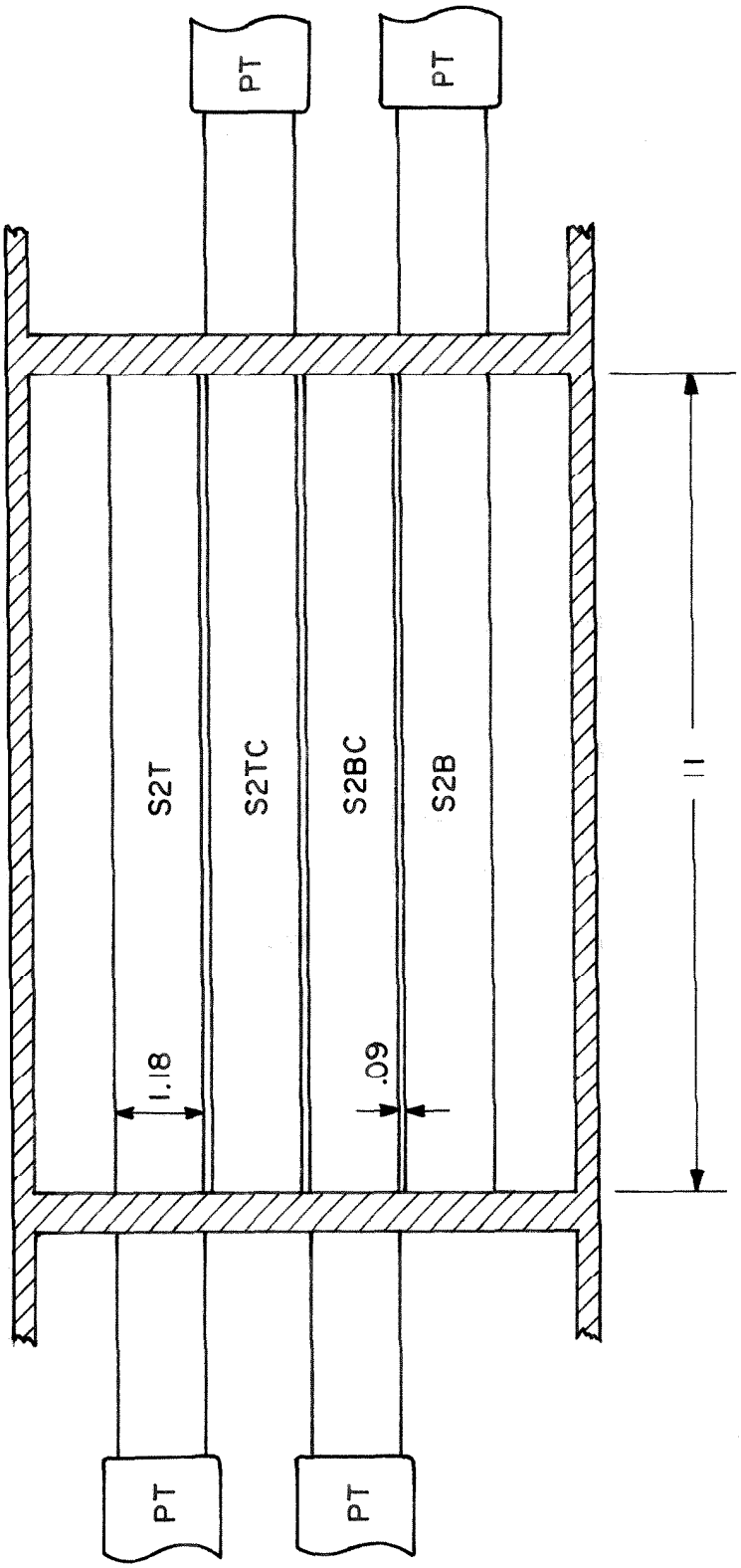

FIGURE 12

THE CONSTRUCTION OF S2

TABLE VI

THE SCINTILLATION COUNTERS

Counter	Dimensions	Material	Phototube Type
A1-12	12" x 2.91" x 0.25"	Pilot B	6810-A
A1-6	6" x 2.91" x 0.25"	Pilot B	6810-A
A2	18" x 4.00" x 0.25"		56AVP
S1	11" x 6.50" x 0.375"	NE-102	2 - 56AVP
S2T, TC, BC, B	11" x 1.18" x 0.25"	Pilot B	1 - 6810-A each
S3	11" x 6.50" x 0.375"	NE-102	6810-A
Fans	25" - 32" x 0.75" x 0.50"		2 - 6810-A

is described in section E of this Appendix. Although this technique has the virtue that the properties of any set of apertures can be calculated from knowledge of the fields, its use is restricted to a small number of central momentum values by its exhaustive nature. Thus, measurements were made at only two momenta, one near the values used in this experiment (~ 800 MeV/c) and the other near saturation of the magnet pole tips (~ 1150 MeV/c). In Table VII(A), the calculated central momenta from the field measurements is compared with the results given by Donoho and Dixon.

Unfortunately, the agreement between the new determinations and Dixon's values are not so good as anticipated. Thus, with two calibrations available, a hard choice between them had to be made. Because of the following considerations, Dixon's calibration was consistently used through the experiment:

a) An estimate of the uncertainty in the field measurement calibration had not been made at the time of the experiment nor were there enough data points to infer the precision from internal consistency.

b) Previous experiments in which Dixon's prescription was used have yielded excitation curves in better agreement with the synchrotron end point calibration than would have been obtained if the field measurements' result had been used.

Somewhat arbitrarily, the central momentum is taken as known to $\pm$ 1%.

The acceptance of the magnet consists of two almost independent factors, the solid angle, $\Delta\Omega$, and the momentum window, $\Delta P/P_o$. The first

TABLE VII

(A) COMPARISON OF SPECTROMETER MOMENTUM CALIBRATIONS

B_o is the uniform field as measured with a proton resonance magnetometer; P_o is the momentum defined by an orbit connecting the center of the hydrogen target with the center of S2 and, at the target, coinciding with the intersection of a horizontal plane and the magnet symmetry plane.

(B) CALCULATED MOMENTUM APERTURES

The apertures are calculated for the S2 scintillator sizes given in Table VI. It is to be noted that the momentum windows, $\Delta P/P_o$, are referred to the magnet central momentum, P_o. The very weak dependence of the spectrometer momentum aperture on the target illumination is illustrated in this table.

(A) Central Momentum vs. Magnetic Field

B_o (kG)	P_o (MeV/c)		
	Donoho	Dixon	This Measurement
10.0	802	768	784.5
15.0	1178	1146	1150.3

(B) Momentum Windows Defined by S2

Counter		$\Delta P/P_o$	
		Uniform Target Illumination	Point Target
	S2T	.0253	.0250
	S2TC	.0241	.0238
	S2BC	.0229	.0227
	S2B	.0218	.0216
Full	S2	.0941	.0931

of these was determined almost entirely by A1. However, the size of the beam at S3 in the non-dispersive direction was slightly larger than that counter. The exact solid angle reduction due to this fact depends upon the details of target illumination, but it has been estimated to be less than 0.6%. The solid angle defined by A1 has been calculated to be 0.00176 sr by use of linear magnet theory (i.e., the effects of the fringing fields are replaced by effective sharp edges and the deviations of orbits from the reference central orbit are calculated to first order only). The calculation is estimated to have a precision of $\pm$ 1%. The solid angle was checked by setting up a small counter in front of the magnet outside the influence of the magnetic field and measuring its efficiency. To ensure that the effective target size was not reduced by the two angular apertures during this test, the small counter's dimensions were chosen to be 3/4" $\times$ 6" and its distance from the target was 91.5"; the solid angle so defined was known to $\pm$ 0.5%. The result of the test was

$$\Delta\Omega = 1.74 \pm 0.03 \times 10^{-3} \text{ sr} \quad ,$$

which is in good agreement with the calculation. Accordingly, the solid angle as calculated has been used in the data reduction and an uncertainty of $\pm$ 1% assigned to it.

The momentum window, $\Delta P/P_o$, has been calculated from the detailed knowledge of the fringing fields of the magnet at 10 kG. Table VII(B) gives the acceptance for each of the four segments of S2 as calculated assuming a uniform 2" vertical illumination of the target.

This simple illumination function hardly describes the actual conditions but the overall acceptance is a very weak function of this assumption as is illustrated in the table. The overall acceptance of 0.0941 agrees quite well with the value, 0.0948, calculated by linear magnet theory which in turn is in good agreement with the stretched wire measurements. Most of the data in this experiment was actually taken using only three segments of S2 with S2BC centered on the momentum aperture. The corresponding sensitivities were obtained by interpolation in Table VII (B). Incidentally, this table also shows the high precision of the assumption that $\Delta P/P_o$ is linear in the size of the counter for small counters centered on the momentum aperture. The uncertainty in $\Delta P/P_o$ has been taken to be $\pm$ 1.5%.

E. Magnetic Field Measurements and Their Analysis

The fringing field measurements upon which were based the calculation of the central momentum and momentum aperture of the spectrometer were made with a Hall effect gaussmeter.* With the nuclear resonance magnetometer, the uniform field was precisely set to a value B', and, with the Hall probe in this field and normal to it, the gaussmeter was adjusted to read zero. Thus, at a point in space where the component of the magnetic field normal to the probe was B', the gaussmeter would again read zero. The uniform field was then set to $B > B'$ and a plot was made of the locus of points at which the field

*D-855 Gaussmeter, Dyna-Empire, Inc., Garden City, New York. The Hall probe element had a diameter of $\lesssim$ 1 mm.

was B'. The probe was maintained parallel to and at a fixed distance from the magnet symmetry plane, S. Thus, the data consists of a contour map of the field component normal to S in a plane parallel to S. Such measurements were made at two values of B, 10 and 15 kG, on the symmetry plane and 1" from it.

The restricted nature of the data does not allow us to calculate precisely the solid angle of the spectrometer since it is primarily determined by other field components. However, it does allow a good calculation of the position of the effective edges of the field from which an excellent approximation to the solid angle can be obtained by linear spectrometer theory.

The momentum dispersion properties of the spectrometer are also readily obtained to a good approximation from knowledge of the effective edges. However, the data are of such a nature that precise orbits can be calculated for particles lying in the symmetry plane and the effective edge approximation dispensed with. A digital computer program for the IBM 7090 was written to calculate this plane motion from the field measurements. The magnetic field was modeled as being everywhere normal to the plane of motion and to consist of three regions: a central uniform field region connected smoothly to two fringing field regions. Outside these regions, the field is taken to be zero. For given initial conditions, the orbit, $y(x)$, of a particle in an inhomogenous magnetic field satisfies a well-known differential equation. However, for computational convenience, the differential equation has been reduced to the following integral equation:

$$y(x) = \int_0^x dx \; \frac{\frac{1}{R_o} \int_0^x b(x, y(x))\, dx}{\left[1 - \left(\frac{1}{R_o} \int_0^x b(x, y(x))\, dx\right)^2\right]^{1/2}}$$

where $b(x,y) = \frac{1}{B_o} B(x,y)$,

$B(x,y)$ = value of field at the point (x,y) ,

R_o = radius of curvature of the motion in a uniform field of magnitude B_o .

The initial conditions assumed in this solution are that the orbit passes through the origin ($x = y = 0$) with zero slope ($y'(0) = 0$). The equation was solved by successive approximations, the process terminating when the last point on the orbit and its slope there had stabilized to within preset tolerances.

The program had several modes of operation, but only two tasks of which it was capable need be considered here:

1. Find the momentum which a particle must have to pass through two given points, one in each field-free region, with a specified direction at one of them. This is the boundary condition problem which was solved to find the central momenta given in Table VII.
2. For rays originating at a given point in a field-free region, find the two-dimensional bundle in direction and momentum accepted by a given aperture system.

The solution of the second problem leads to the momentum aperture of the spectrometer. In figure 13 is shown the two-dimensional acceptance regions of the four S2 segments and the 12" A1 counter for particles originating at the center of the H_2 target. For a source point vertically displaced from the target center, the acceptance regions are displaced in the momentum-angle plane. In fact, when one considers the continuum of source points, the acceptance is a three-dimensional region in a source point-momentum-angle space. By weighting each source point by the photon beam intensity at it and projecting the solid onto the momentum axis, one obtains the momentum resolution function of the aperture system. Furthermore, the area under this function is proportional to the momentum acceptance, $\Delta P/P_o$.

The calculations outlined above leading to the momentum resolution function and acceptance, $\Delta P/P_o$, for the 10 kG data have been carried out by D. Aitken using the momentum-angle acceptance regions for five points in the hydrogen target, on the center and 1" and 1/2" above and below it. The photon beam was weighted equally at all the points. The momentum resolution functions for the four S2 counters are given in figure 14.

This brief account of the results of the field measurements on the spectrometer will be supplemented in detail at a future date in a separate Synchrotron Laboratory report.

FIGURE 13

PHASE SPACE REGIONS ACCEPTED BY S2

The vertical axis is $q = \frac{P - P_o}{P_o}$, where P_o is the momentum of the central ray through the magnet. The horizontal axis is β, the angle in the magnet symmetry plane which a ray makes with the central ray. These regions have been calculated for particles originating at the center of the H_2 target. The angular aperture was taken to be 12" at A1.

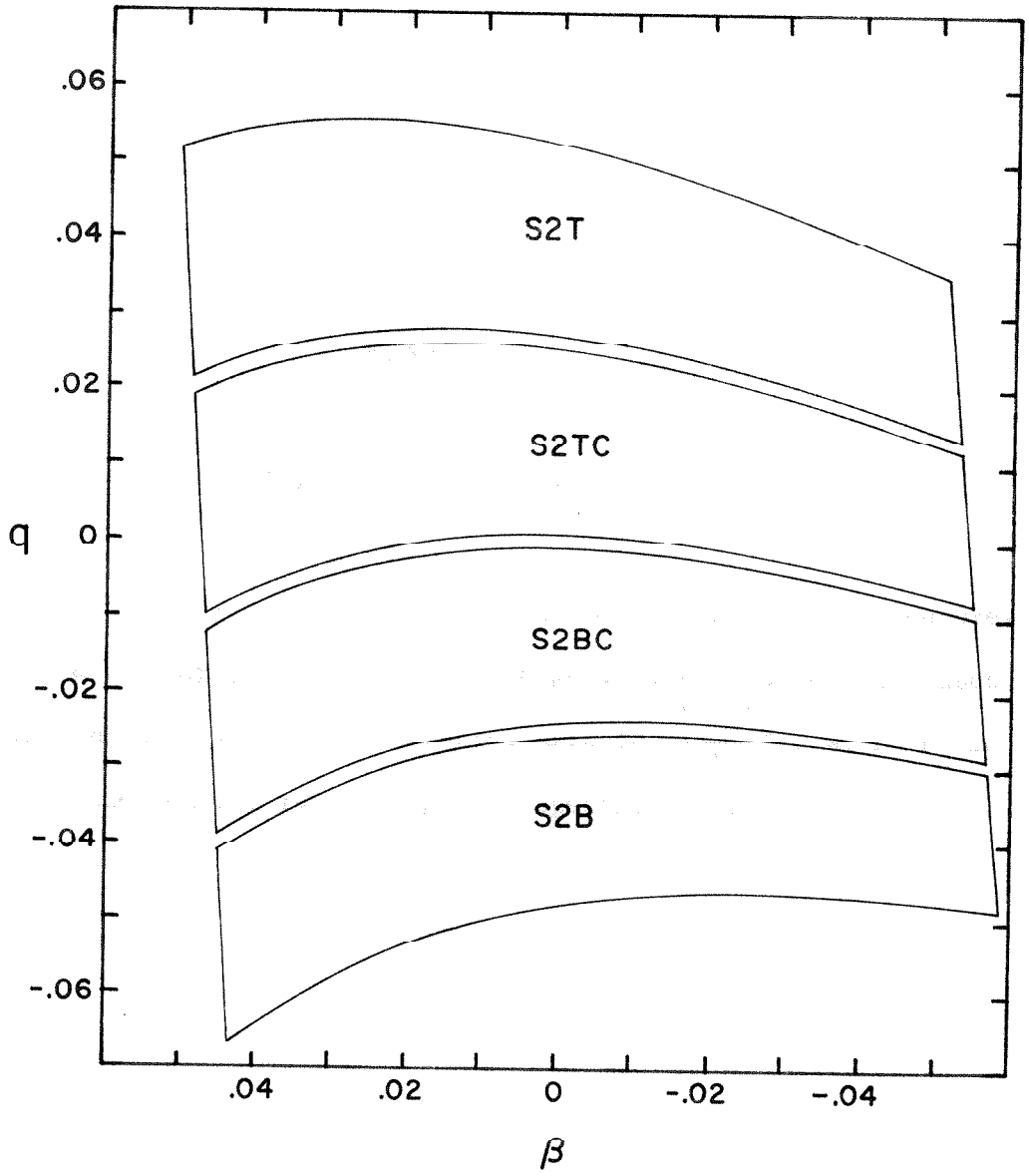
.06
.04
.02
q 0
-.02
-.04
-.06
S2T
S2TC
S2BC
S2B
.04
.02
0
-.02
-.04
β

FIGURE 14

MOMENTUM RESOLUTIONS

These functions have been calculated from the fringing field measurements for a uniformly illuminated 2" target. The S2 dimensions used are given in Table VI. The horizontal axis is $\frac{P - P_o}{P_o}$, where P_o is defined by the central ray through the spectrometer.

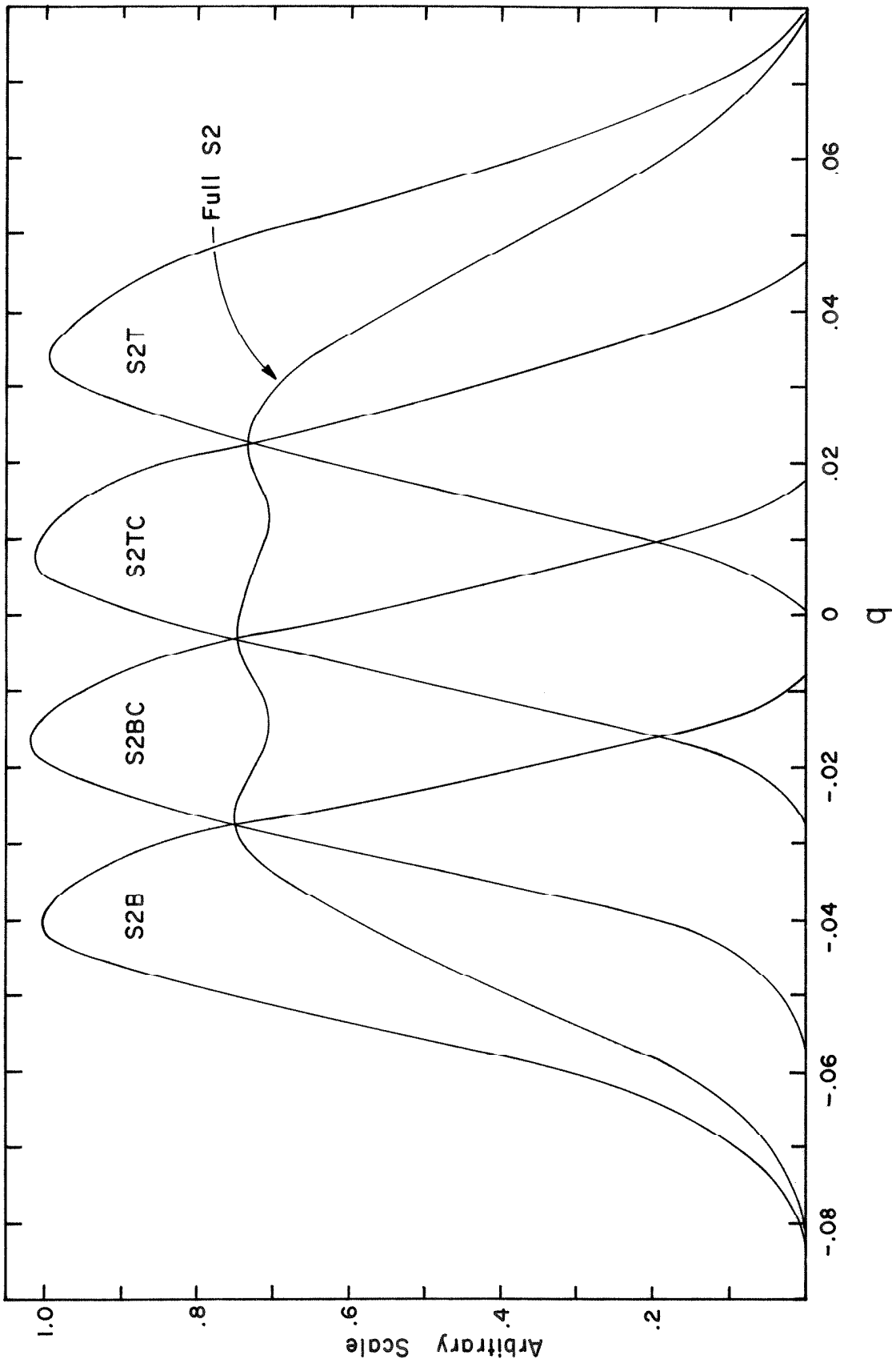
S2B
S2BC
S2TC
S2T
Full S2
Arbitrary Scale
1.0
.8
.6
.4
.2
-.08
-.06
-.04
-.02
0
.02
.04
.06
q

APPENDIX II

CHERENKOV COUNTERS

In this experiment, crucial emphasis was laid on the celebrated Cherenkov effect; almost the entire velocity selection depended upon it. This phenomenon has been extensively studied both theoretically and experimentally[33] and is well understood. For our purposes, only the gross features of the effect were important, viz., the relation between velocity, β, cone angle, θ, and refractive index, n,

$$\cos \theta = \frac{1}{n\beta}$$

and the frequency spectrum of the radiation

$$N(\nu)\, d\nu = \left(\frac{e^2}{\hbar c}\right) \frac{1}{c} \sin^2\theta \, d\nu$$

where $N(\nu)\, d\nu$ is the number of emitted photons per unit length in the frequency interval ν to $\nu + d\nu$. The characteristic polarization of the radiation is favorable for the performance of the two Cherenkov counters but was unimportant. By far the strongest velocity dependence of the effect is in the cone angle, θ, and both instruments capitalized on it. Due to the relatively low efficiency of photocathodes, the average number of photoelectrons produced by the passage of a singly charged particle through the counters was not large enough to allow effective pulse height discrimination. In particular, for a typical photocathode efficiency of 10% and an extended S-11 spectral response, the average number of photoelectrons that can be produced by the light in the full

Cherenkov cone is $75 \sin^2\theta$ per cm. This must, of course, be corrected for geometric light collection efficiency, reflection efficiencies, and attenuation in the material to obtain the actual expected number of photoelectrons for a given instrument. Typically, a few tens of photoelectrons are observed from Cherenkov counters designed to detect a single charged particle, and the instruments described here were no exception.

A. The Focusing Cherenkov Counter

1. Geometry and Expected Characteristics

The focusing Cherenkov counter used in this experiment was conceived and designed by Professor Robert Walker. It is generally similar to an instrument described by Huq and Hutchinson[10], but is unique in the surprisingly large region of particle phase space for which it has a large detection efficiency. The general operational principle is described in the main text and reference can be made there for its geometric construction (figure 3). Of particular note are the following constructional details:

a) The radiator was easily changeable to accommodate different velocities.

b) The mirror was a simple aluminized dish blown from 1/4" Lucite. Its figure was only approximately spherical.

c) The light pipes connecting the aperture in the focal plane to the ten phototubes were hollow aluminized glass transition pieces. Not only did the absence of any material other than

air in the light path avoid attenuation, but also it greatly reduced the sensitivity of the counter to the general background particle flux in the laboratory.

d) The entire structure was built of light weight materials to avoid particle scattering. Special attention was given to the region within the swath of particles swept up and down by the magnet.

If one assumes the mirror to be spherical but ignores aberrations, then it is easy to see (figure 15) that the relation between the mirror radius, R, the angle, Φ, which a bundle of light rays makes with the symmetry axis of the counter, and the distance, d, from the symmetry axis to the focus is

$$d = R \sin \frac{\Phi}{2}$$

Furthermore, in the same approximation, the distance, f, from the mirror center to the focus is given by

$$f = \frac{1}{2} R \cos \frac{\Phi}{2}$$

Of course, these relations are somewhat crude, but in general design they are useful for their representation of the light optics. In detailed design, ray tracings are indispensable. For the configuration shown in figure 3 of the main text, d = 10" and R = 30" so that one obtains $\Phi \cong 39^{\circ}$ and $f \cong 11.5$".

If one considers a particle with trajectory parallel to the counter's axis, then he obtains for the angle Φ of the Cherenkov light in air

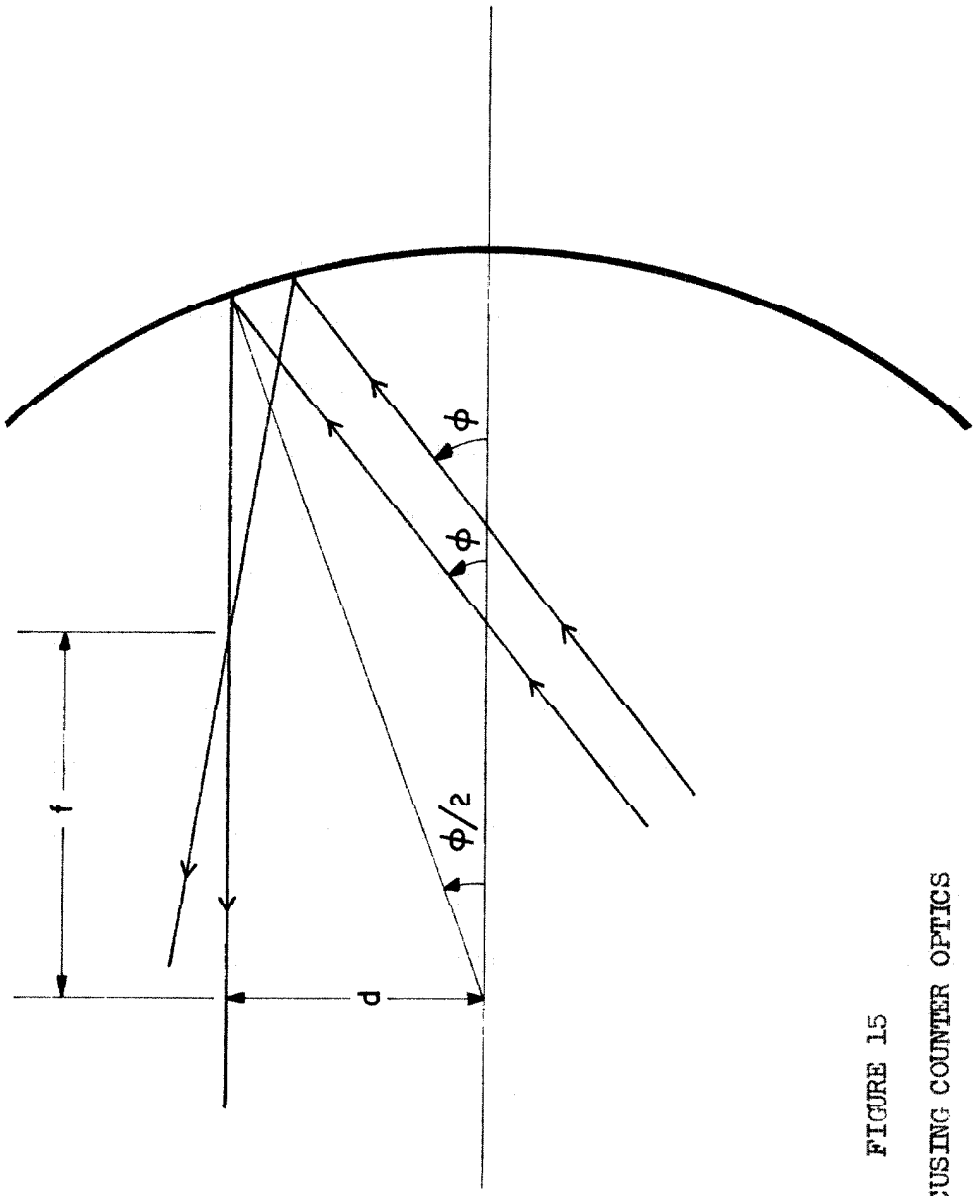

FIGURE 15

THE FOCUSING COUNTER OPTICS

$$\sin^2\Phi = n^2 - 1 - \left(\frac{m}{p}\right)^2$$

where m and p are the mass and momentum of the particle. For a 700 MeV/c K meson, for example, one finds that an index of 1.38 is required if $\Phi = 39^\circ$. Needless to say, the counter was designed so that the refractive indices needed for the momentum range of interest were near to, but greater than, that of water. The index was adjusted by using mixtures of water and glycerine; the tabulation of index vs. concentration from the International Critical Tables was used.

These three simple equations describe the optical characteristics of the counter for the Cherenkov light from particles passing through the counter parallel to its symmetry axis and with a given momentum. Of equal importance are its characteristics for trajectories displaced in position, angle, and momentum from the ideal. To within the approximation of the above equations, positional displacements of trajectories from the axis have no effect. Of course, the radiator and mirror sizes must be large enough to accommodate the beam size. Small angular displacements are more serious since they move the position of the ring of light in the focal plane. The displacement Δd resulting from an angular displacement of $\Delta\theta$ in a particle trajectory is

$$\frac{1}{2} R\left(\cos \frac{1}{2}\Phi\right) \frac{\sqrt{n^2 - \sin^2\Phi}}{\cos\Phi} \Delta\theta$$

With the above geometry and an index of 1.5, one obtains $\Delta d = 24.8'' \Delta\theta$. For the normal running conditions, the particle beam at the focusing counter was defined to about $\pm$ 0.1 radian which results in $\pm$ 2-1/2" of

required aperture in the focal plane. On top of this one must add a width δd resulting from the momentum spread of the beam, Δp;

$$\delta d = R \frac{\cos \frac{1}{2}\Phi}{\sin 2\Phi} (n^2 - 1 - \sin^2\Phi) \left(\frac{\Delta p}{p}\right) \quad .$$

For an index of 1.5 and a geometry as above, this yields $(25" \frac{\Delta p}{p})$, or for a dispersion of $\pm$ 0.05, δd = 1-1/4". Thus, this set of parameters implies a required aperture of 7.5" in the focal plane if no light is to be lost when the particle velocity corresponds to an index of 1.5 (the largest index used). On the other hand, the size of the aperture puts an upper limit on the velocities for which good separation can be achieved between pions and K mesons. At a momentum of 800 MeV/c (which implies $n = 1.33$ to center the K meson Cherenkov light on the aperture), we have

$$d_K = 10" \pm 2.7"$$

$$d_\pi = 15" \pm 2.7"$$

Clearly, then, with an aperture as large as indicated above, the counter would display an intolerable sensitivity to pions at this momentum. In order to maintain a good separation at the highest energies, an aperture of only 4" was used. Actually, the above simple analysis yields somewhat pessimistic aperture requirements; ray traces indicate that a 4" aperture is not as restrictive as implied above. Nevertheless, the counter's behavior deteriorated rapidly at the lower momenta.

In this experiment, two mirrors were actually used in the focusing counter. Measurements with protons (with glycerine as a radiator) were made to determine that the actual angle to which the counter was sensitive was 37°. Because of this, the angular distribution at 1200 MeV could only be carried to 35° c.m. unless we were willing to use radiators with indices less than that of water. Fluorochemicals (FC-75 and FC-43, for example) display the appropriate indices but are prohibitively expensive (and volatile). Another alternative, changing the mirror radius, seemed preferable and, accordingly, a 25.5" mirror was installed in the counter. With this mirror, we determined the central angle to be 46°. The general behavior of the counter, other than the refractive index required for a given momentum, was not much affected by this change.

Since it is the angle of the Cherenkov light <u>in air</u>, which is invariant for a given geometry, the amount of light produced varies inversely as the square of the refractive index. With the original mirror and an index of 1.33, the total number of useful photons in the full cone is 1550. Only 67% of the full cone was used and detailed optical measurements[34] made by Frank Wolverton yielded a light collection efficiency for this fraction of 73%. Hence, the expected number of photoelectrons for a 10% cathode efficiency was 75 when water was used as a radiator.

2. Operating Adjustments

Because of the special importance of this counter in the experiment, care was taken in the selection of the ten 6810A phototubes used in it. Measurements of the relative photocathode efficiencies and gains were made on about twenty available tubes. The very fast spark from a mercury relay was used as the light source in these measurements. The set of tubes with the highest cathode efficiencies and roughly comparable gains were picked for the focusing counter. No noise criteria were set in the selection since the general room background of particles at an electron synchrotron far exceeds typical phototube noise.

It is clear that optimum performance of a counter using several phototubes viewing a common source can only be achieved when all the phototube gains are equal. It was originally intended that the tube characteristics measured with the light pulser would be used to equalize the tube gains. This proved not to be feasible and the gains were adjusted after the completed counter was installed in the spectrometer. A thin piece of scintillation plastic was used in place of the Cherenkov radiator in order to obtain a reasonable signal from each phototube. The gain equalization was then perfectly straightforward. Incidentally, with a scintillator in place of the radiator, the counter missed only 0.04% of the particles (protons were used) defined by the rest of the system.

The refractive index vs. velocity relation for the counter was calibrated using high momentum protons and a glycerine (or Lucite) radiator. Figure 4 in the main text shows the efficiency vs. momentum from such a calibration. Ideally, one would like to verify, with a

copious particle source, that the index chosen for each K velocity used was indeed correct. Furthermore, this would allow a direct measurement of the efficiency of the counter for that velocity. Unfortunately, the highest momentum which the spectrometer was capable of analysing was inadequate to allow direct measurements with protons except for the highest indices used. Pions are useless for this task since in the velocity range of interest they lose a large fraction of their energy in penetrating the 10 cm thick radiator. Accordingly, the calculated index was used and the K meson pulse height distributions in the focusing counter for the three (or four) momentum intervals within the full aperture were recorded. There was never any suggestion that the calculated indices were incorrect.

3. Calculated Performance

As just mentioned, it was not possible to directly measure the efficiency of the focusing counter at each of the several K velocities and bias settings used. For the data reduction, however, it is necessary to know what fraction of the mesons have been lost because of biasing the signal. From the observed pulse height distributions in the focusing counter, the region of biases consistent with a high efficiency was always qualitatively evident. A guess of the efficiency at each configuration would very likely have been adequate, but aesthetically displeasing. The realization that all of the physics involved in a Cherenkov counter is known raised the tantalizing prospect of simply calculating the expected distributions. The author fell victim to the temptation and prepared a program for the IBM-7090 to do it.

The mathematical modelling of the counter is perfectly straightforward. Flat surfaces were taken to be planes, the mirror was assumed perfectly spherical, and the shape of the light pipes was approximated in a fairly realistic but simple manner. A set of several hundred particle trajectories through the spectrometer was selected at random. For each, the amount of light impinging on the ten phototubes was estimated by following about 200 rays through the optics. The actual number of photons getting to the phototubes was corrected to the number effective for producing photoelectrons by taking into account the different relative efficiencies of the tubes used and the radial dependence of photocathode sensitivity. This latter was determined by Frank Wolverton[34] and his curve was used. In figure 16 several such distributions of the average number of effective photons are given. To convert these distributions into observable pulse height spectra, one must scale the number of photons by the average photocathode efficiency and fold the resulting distribution of averages into the Poisson distribution.

In order to compare the predictions with observations, two parameters must be determined, the actual photocathode efficiency and the scale factor relating number of photoelectrons in the counter to channel number in the analyser. Also there was some nonlinearity in the electronics which processed the signal from the focusing counter before it was analysed. The electronic nonlinearity was simply measured and incorporated into the calculation. The other two parameters are less amenable to direct observation. Accordingly, the values were chosen

FIGURE 16

CALCULATED ILLUMINATION FUNCTIONS

FOR THE FOCUSING CHERENKOV COUNTER

These calculations were made for the spectrometer aperture system and radiator refractive index actually used in the experiment. Reference can be made to Table X to determine these.

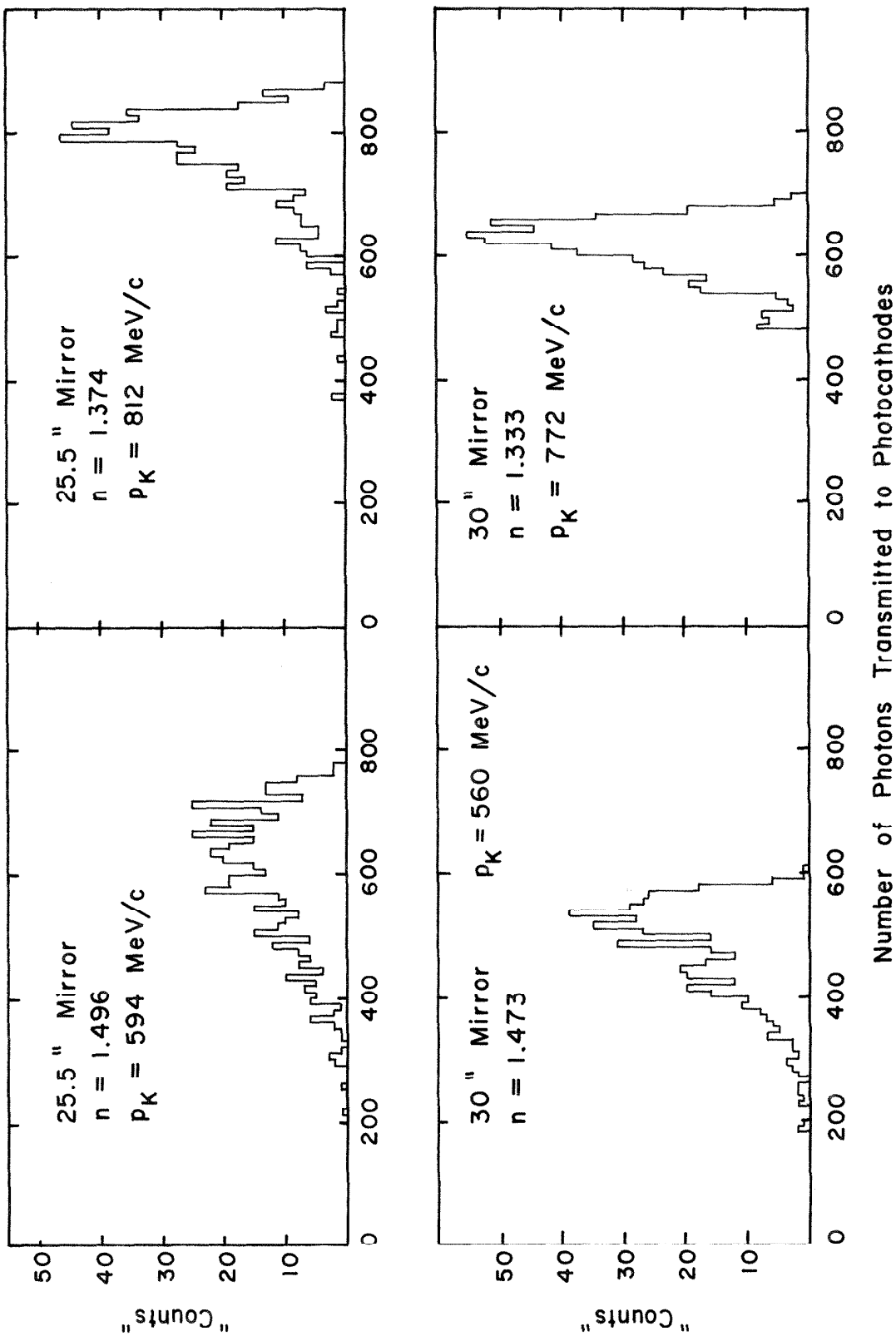
25.5" Mirror
n = 1.496
p_K = 594 MeV/c
25.5" Mirror
n = 1.374
p_K = 812 MeV/c
30" Mirror
n = 1.473
p_K = 560 MeV/c
30" Mirror
n = 1.333
p_K = 772 MeV/c
"Counts"
Number of Photons Transmitted to Photocathodes

statistically by the maximum likelihood method to optimize the agreement between calculation and observation. The excellent experimental distributions obtained with protons were used for this calibration and the two numbers so obtained were incorporated into the calculation of the expected K meson distributions. In figure 17, the comparison between the calculations and observations is presented. In view of the fact that the calculations of the K meson distributions contain no free parameters, the agreement is surprisingly good.

The adjustment of the photocathode efficiency to that which optimizes the fit yielded a value of 0.088. It would be dangerous, however, to assume that this constitutes a measurement of an absolute photocathode efficiency. The difficulty is that this number is the only freedom in the calculation to adjust the calculated width of the distribution to the observed. In fact, there are broadening effects which were not included in the calculation, the most important being the slight gain inequalities between the ten phototubes. The burden of compensating for the approximate nature of all the assumptions in the calculation was carried by this one parameter so that it is smaller than the actual tube efficiency. That it was found to be so near the canonical 10% was encouraging.

On the other hand, Frank Wolverton's measurements indicated that an average of 75 photoelectrons was to be expected if the cathode efficiency were 10% and water were used as a radiator. The computed number for the same assumptions was only 61. The origin of this 20% discrepancy is not known.

FIGURE 17

COMPARISON OF CALCULATED AND OBSERVED DISTRIBUTIONS IN THE FOCUSING COUNTER

The histograms and points were observed experimentally and the smooth curves were calculated.

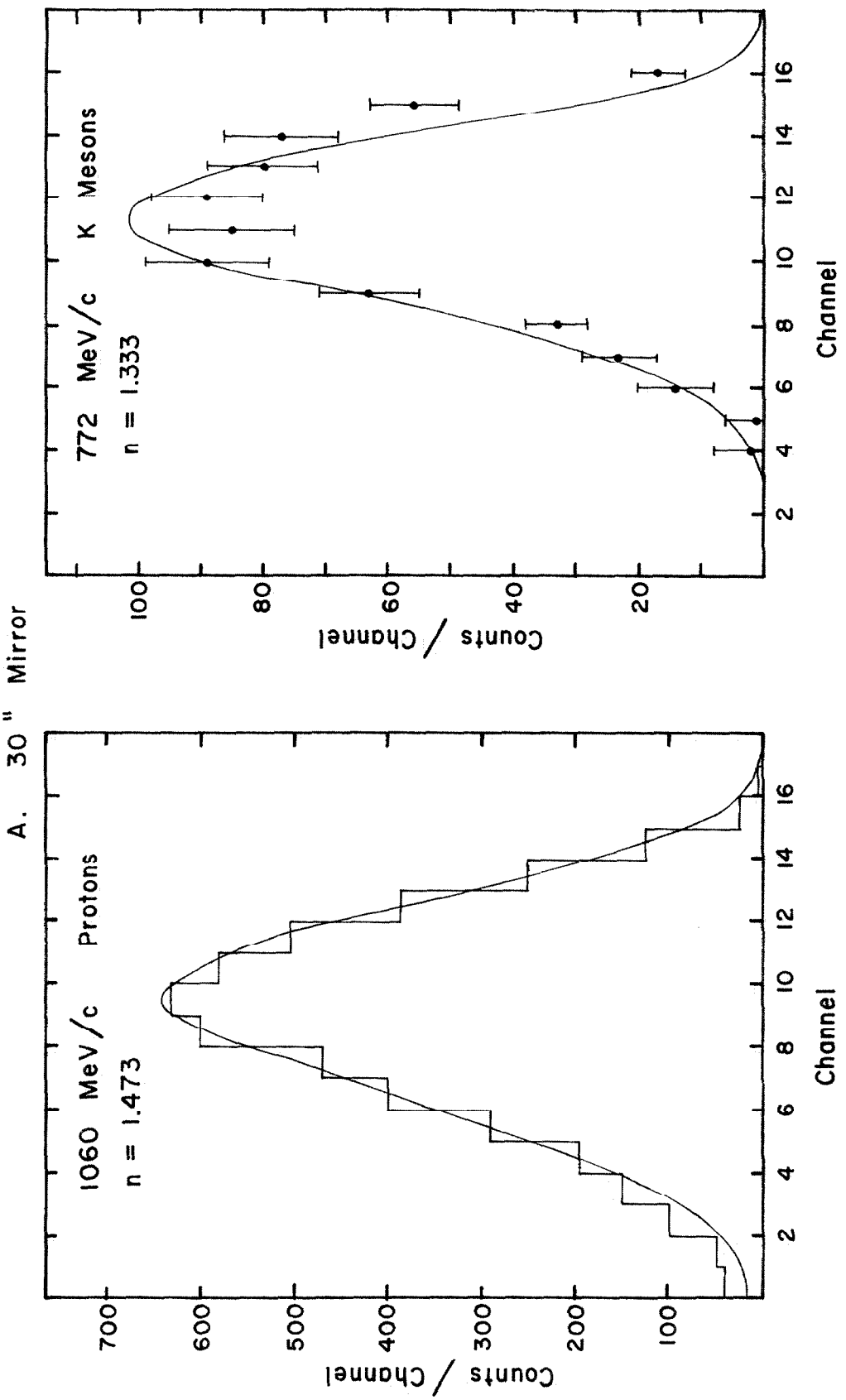
A. 30" Mirror
1060 MeV/c Protons
n = 1.473
772 MeV/c K Mesons
n = 1.333
Counts / Channel
Channel

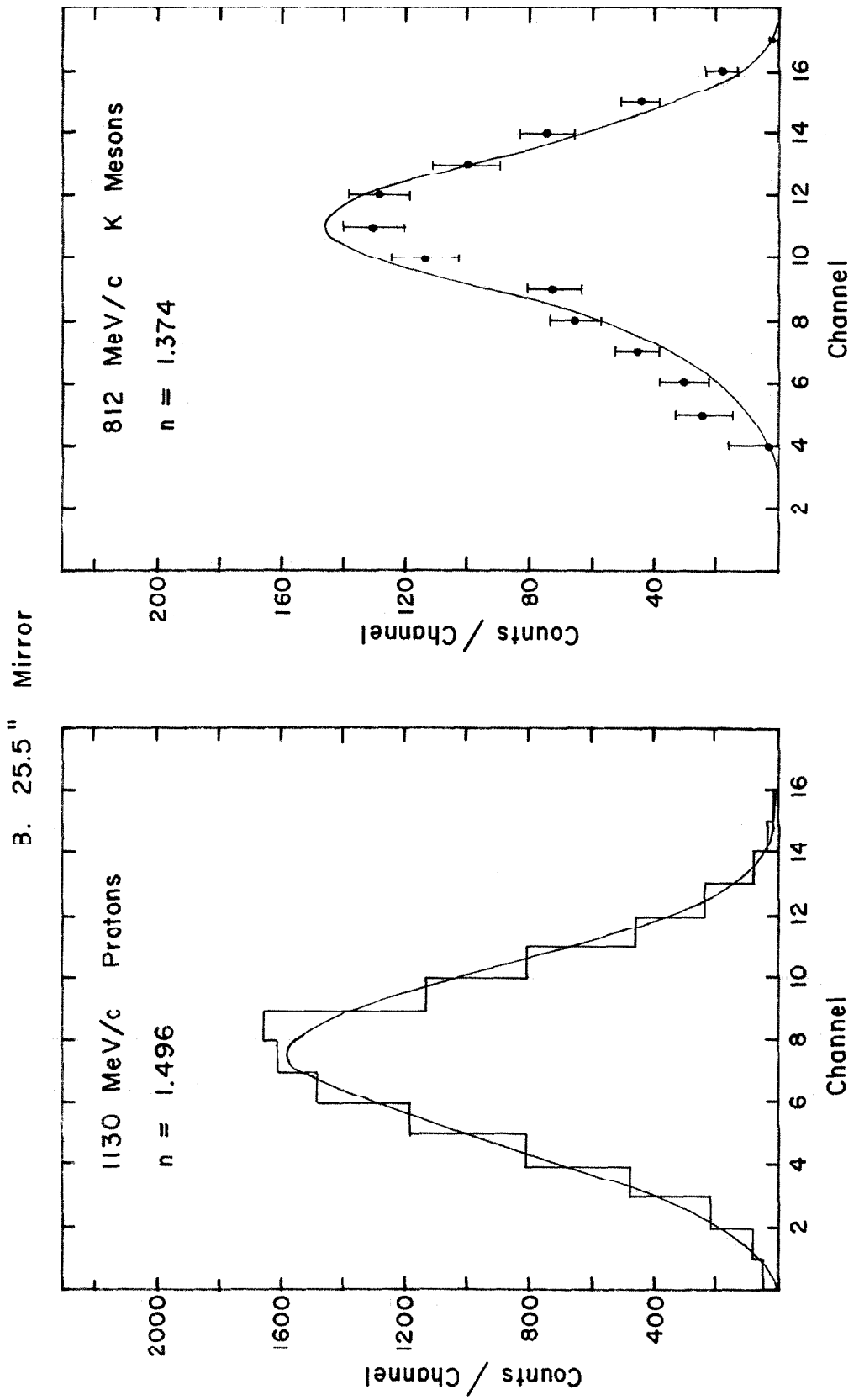
B. 25.5" Mirror
1130 MeV/c Protons
n = 1.496
812 MeV/c K Mesons
n = 1.374
Counts / Channel
Channel
2000
1600
1200
800
400
200
160
120
80
40
2
4
6
8
10
12
14
16

The distributions calculated for K mesons were used to obtain the efficiency of the focusing counter for the biases actually used in the experiment. Since the calculation of a distribution is quite time consuming (about 6 min on the IBM 7090), it was not done for every K momentum used. Rather, for each mirror, only three distributions were obtained. Momenta on either end and at the center of the range used with each mirror were chosen and the efficiencies for intermediate points obtained by interpolation. The results are given in the table of cross section calculations (Table XIII in Appendix VI).

B. The Lucite Cherenkov Counter

This counter was originally used by Brody[29] to veto pions in a K experiment; in his thesis, he has given a full description of its operating principle, construction, and expected performance. For a well collimated beam, the detection efficiency of this counter would drop very quickly when a particle's momentum equaled twice its mass ($\beta \cong 0.9$). With the poor collimation provided by the spectrometer, however, the transition from high efficiency to low is considerably broadened. From the efficiency vs. velocity curve given in Brody's thesis, one would expect a detection efficiency of about 20% at the highest K velocity used in this experiment, $\beta = 0.85$. This would, of course, be intolerably high. In order to ensure a small K meson sensitivity, the performance of the counter was improved by using phototubes with larger cathode efficiencies than were originally installed and by operating with a relatively high bias on the signal. Under these conditions, the detection efficiency

was about 95% for pions but only about 1% for K mesons. In figure 18 the pulse height distribution produced by pions and high energy K mesons in this counter is shown and the electronic bias used is indicated.

It was an easy matter to modify the computer program which was used to analyse the focusing counter to allow a computation of the expected behavior of this simpler Lucite counter. With the exception of the optics, the procedure was the same in both cases. Since the light must penetrate quite thick amounts of Lucite, the absorption for each ray was taken into account. The results of the calculation were that for highly relativistic particles the average light collection efficiency is about 18%, and that its r.m.s. deviation from this mean is about 1.9%. Furthermore, at the highest momentum used in this experiment, the analysis indicated that only about 1% of the K mesons would fire this counter by Cherenkov light. This is consistent with a crude experimental determination and has been used in the data reduction.

FIGURE 18

PION AND K MESON PULSE HEIGHT

DISTRIBUTIONS IN LC

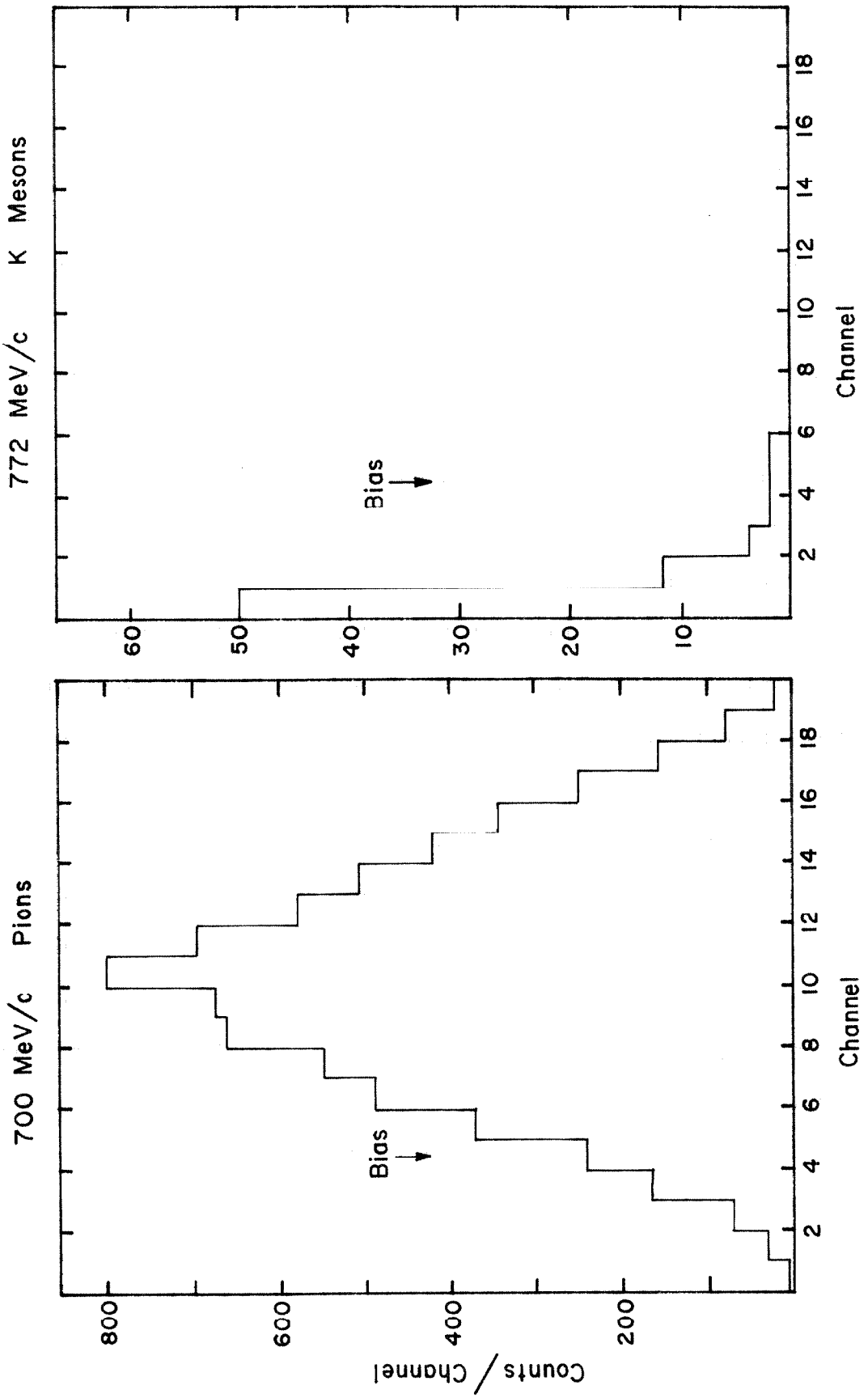
700 MeV/c Pions
772 MeV/c K Mesons
Bias
Bias
Counts / Channel
Channel
Channel
800
600
400
200
60
50
40
30
20
10
2
4
6
8
10
12
14
16
18

APPENDIX III

ELECTRONICS

Whereas the principal mechanical apparatus used in this experiment was either identical or very similar to what has been used in several experiments at the Synchrotron Laboratory, the electronics was sufficiently different in detail to warrant a more elaborate discussion. In line with the current state of the art, the electronics used only transistors as active elements. Nevertheless, the old philosophy of several levels of coincidence logic with progressively longer resolving times has been adhered to. This method is convenient in that the logically more complex signals are very long (0.5 μsec) and can be handled with only minimal precautions. It has the disadvantage that the signal bearing the most information occurs long after the physical event it describes, but, for this experiment, this fact was totally irrelevant.

The principal instruments were designed by M. Sands, J. H. Marshall, and A. Barna and have been described in detail elsewhere.[35,36] The first and fastest level of logic was provided by the TC-4, a two-input coincidence circuit capable of resolving times of a few nanoseconds. Standardized signals 50 nsec long were prepared for the second level of logic by a pulse height discriminator, the TVD1-A. Signals from the discriminators were fed to the TL-1, an eight-input coincidence-veto circuit with 50 nsec resolving time. The coincidence of any combination (as determined by switch settings) of

four inputs results in a 0.5 μsec output at the coincidence terminal (C). Similarly, any combination of four inputs can be selected to be in anticoincidence and the signal incorporating all the logic appears at the terminal CV. These slow pulses were either scaled directly or fed to trivial two-input coincidence circuits. In addition to these standard instruments, two special circuits were designed to economically handle the four-channel multiplexing of the momentum aperture. These consisted of a simplified adaptation of the TL-1 to set the discriminated signals from the four S2 counters into 50 nsec coincidence with one other such signal and a similar arrangement for the 0.5 μsec level of the logic. The overall system proved highly reliable and adequately flexible.

In earlier K^+ experiments at this laboratory, and, indeed, in the early phases of this one, a photographic record was made of all the important signals each time there was a relatively high likelihood that a K meson had been detected. An analysis of the correlated pulse heights was then made and criteria established to select the interesting events. Of course, the logical flexibility afforded by such a scheme is virtually unlimited but, by the same token, the method is very time-consuming and laborious. In this experiment, on the other hand, the selection criteria were of a sufficiently simple sort that correlated pulse height information was not needed and simple coincidence electronic logic could have been used exclusively. However, the focusing counter signal was singularly important and its pulse height distribution was always accumulated in a TMC-401 analyser[37].

The block diagram of the principal electronics used is shown in fig. 19. In addition to what is included in the diagram, several monitoring functions were provided and will be discussed later. The signals from the several phototubes viewing the Cherenkov counters were summed in linear active adders located near the counters. The eleven signals from all the counters were transmitted to the counting room where all the remaining electronics was located. The resolving times of the TC-4's for the coincidences (A1 · S1) and (A2 · S1) were set to about 3.5 nsec. Due to the wide distribution of pulse heights from FC and the Fans, the coincidence resolving times between them and S1 were set to 10 nsec and 15 nsec respectively.

Since it was anticipated that the high singles rate in the Fans would result in a significant number of accidental vetos, a special channel was provided to continuously monitor these accidentals. After passing through the normal (Fan · S1) coincidence circuit, the Fan signal was delayed relative to S1 by 100 nsec (the revolution period of the electrons in the synchrotron) and then fed to the $(\text{Fan} \cdot \text{S1})_{\text{ACC}}$ circuit. The subsequent treatment of the outputs of these two TC-4's was identical.

The signals from the several counters not used in the fastest logic level, the TC-4 outputs, and FC and S1 were fed either directly or after amplification into the voltage discriminators. The bias levels on the scintillator signals were set to approximately one-quarter the average signal produced by the transit of a minimum ionizing particle through the spectrometer. The TC-4 outputs were biased well below the pulse-height distribution produced by true coincidences. For the

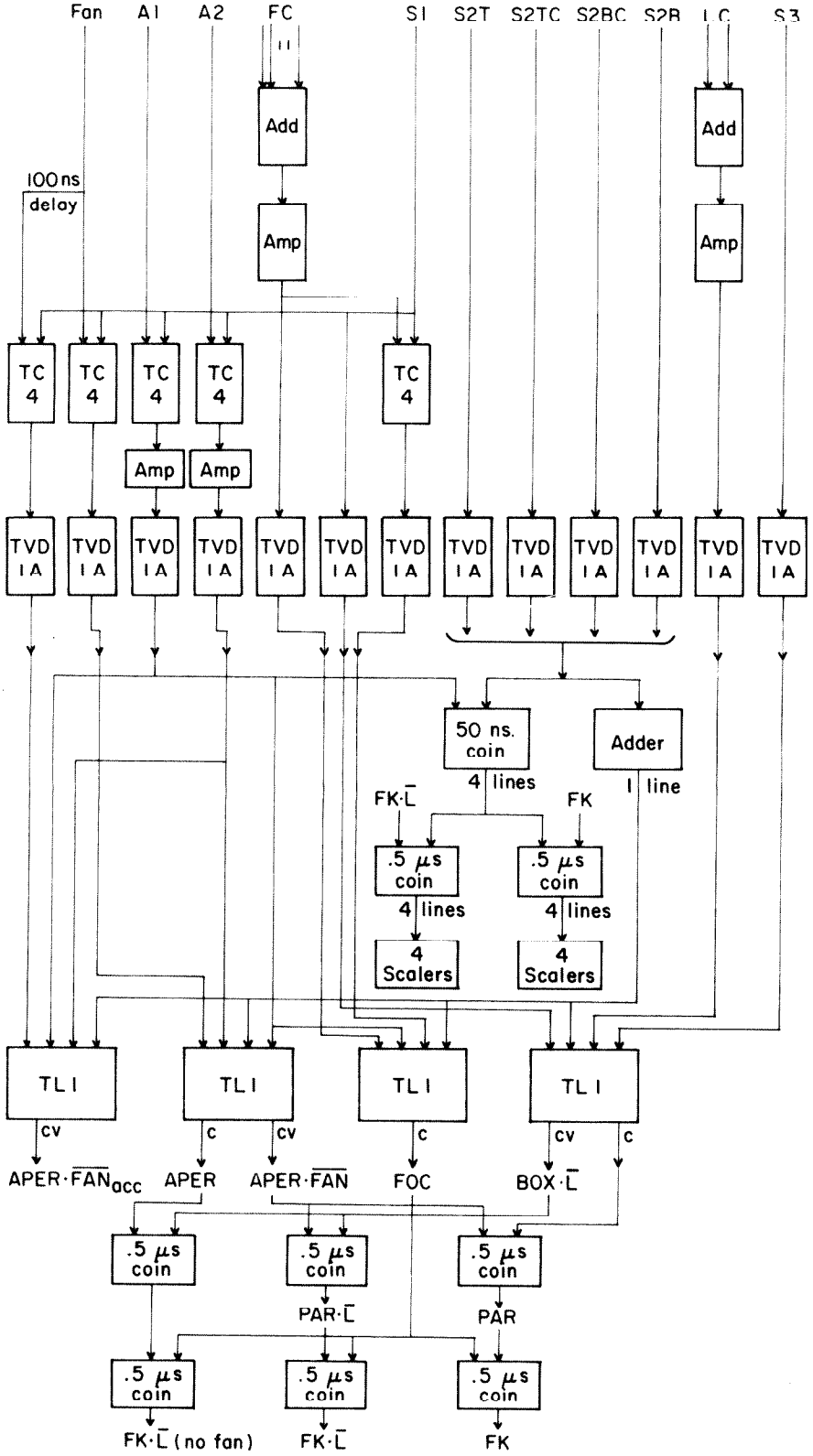

FIGURE 19

ELECTRONICS BLOCK DIAGRAM

Cherenkov counters, the levels were set so as to insure a high K^+ detection efficiency.

The outputs of the four S2 discriminators were logically added and the logical sum used with the several other discriminator outputs to drive the TL-1's. In addition, the four separate lines were set into coincidence with the output of the discriminator on (S1 · A1). The 0.5 μsec signals resulting from these 50 nsec coincidences were sifted through another level of logic before being scaled. For convenience in the block diagram, the other scalers used are not shown, but each labeled signal was fed to one. These signals consist of the outputs of TL-1's and simple coincidences between them. In particular, the switching on the TL-1's was arranged to provide the following logic signals:

$$\text{BOX} = (S1)\cdot(S2)\cdot(S3) \qquad \text{(not scaled)}$$

$$\text{BOX}\cdot\overline{L} = (S1)\cdot(S2)\cdot(S3)\cdot(\overline{LC})$$

$$\text{APER} = (A1\cdot S1)\cdot(A2\cdot S1)\cdot(S2)$$

$$\text{APER}\cdot\overline{\text{FAN}} = (A1\cdot S1)\cdot(A2\cdot S1)\cdot(S2)\cdot(\overline{\text{FAN}\cdot S1})$$

$$\text{APER}\cdot\overline{\text{FAN}}_{\text{ACC}} = (A1\cdot S1)\cdot(A2\cdot S1)\cdot(S2)\cdot(\overline{\text{FAN}\cdot S1})_{\text{ACC}}$$

$$\text{FOC} = (FC)\cdot(A1\cdot S1)\cdot(S2)\cdot(FC\cdot S1)$$

The simple two-fold coincidences between these various signals yielded the following:

$$\text{PAR} = (\text{BOX}) \cdot (\text{APER} \cdot \overline{\text{FAN}})$$

$$\text{PAR} \cdot \bar{L} = (\text{BOX} \cdot \bar{L}) \cdot (\text{APER} \cdot \overline{\text{FAN}})$$

$$\text{FK} = (\text{PAR}) \cdot (\text{FOC})$$

$$\text{FK} \cdot \bar{L} \text{ (no Fan)} = (\text{APER}) \cdot (\text{BOX} \cdot \bar{L}) \cdot (\text{FOC})$$

$$\text{FK} \cdot \bar{L} = (\text{PAR} \cdot \bar{L}) \cdot (\text{FOC})$$

The signal of prime interest was $\text{FK} \cdot \bar{L}$; except for the very low bias set on the focusing counter signal, it measured the (uncorrected) K meson rate. However, due to the very small K meson flux (ranging from 6 to 30 per hour), it was considered essential to monitor several intermediate rates to allow quick detection of malfunctions. The significance and use of each of the scaled signals is the following:

1) $\text{BOX} \cdot \bar{L}$ -- Counted all protons and a small fraction of the pions which passed through the telescope in the counter box. It was quite sensitive to the bias on the Lucite Cherenkov counter signal.

2) APER and $\text{APER} \cdot \overline{\text{FAN}}$ -- The difference of these two rates gave the fraction of pions and protons which the Fan counters vetoed. Furthermore, the individual rates were sensitive to the biases and delay times used with the A1 and A2 fast coincidence channels.

3) APER and $\text{APER} \cdot \overline{\text{FAN}}_{\text{ACC}}$ -- These two rates were used to calculate the fraction of the K mesons which were accidentally vetoed by the Fan counters.

4) FOC -- Used only to check the gross behavior of the FC circuits.

5) PAR -- Measured the total particle flux through the full spectrometer system. This rate was used as the normalization factor in the "Carbon subtraction".

6) PAR $\cdot \bar{L}$ -- Measured the slow particle flux through the system.

7) FK -- Primarily used to monitor the behavior of the focusing counter in the <u>full</u> pion flux.

8) FK $\cdot \bar{L}$ (no Fan) -- The difference between this rate and FK $\cdot \bar{L}$ directly measured the number of K mesons (or K-like objects) vetoed by the Fans.

In general, each of these rates contained but a small fraction of accidentals so that changes in them actually reflected significant variations in the system's operating conditions. For example, in one instance, a small change in the photon beam alignment was signaled by an unusual fluctuation in several of these monitor rates. Normally, over a series of similar runs the several rates which depended upon the A1 and A2 coincidence circuits showed deviations from the average several times larger than expected from counting statistics. This was interpreted as the result of small bias changes in the electronics, to which pion and proton rates are very sensitive. After the experiment was completed, a temperature dependence of a bias in the TC-4 was discovered by D. Groom,[38] and this could easily account for these

observations. Since the cable delays in the A1 and A2 signals were always carefully set for K mesons and the pulse height distributions from the TC-4's were frequently measured, it is believed that the K meson rates were unaffected by these bias fluctuations.

In addition to the monitoring functions provided by the several rates discussed above, provisions were made to conveniently check any electronic signal. Ten percent of any signal was always available at a pickoff for viewing in an oscilloscope or for driving special circuits. Two such were used, a delaying-mixer so that correlated pulse-heights from as many as six sources could be displayed on an oscilloscope triggered by any slow (greater than or equal to 50 nsec) signal, and a TMC-401 pulse height analyser so that the distribution of any one signal could be measured. Furthermore, the 400 word memory of this instrument can be segmented into four identical parts and the signal routed to the one of them selected by a triggering signal. Thus, four separate distributions of the signal from one source, each corresponding to a different logic requirement in the full system, could be simultaneously accumulated. Of course, the several triggers had to be mutually exclusive. In a sense, then, the pulse height analyser performed a function conjugate to that of the delaying-mixer. The input to the analyser could be any of the signals bearing pulse height information (phototube outputs, TC-4 outputs, etc.) and it could be triggered by any signal at least 50 nsec long. Both the trigger and the input could be taken from the 10% pickoffs.

In addition to facilitating circuit adjustments, both the delaying-mixer and the analyser were routinely used during the experiment. The output of the delaying-mixer was displayed on an oscilloscope and photographed in one exposure for an entire run. Of course, the correlation in the pulse heights of the several signals was lost but a qualitative check on several distributions was provided. In fig. 23 in Appendix V, two samples of these photographs are given. The analyser was used to obtain quantitative information about the distributions in the focusing counter. In order to keep a running check on the contamination in the $FK \cdot \bar{L}$ rate due to inadequate selection, the electronic bias on the focusing counter signal was always set very low. The tail of small pulse heights observed in a normal K meson run could then be compared with that observed from a Carbon target run with the E_o set at 1000 MeV (or lower). This operating procedure required an accurate quantitative pulse height analysis of the FC signal. In order to avoid the accidental analysis of a spurious signal falling within the 3 μsec sensitive time of the analyser, the FC signal was gated by the 50 nsec pulse from the discriminator on the $(FC \cdot S1)$ fast coincidence circuit.

Finally, two scalers capable of counting at a rate of 10^7 counts/sec and of being operated by signals at the 10% pickoffs were used to measure singles rates in the various counters. Typically, the shielded counters in the box counted about 5×10^4/sec. At the most forward point (6.3^o lab), the two aperture counters, A1 and A2, counted about 3×10^5/sec while the Fans rate was an order of

magnitude larger. Routinely through the experiment, the singles rates in the focusing counter and one of the aperture counters were monitored. The former was used together with $PAR \cdot \bar{L}$ to calculate the expected number of accidentals in $FK \cdot \bar{L}$; this was always negligible since the rate in the focusing counter was typically only 7×10^3/sec. The observed rate in the aperture counters was used to calculate the dead time in the TC-4 fast coincidence circuits.

In conclusion, the electronic system used in this experiment was certainly more elaborate than would have been essential for its execution. To a large extent, the complexity was introduced to provide monitoring functions and, were it not for the remarkable reliability of the transistorized circuitry, such redundancy would hardly have been feasible.

APPENDIX IV

CONTAMINATIONS

One of the principal tasks faced by an experimentalist is the identification and, if possible, elimination of spurious effects which contaminate his results. In this experiment, as much time was spent investigating such things as in accumulating the data this thesis is based upon. Of course, in photoproduction experiments many sources leading to experimental corrections on the raw data are well known (target structure, accidental coincidences, electronic dead time, etc.) and require no special discussion. In this Appendix, two particular difficulties are singled out since it is believed that they are the largest potential sources of systematic error which can be corrected only by redoing the experiment. The first of these was due to imperfections in the K detection scheme. It was known about during the whole experiment and, in fact, most of the test running was aimed at discovering its origin. The second was discovered in the last days of the experiment when we found that some extraneous matter was condensed on the target structure. It had apparently been there, undetected, through most of the running. With frequent measurement of empty target yields, this problem could have been avoided, but, unfortunately, this was not done.

A. Inadequate K Meson Identification

Since K mesons are produced much more rarely than other particles, small imperfections in the detection scheme can lead to large relative errors. In this experiment, the ratio of protons to K mesons to pions was typically 300 : 1 : 300. A standard test to prove that only K mesons are being detected is to reduce the bremsstrahlung end point energy below that required to photoproduce K mesons. At the mid-angles, the observed rates under these conditions were only 3 - 4% of the normal yields but, at the extremes of the angular range, the ratio rose to 8 - 9%. From the pulse height distributions which these particles made in the focusing counter, it was evident that they were not K mesons (see fig. 5 in the main text). Furthermore, runs with the target empty proved that the contamination originated in the hydrogen. The following several paragraphs describe the several (unsuccessful) tests which were designed to identify the contamination.

In the most unfavorable kinematical regions, about 30% of the particles appeared to be properly momentum-analysed pions and protons. From multiple exposure photographs of the pulse heights in S1 and S3, it was clear, however, that most of the contamination particles had velocities similar to that of K mesons. Furthermore, when the polarity of the magnet was reversed to fully exclude K^+ mesons, this same phenomenon persisted. With the magnetic field set for negative particles and a 1" piece of Lucite for a target (to enhance the yield), the counting rate as a function of the delay in the A1 and A2 signals was measured. In fig. 20 the rates observed in the various scalers

FIGURE 20

(A) VELOCITY SPECTRUM OF NEGATIVE FIELD CONTAMINATION PARTICLES

For comparison, the velocity spectra of other rates are also shown.

(B) FOCUSING COUNTER PULSE HEIGHT SPECTRUM OF NEGATIVE FIELD CONTAMINATION PARTICLES

The integral distribution over FK·L shows the behavior in the focusing counter of highly relativistic particles.

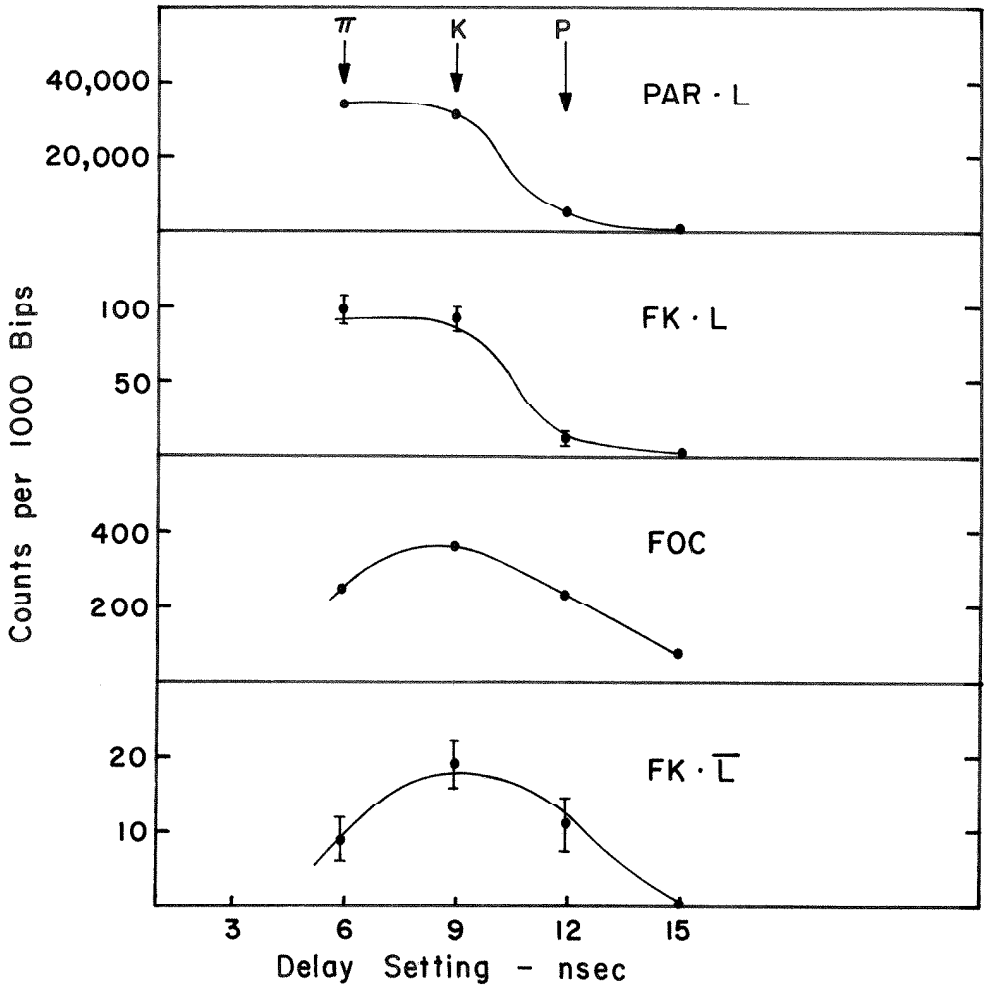
π
K
P
40,000
20,000
PAR · L
100
50
FK · L
400
200
FOC
20
10
FK · L̄
Counts per 1000 Bips
3
6
9
12
15
Delay Setting - nsec

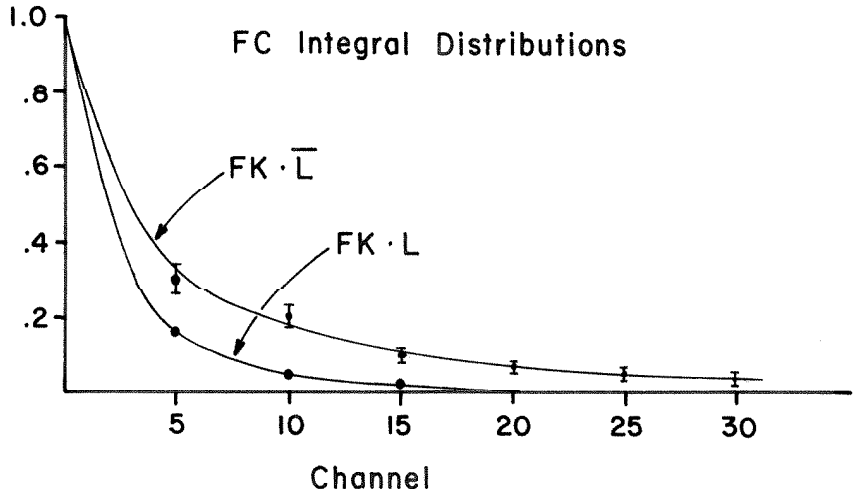
FC Integral Distributions
1.0
.8
.6
.4
.2
FK · L̄
FK · L
5
10
15
20
25
30
Channel

are given; also included are the integral distributions (summed over the several delays) in the focusing counter produced by particles which fired $FK \cdot L$ and $FK \cdot \bar{L}$. It is quite clear that most of the particles defined by $FK \cdot \bar{L}$ are neither pions nor protons with the momentum for which the spectrometer was set. The focusing counter distributions prove that they are not K^- mesons (it was kinematically possible to pair produce K mesons off Carbon). We were forced to conclude that the momentum selection was inferior to the velocity selection.

Somewhat prior to the tests just described, an attempt was made to learn something about this contamination by a range measurement. A very thick (15 cm) Copper energy absorber was placed in front of S3. For particles with the momentum to which the magnet was set (775 MeV/c), it stopped protons but transmitted 42% of the pions and 34% of the K mesons. After passing through it, the pions were still minimum ionizing, but K mesons were slow enough to be from 2.1 to 2.9 minimum ionizing. (This variation was the result of the target size; the absorber was wedge-shaped to correct for the dispersion of the magnet.) For particles with the velocity to which the focusing counter was set, pions were just stopped by the material, but protons could penetrate it and have velocities corresponding to 1.2 to 1.7 minimum ionizing. Thus, if the contamination had penetrated the absorber, it was hoped that its pulse height distribution in S3 would allow an identification. In a series of runs with the end point energy too low to produce K mesons from hydrogen and the absorber in use, only four contamination

counts were recorded whereas without the absorber, 90 were expected. Although this test does not rule out properly momentum analyzed protons, it gives further evidence that the contamination is not normal pions (or K mesons). When the test was made early in the experiment, these two facts were significant, but for our purposes here, it indicates that high momentum scattered protons are not the source of the difficulty. Although in retrospect, further range measurements might have proved useful in isolating the nature of the offending particles, the large amount of time consumed in this one test discouraged us and the attempt was abandoned.

The possibility that either positive or negative particles were scattering from various likely (and unlikely*) parts of the spectrometer was directly tested by shielding such places with a scintillator and measuring its efficiency for detecting the contamination. All results were negative. A more direct test of the scattering hypothesis was then made. A 3" wide, 12" tall scintillator was set up in front of the magnet. Although the statistical precision was somewhat poor, this aperture seemed to have a slightly smaller efficiency for detecting the contamination than for detecting normal particles defined by the spectrometer. Also, during the test made with the front aperture, the size of A2 was reduced to 6". Relative to a normal particle beam, the contamination that missed the front aperture had a slightly enhanced chance of also missing A2. Both these facts

---

*Bob Walker did not have to eat his hat.

suggested that some of the contamination was due to either uncharged particles entering the spectrometer or charged particle scatterings. However, the principal fact which emerged was that the contamination was certainly not dominated by any such effect. One final test was made along these same lines. It has been assumed in the above that the Fan counters eliminated the effects of scattering on the pole pieces of the magnet. This was directly tested by using a narrow (1.25") scintillator in front of the magnet so that the beam defined by it could not hit the pole pieces. Once again, the efficiency of this counter for detecting the contamination was essentially the same as for detecting the normal beam defined by the spectrometer.

Nuclear interactions of pions or protons (or uncharged particles) in either air, the aperture counters, or the focusing counter radiator itself surely lead to a flux of particles with velocities near that of the K mesons. In order to test whether these were the contamination, the amount of matter was doubled, first at the apertures and then at the radiator. Unfortunately, absolute rates rather than efficiencies must be compared in making such a test. However, to within the 30% statistical accuracy with which the comparison was made, the increase of matter did not change the contamination rate.

Finally, the complicated nature of an electromagnetic shower suggests that, in some not well-specified manner, one could masquerade as a K meson. Only one test was made to check this possibility. A 1 cm thick piece of lead was placed in front of S3. Since the

probability that a high energy electron will produce a shower in the lead is quite large, they could be identified by large pulses in S3. Not only was the S3 distribution of the contamination unchanged by the Pb, but also its rate was unaffected. Of course, this test eliminates only one manifestation of the shower hypothesis and processes involving low energy electrons in the counter box are still potential contamination sources.

Aside from electromagnetic showers, the evidence indicates that charged particles enter the magnetic field in the standard manner, manage to negotiate it, but emerge with roughly the velocity of a K meson. One possibility which none of the tests can eliminate is that a pion decays in the magnetic field to a muon with just the right parameters that the muon is injected into a K orbit with the velocity of a momentum analysed K meson. However, ray tracings in the magnetic field rule out this type of event; the decay muon remembers the pion direction much too faithfully to allow the arrangement of orbits suggested. In a similar manner, one might ask about low energy K mesons. Since the K meson has much richer decay possibilities than the pion, there do exist orbits which satisfy the conditions for the contamination. Estimates of the number of low energy K mesons impinging on the magnetic field indicate that there are roughly 50 for each detected K meson. Thus, for these to be the source of a 10% contamination, 0.2% of them must decay with the proper correlation between decay site and decay parameters. Although no detailed calculations of this efficiency have been made, 0.2% seems very large.

The photoproduction of K mesons is one of the rarest processes studied at the Synchrotron Laboratory; its contamination is an order of magnitude more ethereal. Because of this rarity, the several experiments to discover its source could only have been successful if some one effect were the principal contributor. It is certainly possible that the contamination does have in fact a single source which we were unable to identify, but we are inclined to believe that it is a combination of several effects, each contributing but a small fraction of the total. In any case, the empirical "Carbon subtraction" procedure adopted, as outlined in the main text, seemed to be adequate for the level of statistical precision achieved in the experiment.

B. Target Contamination

In the data reduction, an unusual correction of 6.7% is included to account for target contamination. In this section, the history of the experiment as it bears on this problem as well as the data upon which the correction was based will be given.

Before plunging into the central task of measuring the angular distribution at 1200 MeV, we explored the limits of applicability of the experimental technique. Full target rates were measured at 35° and 85° c.m. at 1200 MeV and, to compare our work with that at Cornell, yields were also taken at 48° c.m., 1054 MeV. Immediately thereafter, empty target yields were obtained for the two low momentum points, but, because of a sudden spurt of interest in the K meson identification problem at the low momentum, no empty target

data were taken at 35^{o} c.m. However, the empty target rates observed were consistent with the known construction of the target and the measured rates from a 1" thick piece of Mylar. The target was refilled shortly afterwards, but it remained unused for about a month while other things were done (including some unusual maintenance on the photon source). After this delay, data accumulation was begun in earnest. In Table VIII the calendar dates on which full target yields were measured for the 14 cross sections are given. Although there was less jumping from point to point than is customary in pion photoproduction, for example, adjacent points on the distribution were taken at widely different times. Yields from a 1" Mylar target were taken for each kinematical point. From these, estimates of the empty target backgrounds were made, but during this time no actual empty target rates were measured.

In early October it was decided to terminate the experiment. There remained empty target yields to be measured, especially at the small angles. However, immediately after we emptied the target, it became completely opaque. Since it had been transparent during the entire experiment (any hint of trouble prompted a check of this fact), it was supposed that the extraneous matter had developed during the emptying process. Of course, no data taken with the target opaque could be considered reliable and so it was disassembled for investigation. Immediately after it was opened and before any substantial amount of air or water could condense, a film of material was observed on the outside surface of the Mylar hydrogen cup and on the heat shields. This

TABLE VIII

DATES OF FULL TARGET RUNS

k (MeV)	$\theta_{c.m.}$	Dates (1963)
1200	15°	July 27, 30; Aug. 14, 15
1200	25°	July 16, 19, 23, 25
1200	30°	Aug. 16, 28; Sept. 28; Oct. 2
1200	35°	May 18; July 2
1200	42°	July 10, 11
1200	49°	July 9; Aug. 1
1200	55°	June 27, 28
1200	63°	July 12
1200	70°	June 17 to June 26; July 13
1200	78°	July 16, 17, 18, 23, 25
1200	85°	May 23, 24
1080	46°	Sept. 11, 12, 13, 14, 17, 18
1054	30°	Sept. 18, 19, 20, 21
1054	48°	May 24, 25, 26

presumably was the cause of the opacity. The structure was thoroughly cleaned before reassembly.

Since rather drastic measures had been taken with the target, it was essential to determine the relevancy of empty target yields taken after the episode to full target rates observed before it. This could only be done by comparing K rates from the full target from before and after the target disassembly.* Accordingly, the target was refilled with hydrogen and the 30° c.m. point, which had just been completed, was remeasured. Not only was the $FK \cdot \bar{L}$ rate noticeably smaller, but also the pion rate ($PAR - PAR \cdot \bar{L}$) and the gross proton rate ($BOX \cdot \bar{L}$) were reduced by 8.5% and 7.0% respectively. (The proton rate $PAR \cdot \bar{L}$ was not a good monitor at 30° c.m. because it was very sensitive to the behavior of the fast coincidence circuits.) On the other hand, all rates from the 1" Mylar target were unchanged. These data clearly indicated that at least some of the full target data contained an unknown amount of contamination.

At this juncture, the scientifically best procedure would have been to redo the experiment, but this was hardly feasible. The next best alternative was to seek evidence that the contamination was constant, evaluate its effects, and correct the existing data. The

---

*Of course, if no change in K rates had been found, the constancy of other, better known rates could be used as further evidence in favor of the hypothesis that there had been no trouble. On the other hand, as the K rates decreased, changes in other yields are only of qualitative interest.

empty target runs in May indicate that there was no contamination at that time, but, unfortunately, the early full target data at 35° c.m. does not have sufficient statistical precision to allow a good comparison with the July data. A standard proton counting rate from the hydrogen target (see Appendix V) was frequently measured during the experiment to provide an overall check of the apparatus but, somewhat surprisingly, it proved to be quite insensitive to the target contamination. Therefore, its constancy through the experiment does not constitute good proof of a stable hydrogen target. On the other hand, the statistical precision of the individual K meson rates is inadequate for their internal consistency (see Appendix V) to be good evidence that the target contamination did not change in time. However, Table VIII shows that some part of all but three of the points on the 1200 MeV angular distribution was taken in July and that the two measurements at 49° c.m. bracket these data. These two 49° determinations are in good agreement,* 72.6 ± 3.5 and 71.5 ± 6.0 counts/kiloBIP, but the large uncertainties weaken the evidence. Nevertheless, there is no evidence which suggests either

*Actually a third measurement at 49° c.m. was taken on July 25 in which an anomalously large K rate was observed, 79.7 ± 4.5 counts/kiloBIP. During these runs, the rate in the two-scintillator telescope viewing the hydrogen target was also high and immediately after them a standard proton rate was 3 standard deviations high (see Appendix V). No cause was ever isolated to explain this anomaly but within 12 hours of its occurrence, everything seemed normal again. Either a transitory change occurred in the target or there was an unnoticed experimental error. The latter view is favored.

that the condensation occurred at some definite time during the full target running or that it slowly accumulated during the experiment. It was decided to tentatively accept the hypothesis of a constant contamination and see if further tests were consistent with it.

Four points were selected for detailed remeasurement. They were picked on the basis of good statistical accuracy in the original data and a wide distribution of original running dates. In all four cases, the yields from the freshly cleaned target were smaller than the original. In Table IX the observed K rates (after corrections for deadtime and Fan accidentals) are compared. If it be assumed that the new data are smaller than the old by a multiplicative constant, it is easily determined to be $(1 - 0.067) \pm 0.035$. The last column in the table gives the old data as corrected by this factor. It is seen that the agreement is quite good. Statistically, these data are perfectly consistent with the hypothesis, but the uncertainties in the four individual measurements of the effect are so large that their internal consistency does not carry much weight.

In principle, it would have been better to correct the data using a fixed fraction of the observed yields from Mylar rather than from hydrogen. However, the ratio of these two yields is consistent with being independent of angle over the range of measurements. In view of the more fundamental uncertainties in the procedure adopted, this refinement seemed superfluous and was not used.

Although no solid evidence can be offered to prove that the target contamination did not affect the shape of the angular

TABLE IX

COMPARISON OF K^+ RATES OBSERVED BEFORE AND AFTER CLEANING THE TARGET

k (MeV)	$\theta_{c.m.}$	Yields (counts/1000 BIPS)		
		After	Before	Corrected
1200	15°	94.9 ± 5.60	99.7 ± 5.00	93.0
1200	30°	65.0 ± 4.35	71.5 ± 3.09	66.7
1200	49°	67.5 ± 3.33	71.7 ± 3.11	67.9
1080	46°	48.2 ± 2.92	52.2 ± 2.64	48.7

distribution, there is nothing in the data to suggest that it did. Accordingly, we have not included the 3.5% statistical uncertainty in the target contamination factor in the individual cross section uncertainties but have rather folded it in with the various other systematic effects which affect the absolute cross section scale.

In conclusion, this misfortune was entirely avoidable. More careful attention to empty target yields and an occasional warming of the target would have prevented the whole problem. Evidently, visual inspection of a liquid hydrogen target is not adequate to guarantee that it is uncontaminated. Indeed, on one occasion while the data from the freshly cleaned target were being accumulated, some additional hydrogen was condensed into it. Since, at this time, the author was particularly sensitive to target contamination, a special proton counting rate had been observed immediately prior to the filling operation. The kinematical conditions for this run were chosen so that no proton photoproduced from hydrogen could be detected. Thus, the rate was especially sensitive to heavy nuclei in the target. As filling began, an opacity was noticed developing just below the meniscus of the liquid, and at the completion of the operation the target was opaque. A remeasurement of the proton rate showed it to be completely unchanged whereas a change of 0.02 gm/cm^2 of heavy nuclei could have been detected. Within half an hour, the hydrogen was again clear. Thus, not only is a clear target not necessarily clean, but an opaque one may contain only hydrogen!

APPENDIX V

OPERATING PROCEDURE AND APPARATUS MONITORING

A. Standard K^+ Runs

The settings of the apparatus for each of the cross section measurements are listed in Table X. The data for each measurement were always taken in several identical runs, normally about 1000 BIP long. At the termination of each run, the number of counts in each of the several scalers was recorded and the contents of the pulse height analyser were read out. A comparison of these results with previous ones indicated whether or not the new run contained any abnormalities. If so, they were investigated before proceeding, but if not, another run was begun. In figure 21 the dependence of various counting rates on the K meson c.m. angle for the 1200 MeV data is given. The sharp breaks in PAR, PAR $\cdot \bar{L}$, and APER are due to 1 nsec changes in the delays of the A1 and A2 signals to allow for the varying K meson flight times. The statistical precision of these rates is, of course, excellent but they still show the relatively large fluctuations indicated in the figure. Since these rates are largely determined by electronic efficiencies, the fluctuations reflect electronic instabilities.

In order to monitor the performance of the Fan counters, the electronics configuration was arranged to directly measure their veto rate, both for the general flux of particles through the spectrometer (APER) and for the K mesons (FK $\cdot \bar{L}$). In figure 22(A) the results of these measurements are given. Since it was felt that the laboratory

TABLE X

PRINCIPAL RUNNING PARAMETERS

k	θ_{cm}	P_{target}	P_{magnet}	θ_{lab}	# S2's	Al length	FC Mir. Radius	FC Radiator	Radiator Index	Fraction of running time
1200	15°	815.6	812.2	6.28°	4	6"	25.5"	34% Gly.	1.374	1.00
1200	25°	799.2	796.2	10.50°	3	12"	25.5"	39%	1.379	1.00
1200	30°	788.1	785.1	12.63°	4	6"	25.5"	39%	1.379	1.00
1200	35°	775.2	771.8	14.77°	4	12"	30"	0%	1.333	.25
					3	12"				.75
1200	42°	754.0	750.3	342.19°	3	12"	30"	4.2%	1.338	1.00
1200	49°	729.6	725.8	339.11°	3	12"	30"	13.7%	1.350	.75
					4	6"	25.5"	55.8%	1.405	.25
1200	55°	706.2	702.3	336.44°	3	12"	30"	22.6%	1.362	1.00
1200	63°	671.8	667.7	332.80°	3	12"	30"	40.0%	1.385	1.00
1200	70°	639.0	634.6	329.55°	3	12"	30"	53.0%	1.403	1.00
1200	78°	598.9	594.5	34.26°	3	12"	25.5"	Lucite	1.496	1.00
1200	85°	561.8	556.7	37.37°	4	12"	30"	100%	1.473	1.00
1080	46.5°	598.9	594.5	241.50°	3	12"	25.5"	Lucite	1.496	1.00
1054	31°	598.9	594.5	11.92°	3	12"	25.5"	Lucite	1.496	1.00
1054	48°	561.8	556.7	18.25°	4	12"	30"	100%	1.473	1.00

FIGURE 21

MONITOR RATES FOR 1200 MeV

ANGULAR DISTRIBUTION

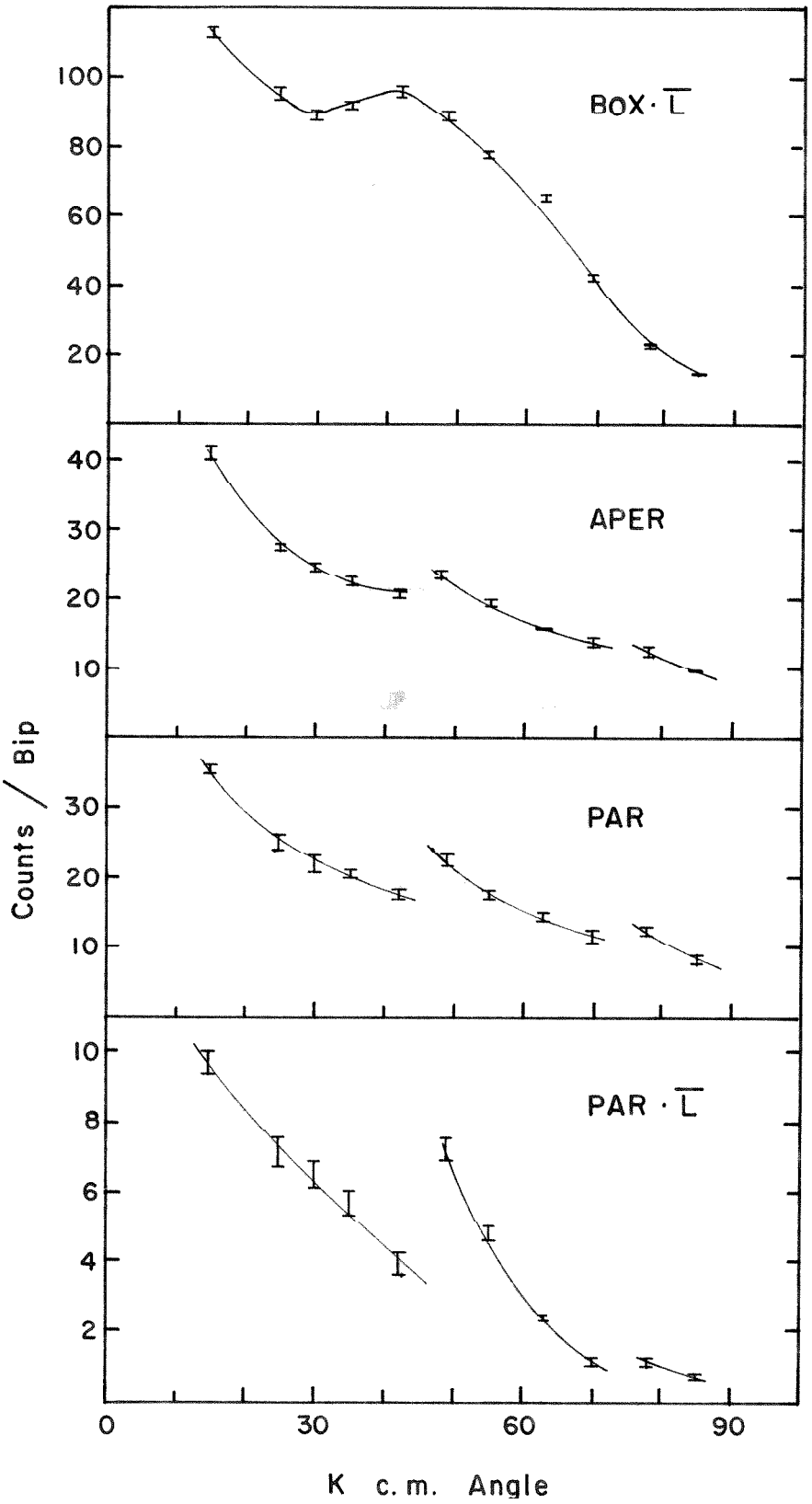
BOX · L̄
APER
PAR
PAR · L̄
Counts / Bip
K c.m. Angle
0
30
60
90

FIGURE 22

(A) FAN COUNTER VETO RATES

(B) UPPER LIMIT TO THE K MESON EFFICIENCY OF THE LUCITE COUNTER

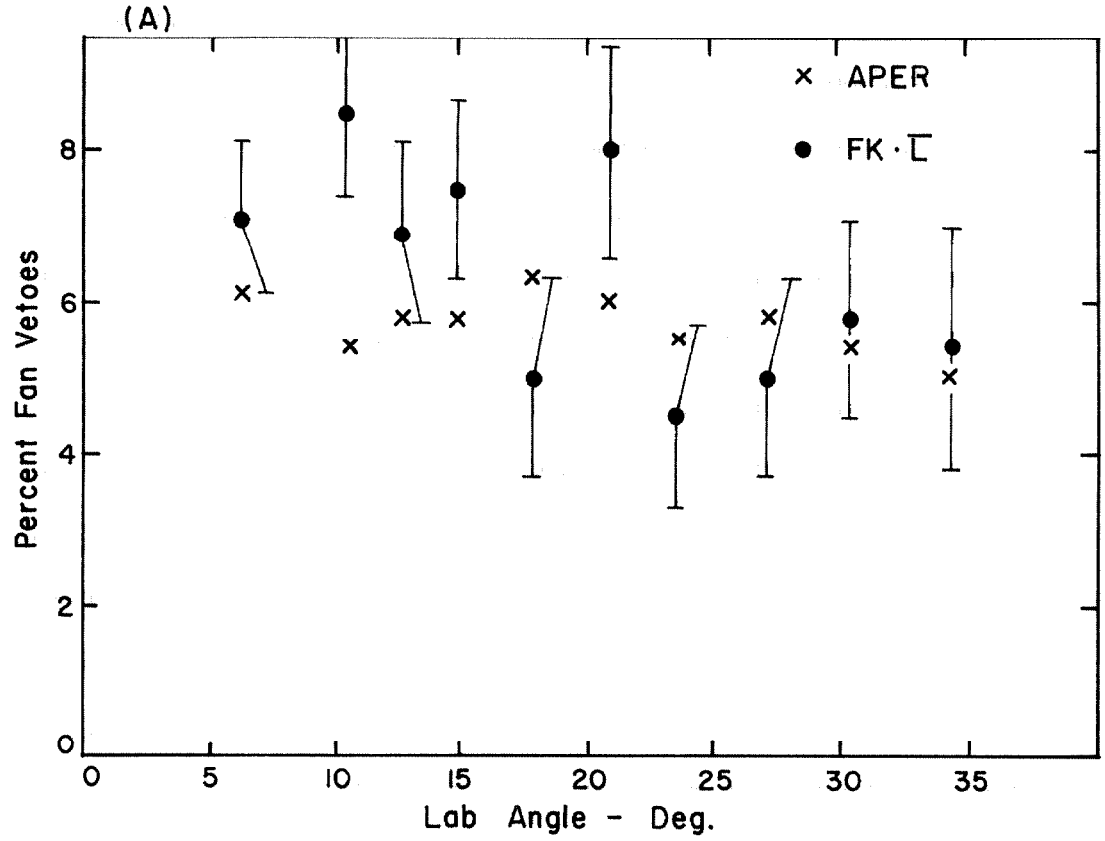
(A)
× APER
● FK · L̄
Percent Fan Vetoes
0
2
4
6
8
0
5
10
15
20
25
30
35
Lab Angle - Deg.

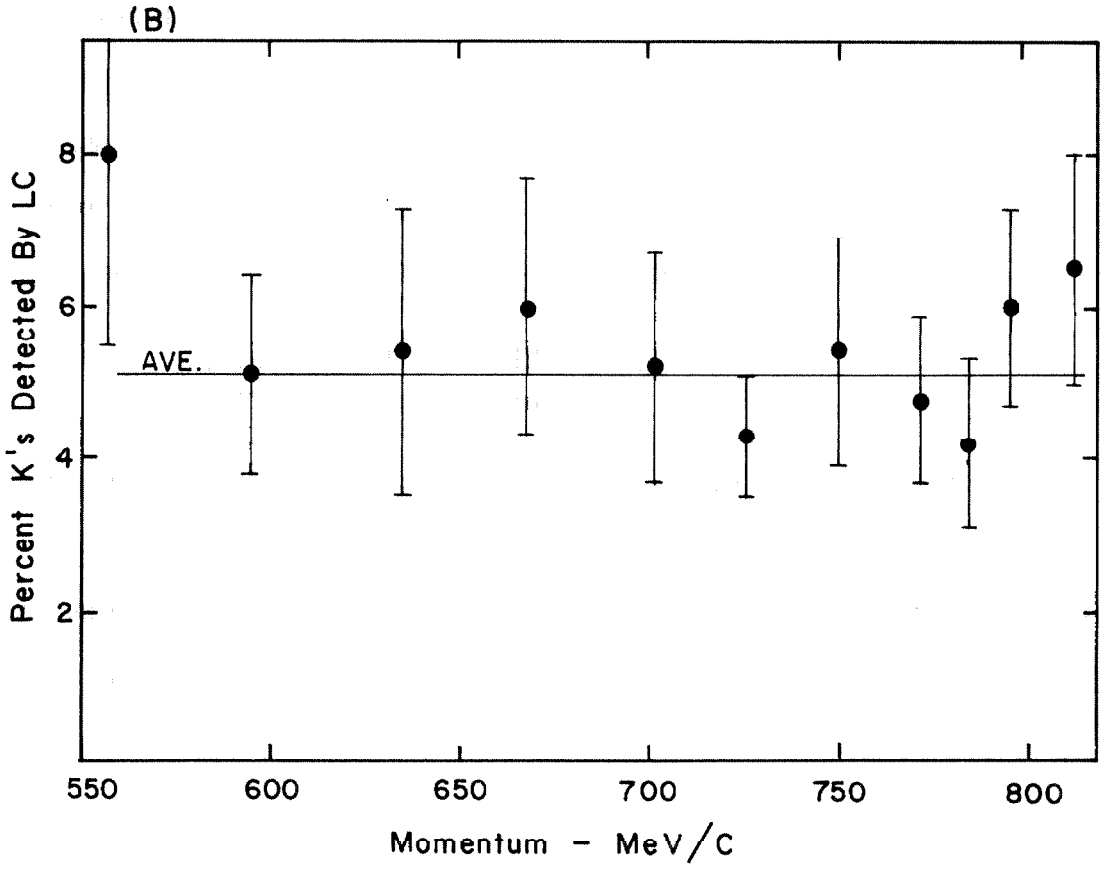
(B)
Percent K's Detected By LC
AVE.
2
4
6
8
550
600
650
700
750
800
Momentum - MeV/C

angle was the most significant parameter with respect to the Fan performance, it has been used as abscissa. The rates plotted have been corrected for accidental vetos. It is apparent that, on the whole, the Fan counters veto the same fraction of particles which satisfy the K meson conditions as of the general flux through the magnet. This suggests that pole piece scatterings do not result in pseudo-K's.

Since an electronic bias much lower than would be used to define a pure K beam was set on the signal from the focusing counter, it was essential to record this counter's pulse height distribution. In fact, however, four spectra were taken. When the momentum aperture was multiplexed into three channels, the FC signal was analysed over $FK \cdot L$, $(FK \cdot \bar{L}) \cdot (S2TC)$, $(FK \cdot \bar{L}) \cdot (S2BC)$, $(FK \cdot \bar{L}) \cdot (S2B)$; when all four momentum channels were in use, the FC spectrum in each was accumulated. We monitored the momentum dependence of the K meson distributions in the focusing counter in order to catch any errors in its velocity tuning. In all cases, the three (four) spectra were indistinguishable. The FC distribution over $FK \cdot L$ not only showed the counter's performance in a pion beam, but also gave us a rough measure of the K detection efficiency of the Lucite counter. In figure 22(B) the ratio

$$\frac{(FK \cdot L) \text{ with FC} \geq \text{channel 10}}{(FK \cdot \bar{L}) \text{ with FC} \geq \text{channel 10}}$$

is plotted for the several momenta used in this experiment. Since this FC bias is always far removed from the pion distribution, this ratio is expected to be a reasonable upper limit to the K detection efficiency of the Lucite counter. The data show no noticeable momentum

dependence and are perfectly consistent with an average of $(5.1 \pm 0.4)\%$. As indicated in Appendix VI, this apparent detection efficiency is interpreted as being primarily the result of K meson decays between the two Cherenkov counters.

As a further monitor, photographs of several signals were taken during the runs. Two examples are given in figure 23. The momenta chosen correspond to c.m. angles of 25° and 78° on the 1200 MeV angular distribution. PAR was triggered by both protons and pions but, for the examples given, the pion rate dominates. The size of a minimum ionizing pulse in the two scintillators is readily read from these photographs. Also, the distribution of large pulses in the Lucite Cherenkov counter is a characteristic pion signature. One can also see the relative values of the bias settings on the outputs of the fast coincidence circuits, $A1 \cdot S1$ and $A2 \cdot S1$, since for particles other than K's, their distributions extend down to the bias levels. Most of the traces triggered by $PAR \cdot \bar{L}$ show the normal behavior of protons in the system. Also since a reasonable fraction (5%) of the pions was not noticed by LC, some pions are included, just enough, in fact, to clearly delineate the LC bias level. Finally, $FK \cdot \bar{L}$ contains almost entirely K mesons, as indicated most clearly in the pictures by the appearance of the $FC \cdot S1$ coincidence output, and the disappearance of any significant distribution in LC (even at the higher momentum). The pulse height distributions in the two scintillators are characteristic of the K meson velocity. Normalizing pulse heights to the average produced by pions, we expect the following average scintillator signals:

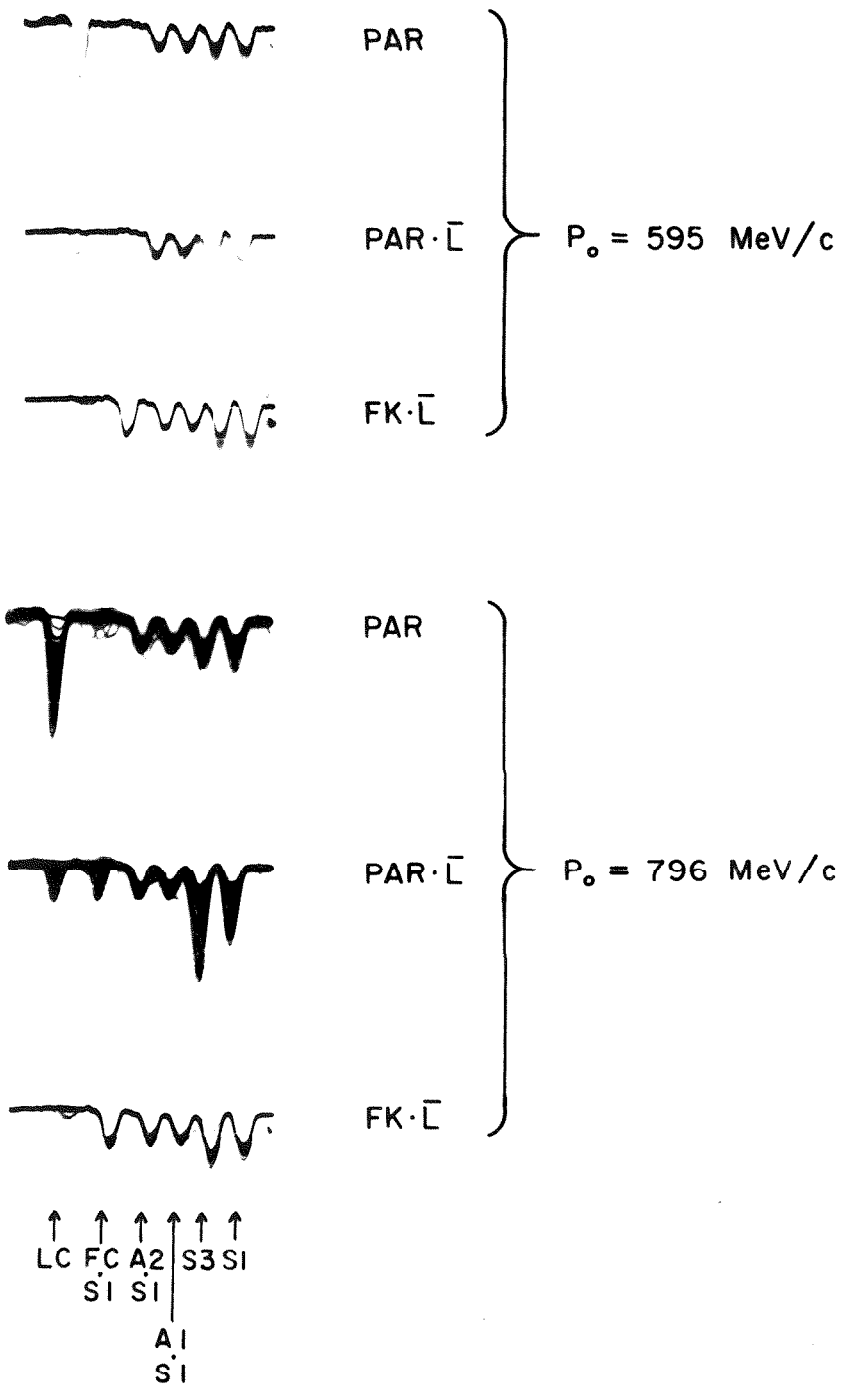

FIGURE 23

TYPICAL MONITOR PHOTOGRAPHS

Momentum	Pion	K	Proton
595 MeV/c	1.00	1.32	2.36
796 MeV/c	1.00	1.11	1.74

During the experiment, it was always reassuring, but not especially significant, to find the expected averages.

During the routine data accumulation, it was always intuitively clear that the $FK \cdot \bar{L}$ rates for the several runs contributing to a given measurement were internally consistent. Of course, there are standard statistical tests which allow one to convert this feeling into an objective measure. The χ^2 goodness of fit test has been applied to the 22 distinct $FK \cdot \bar{L}$ rates which make up the heart of this thesis and the results are summarized in the histogram of figure 24. The smallest χ^2 probability which was observed was 17% and the largest, 96%. Considering the 22 rates as the components of one experiment, one finds an overall χ^2 of 125 for 142 degrees of freedom which has a corresponding probability of 84%. Clearly, the intuitive feeling of internal consistency was justified.

B. Check Runs

1. Proton Rates

As a further check on the stability of the overall system including photon beam, target, and spectrometer characteristics, the proton rate from the hydrogen target with $E_o = 1.2$ BeV, $P_o = 1$ BeV/c, $\theta_{lab} = 15^o$ was frequently measured. Several magnet apertures were used, but all rates have been normalized to a 12" Al counter and all four S2

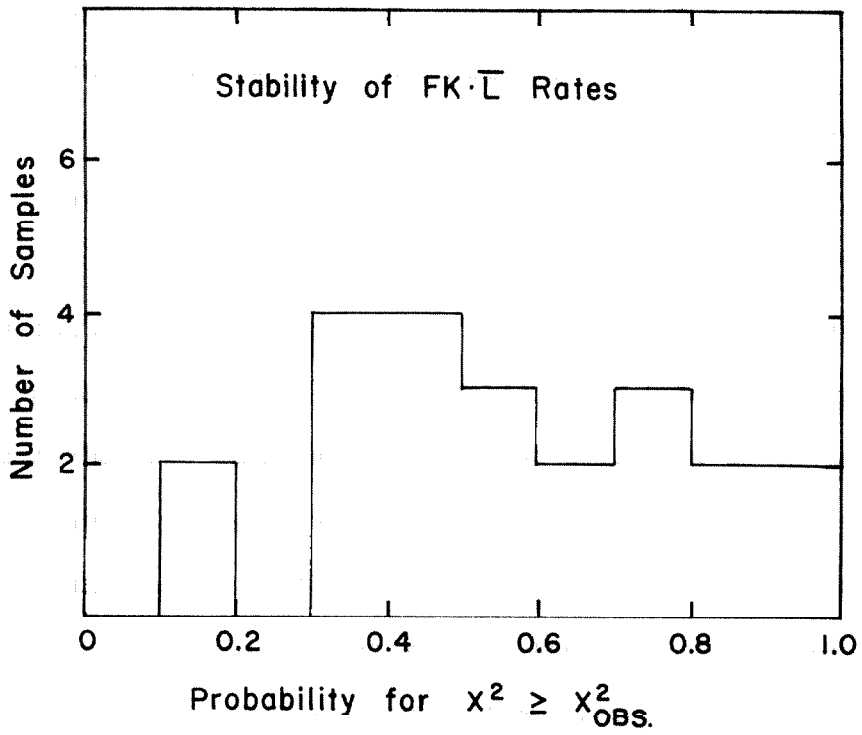

FIGURE 24

DISTRIBUTION OF CHI-SQUARED

PROBABILITIES FOR THE K RUNS

counters ($\Delta\Omega$ = 0.00176 sr, $\Delta P/P_o$ = 0.0941). The results of these measurements are plotted against calendar date in figure 25. The average of the rates measured before cleaning the target is 17.281 $\pm$ 0.086 proton/BIP and the probability of observing a value χ^2 as large or larger than actually obtained is about 25% (χ^2 = 18.7 for 15 degrees of freedom). Not included on the graph or the statistical analysis was a run taken on July 25, shortly after an abnormally large K rate at 49° c.m. was observed. The proton rate at that time was measured to be 18.10 $\pm$ 0.27; its inclusion in the statistical analysis would have increased χ^2 by 10. No data taken in the runs on that date have been used.

The series of runs after cleaning the target show an average of 17.00 $\pm$ 0.16 protons/BIP and a χ^2 probability of 30%. Although this is smaller than the rate observed prior to the discovery of target problems, it is certainly not 6% lower. In fact, the two rates are just consistent with an average of 17.25 (χ^2 probability of 10%). It is this fact which implies that the internal consistency of this monitored rate constitutes, at best, but weak proof for a stable target during the main K runs.

2. Target Contamination Monitor

After the target had been cleaned in early October, a type of run designed to detect any accumulation of extraneous matter in the target was interspersed among the others. At an end point energy of 1.2 BeV, the maximum momentum with which a proton can be photoproduced from hydrogen at a lab angle of 50° is 750 MeV/c. Protons with more

FIGURE 25

PROTON MONITOR RATES THROUGHOUT

THE EXPERIMENT

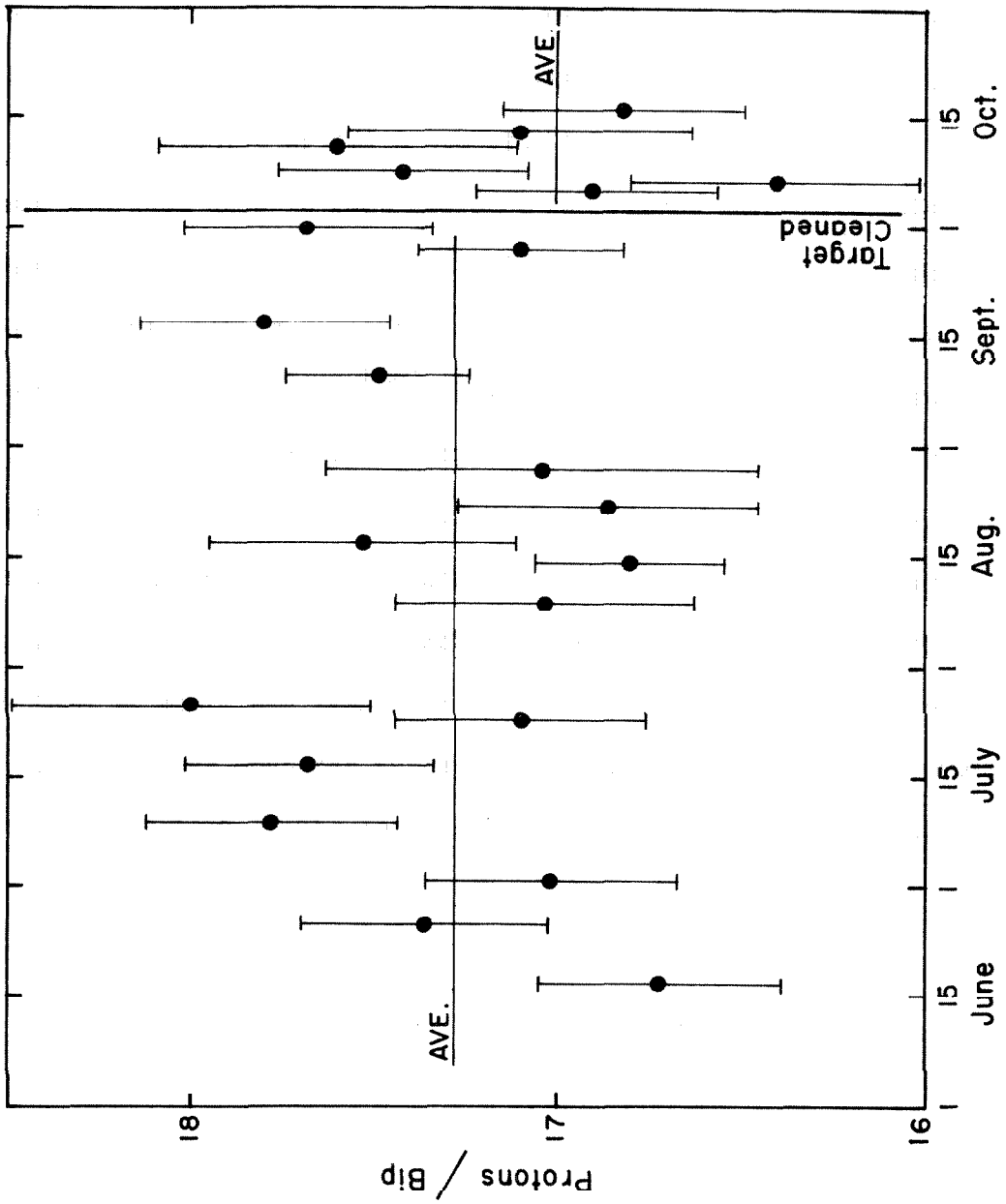
Protons / Bin
18
17
16
AVE.
AVE.
Target Cleaned
June
15
July
15
Aug.
15
Sept.
15
Oct.
15

momentum can only be photoproduced from heavier nuclei, photoproduced from hydrogen and then scattered into this angle, or produced by some other nuclear process. Runs were taken with $E_o = 1.2$ BeV, $\theta_{lab} = 50^\circ$, and $p = 825$ MeV/c with both empty target and full target and the results are plotted in figure 26. The rates have been normalized to a solid angle of 0.00176 sr and a momentum aperture of 0.0941. It is clear that the hydrogen does in fact increase the proton rate by an amount equivalent to 0.021 ± 0.006 gm/cm^2 of Carbon. The cause for this effect was not investigated in detail; it has also been observed in $\pi^o p$ photoproduction experiments.[28] However, the rate increased immediately after filling and decreased immediately after emptying. Since the cup temperature does not change significantly during these processes, it does not seem reasonable that matter condenses on and evaporates from the external walls. Also, a mass spectroscopic analysis of the hydrogen showed that it contained less than 0.4% heavy nuclei. In any case, these data indicate that the target was stable during the tests taken to determine the extent of the contamination during the main experiment.

FIGURE 26

TARGET CONTAMINATION MONITORING

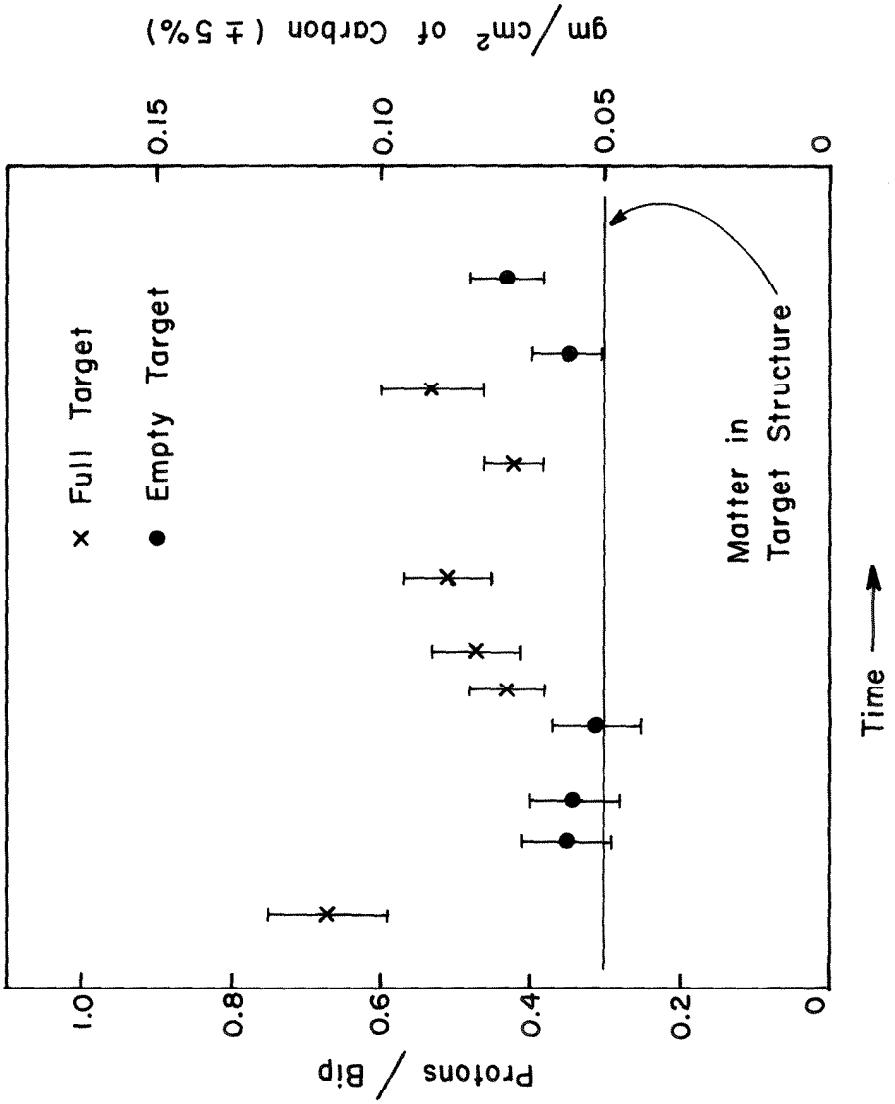
gm/cm² of Carbon (± 5%)
0.15
0.10
0.05
0
× Full Target
● Empty Target
Matter in
Target Structure
Time
Protons / Bin
1.0
0.8
0.6
0.4
0.2
0

APPENDIX VI

DATA REDUCTION

The yield observed in a two-body photoproduction from hydrogen is given by a six-fold integration of the differential cross section and kinematical factors over the target volume and the spectrometer apertures. As these functions are known to be slowly varying over the integration ranges, a priori for the kinematics and a posteriori for the cross section, the integrals are reduced to a simple product of factors by the mean value theorem and the integrand evaluated at the center of the integration ranges. The standard result of this process is:

$$C = \epsilon \, \sigma \, N_\gamma \, N_p$$

where C = number of K mesons detected ,

ϵ = detection efficiency ,

σ = cross section $= \frac{d\sigma}{d\Omega'} \frac{d\Omega'}{d\Omega} \Delta\Omega$,

N_γ = number of photons $= \frac{W}{E_o} \frac{B(k,E_o)}{k} \left(\frac{dk}{dp}\right) \left(\frac{\Delta P}{P_o}\right) P_o$,

N_p = number of hydrogen nuclei per unit area $= N \rho \ell$

In these expressions, $\frac{d\sigma}{d\Omega'}$ is the differential cross section per steradian in the barycentric system; $\frac{d\Omega'}{d\Omega}$ relates the laboratory solid angle to that in the center of mass, and $\Delta\Omega$ is the solid

angle subtended by the spectrometer. In the expression for the number of photons, (W/E_o) (B/k) is the photon number density at energy k, the central energy of the photoproduction, and has been discussed in Appendix I. The other factor is simply the photon energy interval defined by the momentum aperture of the spectrometer. Finally, N is Avogadro's number, ρ the hydrogen density, and ℓ, the effective length of the target. Since no changes were made in either the target or the beam definition relative to earlier work at this laboratory, the results of detailed calculations by Boyden[8] and Kilner[9] of ℓ have been used. These various kinematic and aperture factors either have been discussed earlier or are so well known as to require no special comment.

The terms unique to a given experiment are the yield and the detection efficiency. In Table XI is given the detailed calculation of the yields for the fourteen measured points. The number of counts per 1000 BIP's in the $FK \cdot \bar{L}$ channel with the focusing counter signal above a bias has been corrected for inadequate meson identification (Carbon subtraction), accidental vetos in the Fans and electronic dead time (Acc. and Dead Time) to give the full target counting rate. This has been reduced by 6.7% to account for target contamination in all but two cases and further reduced by the (clean) empty target backgrounds, either measured (m) or calculated (c). The calculated backgrounds were based upon rates observed from a 1" Mylar target. The last column gives the net yield from the hydrogen in the target.

TABLE XI

CALCULATION OF K^+ YIELDS FROM HYDROGEN

All rates are expressed in units of counts/1000 BIP. They have not been corrected to a uniform spectrometer aperture, but they are the observed rates.

k (MeV)	θ c.m.	kilo BIP	FK·$\overline{L}$ FC > Bias	Carbon Subtract.	Acc. and Dead Time	Full Target Yield	Targ. Contam.	Empty Targ. Yield	Hydrogen Yield
1200	15°	5.38	102.6 ± 4.39	- 7.4 ± 1.90	5.7 ± 0.47	100.9 ± 4.77	- 6.7	- 17.5 ± 2.40 m	76.7 ± 5.41
1200	25°	9.24	114.6 ± 3.73	- 3.9 ± 0.93	5.8 ± 0.50	116.5 ± 3.85	- 7.7	- 12.6 ± 2.13 m	96.2 ± 4.44
1200	30°	8.36	74.9 ± 3.01	- 4.1 ± 0.56	1.0 ± 0.20	71.8 ± 3.06	- 4.8	- 4.8 ± 1.46 m	62.2 ± 3.41
1200	35°	9.33	95.3 ± 3.20	- 3.3 ± 0.62	2.6 ± 0.30	94.6 ± 3.27	- 6.3	- 8.5 ± 1.90 m	79.8 ± 3.78
1200	42°	6.40	78.7 ± 3.50	- 2.2 ± 0.56	3.0 ± 0.30	79.5 ± 3.56	- 5.3	- 5.5 ± 0.88 c	68.7 ± 3.67
1200	49°	8.00	72.9 ± 3.03	- 2.4 ± 0.39	1.3 ± 0.18	71.7 ± 3.07	- 4.8	- 5.2 ± 1.70 m	61.7 ± 3.51
1200	55°	6.63	63.6 ± 3.10	- 2.1 ± 0.38	1.4 ± 0.18	62.9 ± 3.14	- 4.2	- 3.5 ± 0.61 c	55.2 ± 3.20
1200	63°	8.00	48.8 ± 2.48	- 1.8 ± 0.59	0.7 ± 0.09	47.7 ± 2.56	- 3.2	- 3.5 ± 0.61 c	41.0 ± 2.63
1200	70°	10.12	34.9 ± 1.86	- 1.2 ± 0.35	0.2 ± 0.03	33.9 ± 1.89	- 2.3	- 2.7 ± 0.49 c	28.9 ± 1.95
1200	78°	9.33	26.6 ± 1.69	- 2.2 ± 0.55	0.1 ± 0.02	24.5 ± 1.78	- 1.6	- 1.1 ± 0.68 m	21.8 ± 1.90
1200	85°	6.50	22.8 ± 1.86	- 2.0 ± 0.92	——	20.8 ± 2.07	——	- 2.2 ± 0.80 m	18.6 ± 2.22
1080	46.5°	8.73	51.0 ± 2.40	- 2.1 ± 0.55	0.3 ± 0.04	49.2 ± 2.46	- 3.3	- 2.3 ± 1.30 m	43.6 ± 2.78
1054	31°	5.65	58.6 ± 3.24	- 3.0 ± 0.85	0.6 ± 0.10	56.2 ± 3.33	- 3.7	- 2.6 ± 1.80 m	49.9 ± 3.81
1054	48°	5.03	47.3 ± 3.10	- 2.8 ± 1.20	——	44.5 ± 3.32	——	- 1.0 ± 1.00 m	43.5 ± 3.47

The detection efficiency of the apparatus, ϵ, consists of three factors, a nuclear absorption factor A, the decay correction D, and electronic efficiencies. All electronic efficiencies have been taken as unity with the exception of those related to the Cherenkov counters and the manner of obtaining these has already been discussed. The correction for nuclear absorption was not measured directly. Rather, it has been calculated from the emulsion data of Zorn and Zorn[39] with a simple version of the optical model. This was used rather than the more direct measurements of Kerth, Kycia, and van Rossum[40] because the newer data extend to a K meson momentum of 670 MeV/c whereas that of Kerth, et al., was at 475 MeV/c. From their data, Zorn and Zorn have derived the complex nuclear potentials for a smooth nuclear density function to describe the nuclear scattering (real part of the potential) and the absorption (imaginary part) by using a sophisticated analysis involving detailed solutions of the Schroedinger equation and exact Coulomb wave function. The analysis which was used to relate their work to the problem at hand was somewhat more prosaic. First, since the bulk of the material causing losses due to nuclear interactions is concentrated near the spectrometer focus, Coulomb and nuclear scattering have been neglected and only the true absorption given by the imaginary part, W, of the potential has been included. Furthermore, its effect was calculated in the original optical model approximation.[41] The result for the absorption cross section, σ_a, of a meson with kinetic energy T and wavelength k is[41]

$$\pi R^2 \left[1 - \frac{1 - e^{-2X}(1 + 2X)}{2X^2} \right]$$

where $X = \frac{1}{2} \frac{W}{T} k R$, and R is the nuclear radius. According to the formula, the absorption is a weak function of momentum for constant W. Also the work of Zorn and Zorn suggests that W contains little energy dependence. Because the approach does not warrant much refinement, a fixed W of 17.5 MeV and an intermediate fixed momentum were used in the calculation. However, the dependence upon the nuclear species is quite strong and was evaluated with the formula. The fraction of the geometrical cross section, πR^2, varied from 0.33 for Carbon to 0.45 for Iron.

The material in the K beam consisted of a fraction which was constant for all the fourteen points and a smaller part which changed from point to point. This latter consisted of the focusing counter radiator and the outside aluminum shell of the hydrogen target which, because of its complex geometry, presented a different effective thickness to the K beam at each lab angle. Although the absorption cross sections are but poorly known at present, better information is potentially available for them. Therefore, in Table XII a detailed listing of the matter in the K beam and the absorption cross sections used is presented.

The flight path from the hydrogen target through the system is quite long and only about 30% of the K mesons produced in the target pass through the full detector without decaying. Since the correction factor for this fact is quite large, considerable care must be taken in its

TABLE XII

MATERIAL IN K BEAM AND ABSORPTION

CROSS SECTIONS

A. Fixed Absorber and Absorption Cross Section

Element	Mass (gm/cm^2)	σ_a (mb)
H	.25	14
C	11.26	100
N	.75	116
Al	.21	218
Fe	.63	425
Cu	.07	485

B. Variable Absorber

k (MeV)	$\theta_{c.m.}$	C (gm/cm^2)	O (gm/cm^2)	H (gm/cm^2)	Al (gm/cm^2)
1200	15°	1.31	7.59	1.01	0
1200	25°	1.55	7.49	1.02	0
1200	30°	1.55	7.49	1.02	0
1200	35°	0	8.22	1.02	0
1200	42°	0.14	8.16	1.02	1.57
1200	49°	0.53	7.98	1.02	1.10
1200	55°	0.87	7.81	1.02	0.89
1200	63°	1.59	7.46	1.02	0.60
1200	70°	2.16	7.21	1.02	0.43
1200	78°	4.55	6.07	1.02	2.04
1200	85°	6.09	4.07	.76	1.50
1080	46.5°	6.09	4.07	.76	1.50
1054	48°	4.55	6.07	1.02	2.04
1054	31°	6.09	4.07	.76	0

evaluation to account for the decays which do not thwart detection. The flight path can be conveniently considered in four parts. First, decay products of any momentum K mesons between target and magnet simply contribute to the general flux of particles from the target and are of no special concern; none of them are counted. Similarly, all K mesons which penetrated the full system but decayed after passing through the Lucite Cherenkov counter were counted since no backward-going decay product has enough velocity to fire this veto counter. (The very small fraction which decay between LC and S3 with no forward going charged product has been neglected.) Ray tracings for those K mesons which have the proper momentum for detection but which decay in the magnetic field or between it and FC show that no decay product can fire the focusing counter. The decays of lower energy K mesons in certain regions of the magnetic field are potentially troublesome and have been discussed in Appendix IV. Finally, the only interesting region is that between FC and LC. The particles which decay here have already behaved normally in the prime K detector, FC, but can be counted only if a slow forward-going charged product results. Furthermore, some fraction of these decays yields large signals in both Cherenkov counters. In order to evaluate these effects, a Monte Carlo program was prepared for the IBM 7090. The results of the calculation were that the number of K mesons which fire both Cherenkov counters is 2.9% of the number detected and that 6.6% of those which decay between the two counters are detected anyway. Both these fractions actually depend on momentum, but very weakly. Of course, only the second fraction is significant in making the decay correction and even so its contribution is almost negligible.

The lifetime given in Rosenfeld's tabulation[42] of 12.24 ± 0.13 nsec was used. Furthermore, the effects of energy loss in the aperture counters, A1 and A2, and in the focusing counter were included. Denoting the decay lengths (in inches) in the three regions, target to apertures, apertures to FC, and FC to LC by λ_1, λ_2, and λ_3, one obtains for the decay correction

$$D = e^{-\frac{163}{\lambda_1}} e^{-\frac{63}{\lambda_2}} \left[e^{-\frac{37}{\lambda_3}} (1 - B) + B \right]$$

where $\lambda_1 = 292.5 \, P_i \left[\text{inches, MeV/c}\right]$,

P_i = momentum in region i ,

B = fraction of decays between FC and LC which are detected ,

and the numerical terms are average flight paths in each region in inches.

The calculation of cross sections from yields is presented in Table XIII.

The various factors relating the yield to the cross section are not perfectly well known, of course, and the accumulation of the uncertainties gives the expected reliability of the absolute scale of the cross section. In Table XIV, the various systematic uncertainties are tabulated. Folding these together by taking the root of the sum of squares, we find that the absolute cross sections are determined to $\pm$ 6%.

TABLE XIII

CROSS SECTION CALCULATION

The table contains all the factors involved in the cross section calculation with the exception of the number of protons in the target, 3.046×10^{23} protons/cm^2. All the quantities have been defined in the text except for:

$$G = \frac{d\Omega'}{d\Omega} \frac{dk}{dp}$$

and Γ = number of counts per 1000 BIPS per 10^{-31} cm^2/sr .

k (MeV)	$\theta_{c.m.}$	p_{mag} (MeV/c)	E_o (MeV)	B	W (10^{12} MeV per BIP)	$\frac{\Delta P}{P_o}$	$\Delta\Omega$ (10^{-3} sr)	G	D	A	ϵ_{FC}	ϵ_{LC}	Γ	Yield (counts per 1000 BIP)	$\frac{d\sigma}{d\Omega}$ (10^{-31} cm^2)
1200	15°	812.2	1280	.83	14.12	.0941	0.88	4.50	.332	.882	.993	.990	20.23	76.7 ± 5.41	3.79 ± .268
1200	25°	796.2	1280	.83	14.12	.0706	1.76	4.45	.324	.881	.994	.990	28.76	96.2 ± 4.44	3.34 ± .154
1200	30°	785.1	1280	.83	14.16	.0941	0.88	4.41	.319	.881	.979	.990	18.22	62.2 ± 3.41	3.41 ± .187
1200	35°	771.8	1280	.83	14.16	.0706	1.76	4.37	.313	.885	.992	.991	26.57	79.8 ± 3.78	3.00 ± .142
1200	42°	750.3	1280	.83	14.13	.0706	1.76	4.29	.303	.877	.988	.992	24.19	68.7 ± 3.67	2.84 ± .152
1200	49°	725.8	1280	.83	14.12	.0706	1.76	4.20	.290	.878	.983	.992	21.87	61.7 ± 3.51	2.82 ± .160
1200	55°	702.3	1280	.83	14.14	.0706	1.76	4.11	.278	.878	.988	.992	19.98	55.2 ± 3.20	2.76 ± .160
1200	63°	667.7	1280	.83	14.13	.0706	1.76	3.96	.260	.878	.980	.993	17.00	41.0 ± 2.63	2.41 ± .155
1200	70°	634.6	1280	.83	14.15	.0706	1.76	3.81	.242	.877	.970	.994	14.34	28.9 ± 1.95	2.02 ± .136
1200	78°	594.5	1280	.83	14.12	.0706	1.76	3.61	.220	.863	.960	.995	11.24	21.8 ± 1.90	1.94 ± .169
1200	85°	556.7	1280	.83	14.21	.0941	1.76	3.41	.198	.869	.960	.995	12.09	18.6 ± 2.22	1.54 ± .184
1080	46.5°	594.5	1160	.84	13.80	.0706	1.76	4.12	.220	.869	.960	.995	15.64	43.6 ± 2.78	2.79 ± .178
1054	31°	594.8	1130	.85	13.70	.0706	1.76	4.34	.220	.877	.960	.995	17.58	49.9 ± 3.81	2.84 ± .217
1054	48°	556.7	1130	.85	13.75	.0941	1.76	4.10	.198	.873	.960	.995	18.63	43.5 ± 3.47	2.33 ± .186

TABLE XIV

LISTING OF SYSTEMATIC UNCERTAINTIES

Target and Spectrometer constants	$\pm$ 2.0 %
Decay corrections	$\pm$ 1.5 %
Absorption corrections	$\pm$ 3.0 %
FC and LC efficiencies	$\pm$ 0.7 %
Number of equivalent quanta, $\frac{W}{E_o}$	$\pm$ 1.5 %
Bremsstrahlung shape factor, B	$\pm$ 0.7 %
Target contamination	$\pm$ 3.5 %
Total	$\pm$ 6 %

REFERENCES

1. P.L.Donoho and R.L.Walker, Phys. Rev. 112, 981 (1958); B.D.McDaniel, A.Silverman, R.R.Wilson, and G.Cortellessa, Phys. Rev. 115, 1039 (1959); H.M.Brody, A.M.Wetherell, and R.L.Walker, Phys. Rev. 119, 1710 (1960).
2. R.L.Anderson, E.Gabathuler, D.Jones, B.D.McDaniel, and A.J.Sadoff, Phys. Rev. Letters 9, 131 (1962).
3. A.J.Sadoff, R.L.Anderson, E.Gabathuler, and D.Jones, Bull. Am. Phys. Soc. 9, 34 (1964).
4. H.Thom, E.Gabathuler, D.Jones, B.D.McDaniel, and W.M.Woodward, Phys. Rev. Letters 11, 433 (1963).
5. J.G.Taylor, M.J.Moravcsik, and J.L.Uretsky, Phys. Rev. 113, 689 (1959); M.J.Moravcsik, Dispersion Relations (Interscience Publishers, Inc., New York, 1961), p. 117.
6. M.J.Moravcsik Phys. Rev. Letters 2, 352 (1959); J.J.Sakurai, Nuovo Cimento 10, 1212 (1961).
7. R.L.Walker, Proceedings of the Tenth Annual International Conference on High Energy Physics at Rochester, 1960 (Interscience Publishers, Inc., New York, 1960) p. 17.
8. J.H.Boyden, Ph.D. Thesis, California Institute of Technology (1961).
9. J.R.Kilner, Ph.D. Thesis, California Institute of Technology (1963).
10. M.Huq and G.W.Hutchinson, Nuclear Instr. and Meth. 4, 30 (1959).
11. B.D.McDaniel, R.L.Anderson, E.Gabathuler, D.P.Jones, A.J.Sadoff, and H.Thom, 1962 International Conference on High Energy Physics at CERN (Interscience Publishers, Inc., New York, 1962), p.266.
12. S.Iwao, Nuovo Cimento 23, 516 (1962); N.J.Sopkovich, Ph.D.Thesis, Carnegie Institute of Technology (1962).

13. F.Ferrari, Nuovo Cimento 9, 842 (1958).

14. G.T.Hoff, Phys. Rev. 131, 1302 (1963).

15. M.Gell-Mann, Phys. Rev. 106, 1296 (1957).

16. N.M.Kroll and M.A.Ruderman, Phys. Rev. 93, 233 (1954).

17. R.K.Adair and E.C.Fowler, Strange Particles (Interscience Publishers, Inc., New York, 1963), p. 56.

18. A.Kanazawa, Phys. Rev. 123, 993 (1961).

19. T.K.Kuo, Phys. Rev. 129, 2264 (1963).

20. N.A.Beauchamp and W.G.Holladay, Phys. Rev. 131, 2719 (1963).

21. M.Rimpault (to be published).

22. S.Matsukade and H.J.Schnitzer, Phys. Rev. 128, 468 (1962).

23. Ibid, Phys. Rev. 132, 1301 (1963).

24. M.Gourdin, Nuovo Cimento 10, 1035 (1961); M.Gourdin and J.Dufour, Nuovo Cimento 27, 1410 (1963).

25. M.Cini and S.Fubini, Annals of Physics 3, 352 (1960); S.Fubini, Dispersion Relations (Interscience Publishers, Inc., New York, 1961), p. 259.

26. W.C.Davidon, ANL-5990 Rev. (1959), unpublished.

27. R.Gomez, Beam Monitoring at the Caltech Synchrotron (1962), unpublished.

28. A complete description of the target is given by R.E.Diebold, Ph.D. Thesis, California Institute of Technology (1963).

29. H.Brody, Ph.D. Thesis, California Institute of Technology (1959).

30. P.L.Donoho, A Magnetic Spectrometer for Analysis of Charged Particles at Momenta up to 1200 MeV/c (1957), unpublished.

31. The author is unaware of any written description of this work; however, the results are given on a Synchrotron Laboratory graph, SL 363 (R.L.Walker, private communication).

32. F.P.Dixon, Ph.D. Thesis, California Institute of Technology, (1960).

33. J.V.Jelley, Cherenkov Radiation, (Pergamon Press, New York, 1958).

34. F.Wolverton, Optical Efficiency of the Focusing Cherenkov Counter (1962), unpublished.

35. A.Barna, J.H.Marshall, and M.Sands, Nuclear Instr. and Meth. 7, 124 (1959); Nuclear Instr. and Meth. 12, 43 (1961); CTSL 17 (1961).

36. A.Barna and J.H.Marshall, CTSL 18 (1961).

37. Technical Measurements Corp., North Haven, Conn.

38. D.Groom, private communication.

39. B.S.Zorn and G.T.Zorn, Phys. Rev. 120, 1898 (1960).

40. L.T.Kerth, T.F.Kycia, and L.VanRossum, Phys. Rev. 109, 1784 (1958).

41. S.Fernbach, R.Serber, and T.B.Taylor, Phys. Rev. 75, 1352 (1949).

42. A.H.Rosenfeld, UCRL-8030 Rev. (1963).

43. M.D.Daybell, Ph.D. Thesis, California Institute of Technology (1962).